NOTICE

The quality of this microform is heavily dependent upon the quality of the original thesis submitted for microfilming. Every effort has been made to ensure the highest quality of reproduction possible.

If pages are missing, contact the university which granted the degree.

Some pages may have indistinct print especially if the original pages were typed with a poor typewriter ribbon or if the university sent us an inferior photocopy.

Reproduction in full or in part of this microform is governed by the Canadian Copyright Act, R.S.C. 1970, c. C-30, and subsequent amendments.

AVIS

La qualité de cette microforme dépend grandement de la qualité de la thèse soumise au microfilmage. Nous avons tout fait pour assurer une qualité supérieure de reproduction.

S'il manque des pages, veuillez communiquer avec l'université qui a conféré le grade.

La qualité d'impression de certaines pages peut laisser à désirer, surtout si les pages originales ont été dactylographiées à l'aide d'un ruban usé ou si l'université nous a fait parvenir une photocopie de qualité inférieure.

La reproduction, même partielle, de cette microforme est soumise à la Loi canadienne sur le droit d'auteur, SRC 1970, c. C-30, et ses amendements subséquents.

Canada

Objective Measurement of Subjective Image Quality

Wajih Walid Bishtawi

A Thesis

in

The Department

of

Electrical and Computer Engineering

Presented in Partial Fulfillment of the Requirements

for the Degree of Master of Applied Science at

Concordia University

Montréal, Québec, Canada

March 1996

ISBN 0-612-10824-4

Canada

ABSTRACT

Objective Measurement of Subjective Image Quality

Wajih Walid Bishtawi

The development of image coders, has been traditionally obstructed by the lack of a clear relation between designing procedures and the perceptual coder performance; this is due to unavailability of a reliable objective image quality technique that can measure the error in compressed images as perceived by human observers. In the past, there were many attempts to predict image quality based on the Human Visual System (HVS). Most of these attempts used visual criteria such as the frequency sensitivity and frequency masking properties of the eye. These attempts were unable to predict two important image quality factors: type and location of error. Summaries of some of these attempts are presented. In this thesis, the Impairment Detection Method (IDM) is introduced. It is a first step in developing an objective measure of subjective image quality. It detects and measures certain types of image artifacts that are common with block transform coding techniques: blocking, blurring, and spatial edge noise (*ringing*). IDM is a relative measurement where both original and reconstructed images are required. Simulation results show that IDM isolates each type of artifact within its c ıtext and produces three output primitives; each primitive measures the amount of error that is introduced by a single type of artifact. These primitives are monotonic; one decreases as the presence of blurring artifact increases, and the others increase as the presence of blocking and ringing artifact increase. Note that IDM is restricted only to the luminance part of images.

ACKNOWLEDGEMENTS

I would like to express my sincere appreciation to my supervisor, Dr. William Lynch, for his invaluable help, patience, guidance and support. I would also like to thank from the department: Dr. M. Gawargy, Dr. H. Hum and Kim Adams for their continuous help and support. A special thanks go to my friends for their help, patience, companion and fellowship. In particular I would like to mention Ahmed El-Husseiny, Ali Shatnawi, Hani Sorial, Mohanad Al-Ata and Nasser Ismail.

Thanks also go to the organizations that provided financial support to me through the grants awarded to my supervisor; Concordia University through its Faculty Research Development Program Grant and National Sciences and Engineering Research Council of Canada through their Operating Grant.

Finally, I express my deepest gratitude to my parents and my brother who without their love, support and encouragement I would never have reached this level.

TABLE OF CONTENTS

LIST OF FIGURES viii

LIST OF TABLES xii

1 Introduction **1**

1.1 Image Compression and Quality Measurement 1

1.2 Weaknesses of MSE 7

1.3 Problem Statement 10

1.3.1 Solving Mechanism 10

1.3.2 Evaluation 11

1.4 Thesis Summary 12

2 Quality Measurement Techniques **13**

2.1 Introduction 13

2.2 Subjective Measurements 15

2.3 Graphical Measurement 17

2.4 Measurements Based on a Multiple Channel HVS model 21

2.4.1 Image Quality Criterion 22

2.5 Picture Quality Scale Method 24

2.6 Impairment Quality Rating 27

2.6.1 Gradient Magnitude and Angle Histogram 31

2.6.2 Features Extracted from SIH(r,θ) 31

2.6.3 Combining the Features into Parameters 37

2.7 Conclusions 38

3 Impairments Detection Method **40**

3.1 Introduction 40

3.2 Block Classification 44

3.2.1 Edge Block Detector 48
3.2.2 Edge Connectivity 52
3.2.3 Edge Contour 55
3.2.4 Edge Continuity 57
3.2.5 Edge Extraction 57
3.3 Image Analysis 63
3.3.1 Spatial Information Histogram 63
3.3.2 Edge Measurements 65
3.4 Impairments Measurements 66
3.4.1 Blurring Artifact 67
3.4.2 Blocking Artifact 68
3.4.3 Spatial Edge Noise Artifact *(Ringing)* 68
3.5 Simulation Results 69
3.5.1 Discussion 70
3.5.2 Low Frequency Blocks Results 74
Discussion 76
3.5.3 Texture Blocks Results 80
Discussion 80
3.5.4 Sharp Edge Blocks Results 86
Discussion 90
3.5.5 IDM vs. IQR 94
Compressing the Texture Blocks 94
Compressing the Sharp Edge Blocks 95
Compressing the Flat Blocks 98
3.5.6 Results of Other Images 101
3.6 Conclusions 107

4 Conclusions and Further Research **108**

4.1 Conclusions 108

4.2 Further Research 110
MOS Emulation 110
Inclusion of More Types of Artifacts 111
Practical Problems and Refining 112

BIBLIOGRAPHY 113

A IDM and IQR Simulation Results **119**

LIST OF FIGURES

1.1 Part of Lena's Face and Shoulder: (a) Original, (b) Showing the Blocking Artifact 4

1.2 Right Shoulder of Lena: (a) Original, (b) Showing the Spatial Edge Noise Artifact 1

1.3 Original 512×512 Lena 5

1.4 Third Generation Low-pass Filtered Lena 6

1.5 Compressed Lena Using PVRG-JPEG CODEC at -q= 300 (compression ratio of 42:1) 9

2.1 Block Diagram of the Visible Differences Predictor 18

2.2 Masking Model: logarithmic relation between the visibility threshold C_T and the background contrast C_M 22

2.3 Original 512×512 Pepper 32

2.4 SIH(r,θ) of Original Pepper 33

2.5 Compressed Pepper Using PVRG-JPEG CODEC at -q = 400 (compression ratio of 53:1) 34

2.6 SIH(r,θ) of the Degraded Pepper 35

3.1 IDM Block Diagram 43

3.2 Compressed Lena using PVRG-JPEG CODEC at -q=100 (compression ratio of 18:1) 45

3.3 Blurred Lena 46

3.4 The Magnitude of the Sobel Filtered Lena 47

3.5 Low Frequency Blocks of Original Lena 49

3.6 High Frequency Blocks of Original Lena 50

3.7 Mapping of Two Sobel Operators to the Sharp Edge Region 51

3.8 Sharp Edge Block Acceptable Situations 52
3.9 Output of the Edge Block Detector (Sharp Edge Blocks) 53
3.10 Output of the Edge Block Detector (Texture Blocks) 54
3.11 8-Neighbors and 4-Neighbors of the Center Pixel 55
3.12 (a) Two Edge Regions (b) Their Edge Identification Numbers (c) Their Edge Contours (d) The Edge Identification Numbers of The Contours 56
3.13 The Sharp Edge Region after the Edge Length Test 58
3.14 8×8 Block Division into Frame and Interior 59
3.15 Sobel Masked Image of the Sharp Edge Blocks after the Continuity Test 60
3.16 Sobel Masked Image of the Texture Blocks after the Continuity Test . 61
3.17 Sharp Edge Pixels 62
3.18 An Example of a SIH(r,θ) Construction 64
3.19 Graphical Representation of the Area of the Horizontal and Vertical Feature (*shaded area*) 66
3.20 Degraded Lena at $q = 100$ Showing the Blocks of Interest 72
3.21 Block (8,112) of Degraded Lena of $q = 100$ 73
3.22 Block (112,168) of Degraded Lena of $q = 100$ 73
3.23 Block (40,224) of Degraded Lena of $q = 100$ 73
3.24 Simulation Results of Low Frequency Block, $\alpha = 5°$ 74
3.25 Compressed Lena Using PVRG-JPEG CODEC at -q=500 (compression ratio of 65:1) 75
3.26 Simulation Results of Low Frequency Block, $\alpha = 0°$ 77
3.27 DCT Coefficients of the Block Located at (8,112) of the Original Lena (Left) and the Degraded Lena at -$q = 100$ (Right) 78

3.28 For the Block located at (8,112): (a),(c) Horizontal Sobel Filter of the Original and the Degraded Lena at -q = *100* respectively (b),(d) Vertical Sobel Filter of the Original and the Degraded Lena at -q = *100* Respectively 79
3.29 Simulation Results of Texture Blocks, $\alpha = 5°$ 82
3.30 Compressed Lena Using PVRG-JPEG CODEC at q= 150 (compression ratio of 25:1) 83
3.31 Simulation Results of Texture Blocks, $\alpha = 0°$ 84
3.32 For the Block located at (112,168): (a),(c) Horizontal Sobel Filter of the Original and the Degraded Lena at -q = *100* respectively (b),(d) Vertical Sobel Filter of the Original and the Degraded Lena at -q = *100* respectively 85
3.33 DCT Coefficients of the Block Located at (112,168) of the Original Lena (Left) and the Degraded Lena at -q = *100* (Right) 86
3.34 Simulation Results of Sharp Edge Blocks, $\alpha = 5°$ 88
3.35 Simulation Results of Sharp Edge Blocks, $\alpha = 0°$ 89
3.36 For the Block Located at (40,224): (a) Horizontal Sobel Filter of the Original Lena (b) Vertical Sobel Filter of the Original Lena 91
3.37 For the Block Located at (40,224): (a),(c) Horizontal Sobel Filter of the Degraded Lena at -q = *100 and 400* respectively (b),(d) Vertical Sobel Filter of the the Degraded Lena at -q = *100 and 400* respectively 92
3.38 DCT Coefficients of the Block Located at (40,224), (a) the Original Lena, (b) the Degraded Lena at -q = *100*, (c) the Degraded Lena at -q = *400* 93
3.39 The Feather Blocks of Lena are Compressed at a Rate 31:1 96
3.40 Simulation Results of Changing the Compression Ratio for Lena's Feather Blocks 97

3.41 Sharp Edge Blocks of Lena are Compressed with a Compression Ratio of 42:1 99
3.42 Simulation Results of Changing the Compression Ratio for Lena's Sharp Edge Blocks 100
3.43 Flat Blocks of Lena are Compressed with a Compression Ratio of 36:1 102
3.44 Flat Blocks of Lena are Compressed with a Compression Ratio of 59:1 103
3.45 Simulation Results of Changing the Compression Ratio for Lena's Flat Blocks 104
3.46 Original 512×512 Bank 105
3.47 Original 256×256 Girl 106
3.48 Original 256×256 House 106

LIST OF TABLES

1.1 MSE and PSNR for Different Types of Artifacts in Lena 8

2.1 Rating Scale Recommended by CCIR-500 for Subjective Evaluation 16
2.2 Sobel Operators $S_h(x,y)$ and $S_v(x,y)$ 29
2.3 Summary of the Capabilities of the Introduced Image Quality Measures 39
2.4 Summary of the Output Format and the Measurement Type of the Introduced Image Quality Measures 39

3.1 3×3 Neighborhood Averaging Low Pass Filter 44
3.2 Blocks Classes and Their Classification Conditions 59
3.3 Summary of the IDM's Measurement Locations for Each Type of Artifact 69

A.1 Image Compression Ratios of the Used Q-Factor ($-q$) 120
A.2 Lena, Low Frequency Blocks (Block Frame), $\alpha = 5°$ 121
A.3 Lena, Low Frequency Blocks (Block Interior), $\alpha = 5°$ 121
A.4 Lena, Texture Blocks (Block Frame), $\alpha = 5°$ 122
A.5 Lena, Texture Blocks (Block Interior), $\alpha = 5°$ 122
A.6 Lena, Sharp Edge Blocks (Block Frame), $\alpha = 5°$ 123
A.7 Lena, Sharp Edge Blocks (Sharp Edge pixels), $\alpha = 5°$ 123
A.8 Lena, Sharp Edge Blocks (Background pixels), $\alpha = 5°$ 124
A.9 Lena, Simulation Results of IQR, $\alpha = 5°$ 124
A.10 Lena, Low Frequency Blocks (Block Frame), $\alpha = 0°$ 125
A.11 Lena, Low Frequency Blocks (Block Interior), $\alpha = 0°$ 125
A.12 Lena, Texture Blocks (Block Frame), $\alpha = 0°$ 126
A.13 Lena, Texture Blocks (Block Interior), $\alpha = 0°$ 126
A.14 Lena, Sharp Edge Blocks (Block Frame), $\alpha = 0°$ 127

A.15 Lena, Sharp Edge Blocks (Sharp Edge pixels), $\alpha = 0°$ 127
A.16 Lena, Sharp Edge Blocks (Background pixels), $\alpha = 0°$ 128
A.17 Lena, Simulation Results of IQR, $\alpha = 0°$ 128
A.18 Bank, Low Frequency Blocks (Block Frame), $\alpha = 0°$ 129
A.19 Bank, Low Frequency Blocks (Block Interior), $\alpha = 0°$ 129
A.20 Bank, Texture Blocks (Block Frame), $\alpha = 0°$ 130
A.21 Bank, Texture Blocks (Block Interior), $\alpha = 0°$ 130
A.22 Bank, Sharp Edge Blocks (Block Frame), $\alpha = 0°$ 131
A.23 Bank, Sharp Edge Blocks (Sharp Edge Pixels), $\alpha = 0°$ 131
A.24 Bank, Sharp Edge Blocks (Background pixels), $\alpha = 0°$ 132
A.25 Girl, Low Frequency Blocks (Block Frame), $\alpha = 0°$ 133
A.26 Girl, Low Frequency Blocks (Block Interior), $\alpha = 0°$ 133
A.27 Girl, Texture Blocks (Block Frame), $\alpha = 0°$ 134
A.28 Girl, Texture Blocks (Block Interior), $\alpha = 0°$ 134
A.29 Girl, Sharp Edge Blocks (Block Frame), $\alpha = 0°$ 135
A.30 Girl, Sharp Edge Blocks (Sharp Edge Pixels), $\alpha = 0°$ 135
A.31 Girl, Sharp Edge Blocks (Background pixels), $\alpha = 0°$ 136
A.32 House, Low Frequency Blocks (Block Frame), $\alpha = 0°$ 137
A.33 House, Low Frequency Blocks (Block Interior), $\alpha = 0°$ 137
A.34 House, Texture Blocks (Block Frame), $\alpha = 0°$ 138
A.35 House, Texture Blocks (Block Interior), $\alpha = 0°$ 138
A.36 House, Sharp Edge Blocks (Block Frame), $\alpha = 0°$ 139
A.37 House, Sharp Edge Blocks (Sharp Edge Pixels), $\alpha = 0°$ 139
A.38 House, Sharp Edge Blocks (Background pixels), $\alpha = 0°$ 140
A.39 Pepper, Low Frequency Blocks (Block Frame), $\alpha = 0°$ 141
A.40 Pepper, Low Frequency Blocks (Block Interior), $\alpha = 0°$ 141
A.41 Pepper, Texture Blocks (Block Frame), $\alpha = 0°$ 142
A.42 Pepper, Texture Blocks (Block Interior), $\alpha = 0°$ 142

A.43 Pepper, Sharp Edge Blocks (Block Frame), $\alpha = 0^{\circ}$ 143
A.44 Pepper, Sharp Edge Blocks (Sharp Edge Pixels), $\alpha = 0^{\circ}$ 143
A.45 Pepper, Sharp Edge Blocks (Background pixels), $\alpha = 0^{\circ}$ 144

Chapter 1

Introduction

1.1 Image Compression and Quality Measurement

One of the important benefits of digital waveform representation is the fact that digital signals are less sensitive than analog signals to transmission noise. Digital signals have the advantages of being easy to: *regenerate, store, error-protect, multiplex, packetize,* and *mix.* Digitizing also permits the application of powerful digital signal processing techniques [1]. Images are among the signals that can benefit from digitizing. In this thesis, we are concerned with digital images.

An enormous amount of data is produced when a 2-D light intensity function is sampled and quantized to create a digital image. In fact, the amount of data generated may be so great that it results in impractical storage, processing, and communication requirements. For example, assuming one byte per pixel, a 512×512 pixel monochrome image occupies 262,144 bytes of storage. This is equivalent to about 87 pages of dense text at one byte per character. Color images may require as much as three times the storage amount required by monochrome images. This massive storage and bandwidth requirements are a serious concern for many applications involving imagery. Image compression alleviates a solution to this problem by reducing the number of bits or the range of frequencies needed. The amount of

reduction determines the loss in image quality. But, how much quality is sacrificed for how much compression?

Numerous image compression techniques ([2], [3], [4], [5], [6]) exist today with a common goal of reducing the number of bits needed to store or transmit images. The efficiency of a compression algorithm is generally measured using three criteria [7]:

1. resulting distortion
2. amount of compression, and
3. implementation complexity.

Amount of compression can be measured by calculating the compression ratio. Algorithmic complexity on the other hand, can be measured by considering the type and the number of operations required. The main difficulty in evaluating lossy compression techniques comes from the fact that there is no reliable objective measure for determining the nature and the location of distortions resulting from the loss. While objective measures utilize the computers, which make the evaluation easier, faster, and cheaper, currently used objective measures such as Mean Square Error (MSE) and Peak Signal to Noise Ratio (PSNR) do not compute the perceptual error as detected by the human eye. Section 1.2 will discuss the weaknesses of such measures. The subject of this thesis is to attempt to develop a reliable objective measure that is able to determine the nature and the location of distortions in reconstructed images.

Standard lossy digital image compression techniques such as block coding techniques (JPEG [8], MPEG [9], H.261 [10] ... etc), result in different types of impairments in the reconstructed images. Among the common types of artifacts that such compression techniques produce are:

- *Blocking:* A distortion of the image characterized by the appearance of an underlying block encoding structure [11].

- *Blurring:* A global distortion over the entire image, characterized by reduced sharpness of edges and spatial details [11].

- *Spatial Edge Noise (Ringing):* A form of busyness characterized by spatially varying distortion in close proximity to the edge of objects [11].

Figures 1.1, 1.2 show examples of blocking and ringing artifacts respectively, while Figures 1.3, 1.4 show an example of blurring artifact. The detection and measurement techniques of these types of artifacts will be discussed in Chapters 2 and 3.

Although the objective assessment methods utilize the computers to predict image quality, the subjective assessment methods utilize human observers to view and rate image quality. Subjective assessment methods are the only satisfactory methods for assessing coding quality as perceived by the human observers [12], they have the disadvantage of being costly and time consuming. Objective measures, which are repeatable and do not depend on the viewing conditions or the mood of the viewer, need to be developed. Such measures are not only needed for comparing images produces by different compression techniques, but they are also important in designing image compression algorithms.

Because the human eye is the final arbiter of image quality, it is essential to understand the Human Visual System (HVS) in order to understand the ingredients of image quality. HVS-weighted measurements result in a strong correlation with subjective evaluation [13, 14]. The HVS gives unequal weighting to different types of impairments [15, 16, 17]. For example, subjective studies showed that blocking distortion is ten times more objectionable than equal energy white noise [18]. In addition, humans tend to realize degradation in flat areas more than detailed areas [19]. In other words human observers are sensitive to the structure of the noise and not just the noise energy [18]. Therefore, it is necessary to develop a quality measure that is capable of determining:

(a) (b)

Figure 1.1: Part of Lena's Face and Shoulder (a) Original (b) Showing the Blocking Artifact

(a) (b)

Figure 1.2: Right Shoulder of Lena (a) Original (b) Showing the Sharp Edge Noise Artifact

Figure 1.3: Original 512 × 512 Lena

Figure 1.1: Third Generation Low-pass Filtered Lena

1. the area of degradation,

2. the type of degradation, and

3. the amount of degradation.

in reconstructed images.

1.2 Weaknesses of MSE

Today, Mean Square Error (MSE) is widely used by researchers as an objective quality measure, but it is equally widely criticized [6]. In previous work, Marmolin [20] conducted a test of the applicability of MSE as a measure of perceived similarity between the original and the degraded images. His results showed that MSE is an unsatisfactory measure. Eskicioglu, Fisher, and Chen [21] tested the performance of MSE and reached the same results as Marmolin.

The fact that the properties of the HVS are not taken into account in calculating MSE [22] makes MSE produces outputs that are badly correlated with subjective quality measures. MSE suffers from several significant weaknesses [23]:

1. An arbitrary increase in the MSE does not always lead to a decrease in image quality.

2. Equal values of MSE for two degraded images do not imply similar visual quality.

3. MSE does not specify the types of artifacts.

4. MSE is not capable of specifying the locations of the artifacts.

As a solution for the first weakness, Eskicioglu and Fisher [24] tried to replace MSE by the variance of the error, but their method did not solve the other weaknesses of MSE. These weaknesse. of MSE are not surprising; it is a fact that the human

observers do not sum the error over the entire picture but process it in much more complicated way [3, 17, 20, 22]. MSE is given by:

$$MSE = \frac{1}{MN} \sum_{m=1}^{M} \sum_{n=1}^{N} [i(m,n) - \tilde{i}(m,n)]^2 \tag{1.1}$$

while Peak Signal to Noise Ratio (PSNR) is given by:

$$PSNR = 10 * \log\left(\frac{255^2}{MSE}\right) \tag{1.2}$$

where M and N are the number of rows and columns of an image respectively, $i(m,n)$ and $\tilde{i}(m,n)$ are original image pixels and reconstructed image pixels located at (m,n) respectively.

An example is given in Table 1.1 and Figures 1.4, 1.5 to show one of the weaknesses of MSE. Figure 1.4 is the third generation of low-pass filtered Lena, and Figure 1.5 is the reconstructed Lena after using PVRG-JPEG CODEC [25] with the Q-Factor option (-q) set to 300 (compression ratio of 42:1). Where JPEG refers to a definition of a still-image compression algorithm established by the Joint Photographic Experts Group committee, and the Q-Factor option specifies a multiplicative factor for the quantization: each quantization coefficient of the default quantization matrix is scaled by (Q-Factor/50) [25]. From Table 1.1 it can be seen that both images of Figure 1.4 and Figure 1.5 almost have the same MSE value and PSNR value, while by looking at Figure 1.4 and Figure 1.5 one can see that both images do not have the same visual quality. It can be seen that the artifacts presented in one of the images are more annoying than the artifacts of the other image. That makes their visual quality unequal. This example shows that equal values of MSE for two images does not imply similar visual quality.

Lena Image	MSE	PSNR
Blurred	83.55	28.91
PVRG-JPEG -q 300	83.88	28.89

Table 1.1: MSE and PSNR for Different Types of Artifacts in Lena

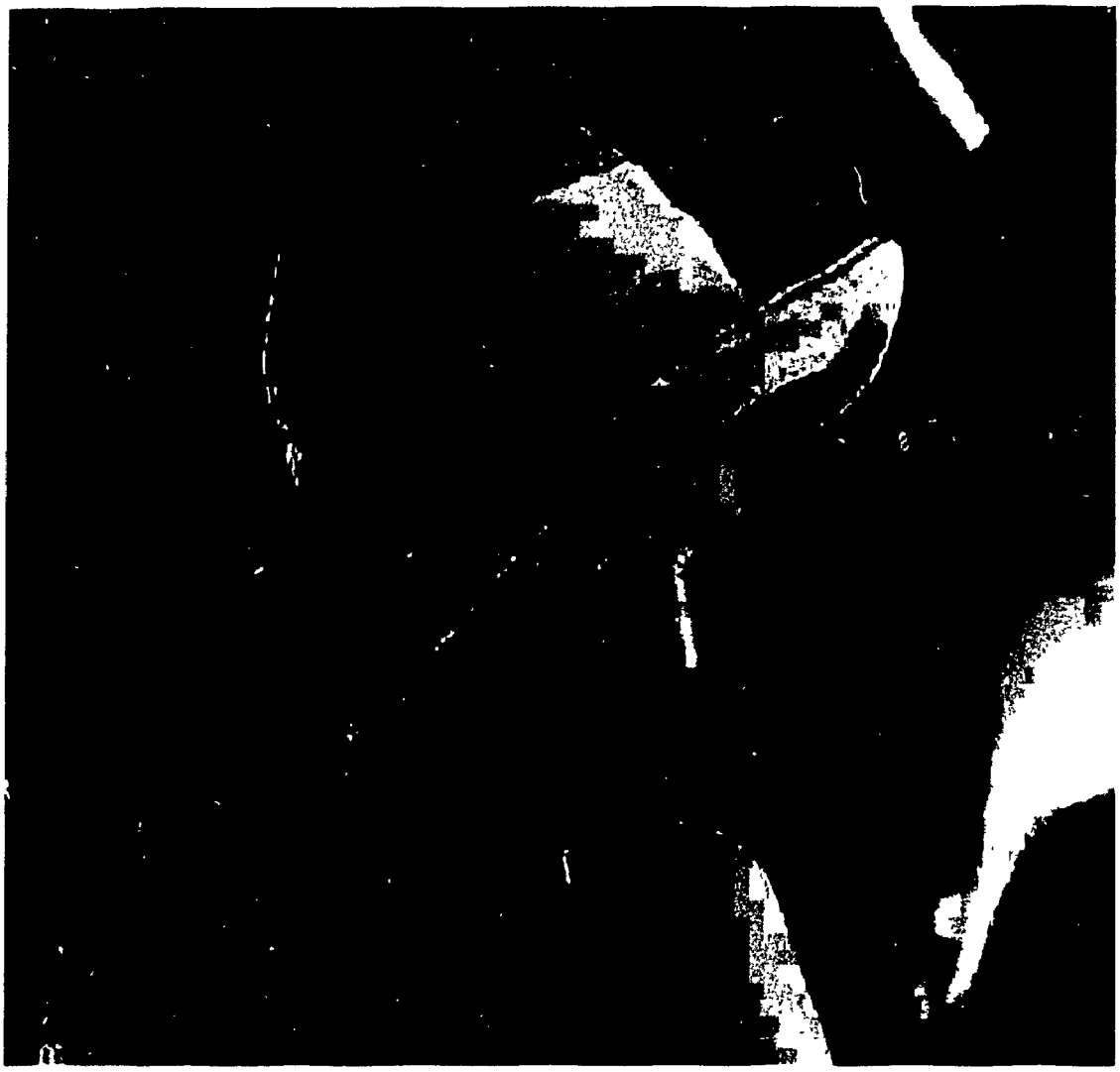

Figure 1.5: Compressed Lena Using PVRG-JPEG CODEC at q = 300 (compression ratio of 12:1)

1.3 Problem Statement

As mentioned earlier, the only reliable measures of perceived image quality are the subjective assessment methods. These methods are expensive and time consuming. Current objective image quality assessment methods such as MSE are easy to compute but do not measure well the perceptual distortions of images. The development of an objective technique that combines the best of subjective and objective measures, by being easy to compute and sensitive to the properties of the HVS, is needed for comparing images produces by different compression techniques and is also important in designing image compression algorithms.

There are different types of artifacts that are associated with different compression techniques. This thesis is concerned with block transform coding techniques of gray scale images, where there are three common types of artifacts, namely: *Blocking Distortion, Blurring, and Spatial Edge Noise (Ringing)*. This thesis is restricted only to the subset of these three types of artifacts.

1.3.1 Solving Mechanism

The problem of objectively evaluating the quality of compressed images can be handled in two steps:

1. by measuring number of primitives for each type of artifact.
2. by putting the measured primitives in an equation that emulate the MOS of subjective evaluation tests.

As mentioned in section 1.1 the HVS gives unequal weighting to different types of impairments. For example, subjective studies showed that blocking distortion is ten times more objectionable than equal energy white noise [18]. So in the first step, the developed method should isolate different types of artifacts from each other so they can be weighted differently in the second solution step.

In addition to the type of error, the context of error is a very important image quality factor: humans tend to realize degradations in flat areas (low frequency areas) more than in detailed areas (high frequency areas) [19]. So, the developed method should also check the context of each type of artifact.

Keeping in mind what will happen in the second problem solving step, sufficient data should be available by computing number of primitives that measure each type of artifact in in each artifact context. The output of this step is required to carry out the second step.

In the second problem solving step, all the necessary computed primitives for each type of artifact can be given different weights, depending on the weighting scheme of the HVS, then they should be put together in an equation that emulate. the MOS, where a single number is produced as an output that represent the quality of an image. This can be achieved by using statistical analysis techniques such as regression analysis.

In this thesis, only the first solving step is handled, while the second solving step is a big problem and beyond the subject of this thesis.

1.3.2 Evaluation

The results of the first problem solving step mentioned in section 1.3.1 can be evaluated and said to be good if:

1. they indicate that each type of artifact is isolated from the other types. Where the presence or the disappearance of a single artifact should not affect any primitive except its own.

2. by looking at the output of the context isolation process, the artifact's contexts should be seen to be separated.

3. the primitives of each type of artifact are monotonic with the compression ratio of its context. And the primitives should have one to one relation with

the perceptual presence of their corresponding type of artifact.

1.4 Thesis Summary

Objective assessment methods will eliminate the difficulties of the subjective assessment methods and will expand the field of image coding by leading to more systematic design of image coders. The development of an objective assessment method, that combines computational simplicity, and sensitivity to the properties of the human visual system, would be an important tool in the development of compression techniques.

In the past, there have been many attempts to predict image quality based on HVS. Chapter 2 summarizes some of these previous attempts in addition it summarizes the techniques used in subjective measurements.

Coded images usually have common types of artifacts such as blocking, blurring, and spatial edge noise. The detection and measurement of these artifacts are addressed by the Impairment Detection Method (IDM) in Chapter 3. Note that Chapter 3 represents our work.

Finally, Conclusions and further research are discussed in Chapter 4.

Chapter 2

Quality Measurement Techniques

2.1 Introduction

Although there is no standard objective image quality measure available, most researchers frequently use Mean Square Error (MSE) and Peak Signal to Noise Ratio (PSNR) because of their computational simplicity. From the literature [3, 7, 20, 22] and as it can be seen in section 1.2, MSE and PSNR do not correlate reasonably well with the subjective quality measurements.

The determination of a good objective quality scale for image coding is a difficult problem. In this chapter, subjective measurement techniques and some of the promising objective measures are illustrated briefly.

Subjective assessment methods are widely used to evaluate the picture quality of coded images [26]. As mentioned earlier, subjective methods depend on human observers to view and rate the quality of coded images. However, the subjective results fluctuate depending on the test conditions, and the assessment tests take considerable amount of time and money. Section 2.2 will discuss the subjective techniques.

Since human observers are the end users of images, an objective image quality measurement that is based on the human visual perception is more appropriate in

predicting and measuring images visual quality. Although the HVS is too complex, a number of experiments [13, 14, 19, 27, 28] with simplified HVS models showed that the inclusion of a model of the HVS generally produces results that are in better correlation with the perceived image quality. These trial models took into consideration various recognized characteristics of the HVS. They are however limited in validity and scope [7]. Ahumada, Null, and Hearty [29, 30] pointed out that the visual quality may have more than a single dimension. Taking that into consideration in designing a better HVS model will lead to a better quality measurement.

Graphical measures are multi-dimensional measures. Their final outputs are presented as graphical maps, histograms, plots, or charts. The interpretation of these graphical outputs determines type, location and amount of degradations. Section 2.3 will present the graphical quality measurement techniques.

On the other hand, numerical measures most of the time end up with a single number as their final output. Some of the numerical measures will be presented in this chapter, these measures are the work of Comes [31, 32], Algazi [15, 33, 34], and Wolf [35, 36, 37]. In all of them distortion factors are extracted based on the properties of the HVS. These factors are used later on in equations that simulate the Mean Opinion Score (MOS) of subjective measurements.

In Section 2.4, a quality measure based on a multiple channel HVS model will be illustrated, where Comes masked the invisible noise then used a weighted MSE of the visible noise to compute image quality.

Algazi, Kato, Miyahara, and Kotani introduced the Picture Quality Scale (PQS). In their method, they identified five different distortion factors. The first two factors refer to random errors with different weighting, the third factor refers to the end of block disturbances, and the last two factors measure the structured errors, such as spatial edge noise. The PQS will be illustrated in Section 2.5.

Section 2.6 will discuss the Impairment Quality Rating (IQR). The IQR is a

video quality assessment technique. Its formulation is based on a functional combination of distortion measures. These distortion measures combine two temporal measures and a spatial measure. The spatial distortion measure is based on the Sobel filter [5]. Since this thesis is limited to still images, only the spatial distortion measure and its enhancement will be discussed in Section 2.6. This measure represent the base of our work that will be presented in Chapter 3.

Finally, the conclusions will be discussed in Section 2.7.

2.2 Subjective Measurements

As the end user of images are humans, the most reliable image quality measure is the subjective rating by human observers [7]. Generally in subjective rating experiments, images and their perceptual errors are checked and rated by humans then the observers MOS is statistically calculated.

In such experiments, both expert and non-expert observers are used; non-experts represent the average viewer while experts give better assessments of image quality since they are familiar with images and their distortions. There are a certain viewing conditions that should be set before the evaluation is taking place [38]. Among them, viewing distance, viewing angle, monitor size, peak luminance of the screen, room lighting, and number of assessors. There are different evaluation techniques:

- *The absolute evaluation:* The observers view an image and assess its quality by assigning to it category in a given rating scale.
- *The comparative evaluation:* A set of images are ranked from best to worst by the observers.
- *Bubble sort evaluation:* The observer compares two images A and B from a group of images and determine their order. Assuming that the order is AB, the

observer takes a third image and compares it with B to establish the order ABC or ACB. If the order is ACB, then another comparison is made to determine the new order. The procedure continues until all the images have been used, allowing the best pictures to bubble to the top if no ties are accepted [3, 13].

The most commonly used technique is the first one. It uses the rating scale that has been accepted by the CCIR in recommendation 500 [26] and appeared in the relevant literature [3, 31, 33, 35]. Table 2.1 list this rating scale. The mean rating of a group of observers who join the evaluation is usually computed by [21]:

$$R = \frac{\left(\sum_{k=1}^{n} s_k n_k\right)}{\left(\sum_{k=1}^{n} n_k\right)} \tag{2.1}$$

where s_k=the score corresponding to the kth rating, n_k=the number of observers with that rating, and n=the number of grades in the scale.

It is important to note that the results of subjective rating are affected by a number of factors including

- type of images,
- level of expertise of the observers, and
- experimental conditions.

Note	*Impairments*	*Quality*
5	Imperceptible	Excellent
4	Perceptible, but not annoying	Good
3	Slightly annoying	Fair
2	Annoying	Poor
1	Very annoying	Bad

Table 2.1: Rating Scale Recommended by CCIR-500 for Subjective Evaluation

2.3 Graphical Measurement

Eskicioglu [39] claimed that scalar image quality measures are not able to describe either the degradation type or the local error in a compressed image. Graphical image quality measurement techniques are multi-dimensional measures. Unlike most image quality metrics, graphical techniques do not represent their outputs in numerical format. Instead, their outputs are presented in a graphical format such as maps, histograms, plots, or charts. Features showing type of impairments, location of impairments, or both are computed then plotted. The plots identifies type, location, and amount of errors.

The graphical measures that have general applicability in the field of image compression are [7]:

1. Visible Differences Predictor (VDP)
2. Histogram of the compression error
3. Hosaka plots
4. Eskicioglu charts

These measures are described briefly as follow:

- The Visible Differences Predictor (VDP) [40] consists of components for calibration of the input images, a HVS model, and a method for displaying the HVS predictions of the detectable differences as shown in Figure 2.1. The input of the algorithm includes two images (original and degraded), and parameters for viewing conditions and calibration such as viewing distance and physical pixel spacings. Input images are passed through a display model that should be supplied by the user. The HVS model used in the VDP has three main components that measures the variations in visual sensitivity as a function of light level, spatial frequency, and signal content. The output of VDP is a map

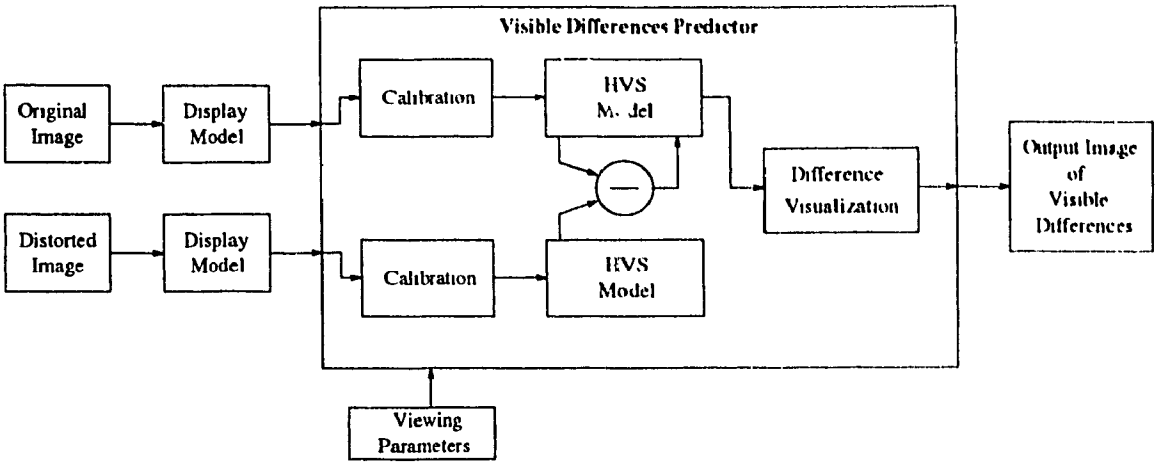

Figure 2.1: Block Diagram of the Visible Differences Predictor

of the probability of detecting the differences between the two images as a function of their location in images. The map indicates the shape and location of the predicted visual differences. Daly [40] claims that VDP can be used for all types of image distortions. A drawback to the VDP is that it is a very complex algorithm. Another drawback is that there are many experiments for an image with distortions, since there is essentially an experiment for each local artifact.

- A histogram of the compression error is constructed by plotting the number of times a specific value occurs in the difference image versus the value itself. Typically the histogram look like a Gaussian curve [7]; the more it resembles a spike at $x = 0$, the better the quality of the degraded image. Eskicioglu, Fisher, and Chen [21] found that histograms clearly represent the amount of degradation, but still they cannot express the type or the location of degradation.

- Hosaka started with the quadtree decomposition [3, 41] to segment the original image into certain activity regions. Five classes of blocks are formed with this decomposition; a smaller block size denotes a higher frequency region of the

image. There are two features computed for each class:

1. the average standard deviation of the blocks
2. the average mean of the blocks less the average mean of the classes

With the same segmentation, these features are also computed for the degraded image. The Hosaka plot [18] is constructed in polar coordinates after obtaining the absolute error for each class in the corresponding features. The absolute errors of the first feature are plotted in the left half plane while the absolute errors of the second feature are plotted in the right half plane, all equally spaced. These plots represent the error in its size and the type of distortion in its pattern. However, the use of these plots in specifying the major type of impairment is limited [42]. They can not properly describe the type of loss, i.e. the nature of error. They clearly display blocking artifact but not equally successful in showing blurring artifact when both of them are present in the same image [21]. Another drawback is that the selection of two critical parameters for the block size and the variance threshold is not trivial and depends on the compression ratio, compression technique, and the frequency contents of the impaired image [39].

- Eskicioglu [39] as in the case of Hosaka plots, divided the original and the degraded images into areas with certain activity levels using the quadtree decomposition [3, 41]. He used in his decomposition 4 classes of blocks, where the largest and the smallest block sizes are 16 and 2, respectively. Class i represents the collection of ixi blocks; a higher value if i denotes a lower frequency area of the image. After obtaining the quadtree decomposition of the image for a specified value of the variance threshold(20), three normalized values for each class i (i=2, 4, 8, 16), are computed:

  1. The number of pixels / the number of pixels of the entire image.

2. The number of distinct pixel values / the number of possible pixel values(256).

3. The average of the standard deviations in the blocks / a preset maximum standard deviation(8).

Then the essential characteristics of the original and the degraded images are graphed in the normalized bar charts. An evaluation of the type and amount of distortion that is affecting a degraded image can be made through a comparison between the bar chart of the original image and the degraded one. Eskicioglu claims that Eskicioglu charts specify and measure the blocking artifact since blockiness leads to a drastic change in average standard deviations, the number of distinct pixel values, and the number of pixels in the classes. A drawback is that this technique can not distinguish between blurriness or blockiness since both blockiness and blurriness leads to a change in average standard deviations, the number of distinct pixel values, and the number of pixels in the classes.

In a recent paper by Eskicioglu [23], he added one more dimension to the Eskicioglu charts. The fourth dimension is associated with the end of block disturbances, these are discontinuities at block borders. The disturbance of a block of size M×N is measured by *EOBD* [23],

$$EOBD = \{E[\Delta f(m, N)] + E[\Delta f(M, n)]\}^{1/2} \tag{2.2}$$

with

$$\Delta f(m, N) = [f(m, N) - f(m, N + 1)]^2 \tag{2.3}$$

and

$$\Delta f(M, n) = [f(M, n) - f(M + 1, n)]^2 \tag{2.4}$$

where $f(m, n)$ denotes a pixel value and $E[\ ]$ is the expectation operator. This definition is modified for the blocks located along the bottom or right side of an image by omission of an expectation term. EOBD is not defined for the bottom

right side corner block. The fourth feature for each class is then given by the average of the end of block disturbances normalized by a preset maximum disturbance. A drawback to this fourth dimension of Eskicioglu charts is that it is affected by both blocking and blurring artifacts. i.e. for a degraded image that is affected by blockiness and blurriness, the fourth dimension of Eskicioglu charts will measure both artifact together and can not distinguish between them.

2.4 Measurements Based on a Multiple Channel HVS model

According to the psychovisual model of tuned channels the visual information is received inside the human eye through perceptual channels which perform a decomposition with respect to the location in the visual field, the orientation and the spatial frequency of the stimuli [32]. Each perceptual channel is characterized by its own visibility threshold. For a perceptual channel, the threshold depends on the contents of the background image in the corresponding tuned channel. This phenomenon is called *masking*. The visibility of a noise pattern that has been generated by a coding technique depends on the type of the background (i.e if it is uniform or texture).

The psychovisual model of tuned channels has been used previously in many image quality techniques [31, 43, 44]. Comes, Bruydonckx, and Macq [32] used the *masking* phenomenon to develop an image quality criterion that utilizes the unmasked MSE in an equation that simulates the CCIR-500 [26] five-grade quality scale shown in Table 2.1.

The contrast is defined as a representation to the dynamic range of luminance in a region of an image. The definition of the contrast C that will be used is [31]:

$$C = \frac{L_{max} - L_{min}}{2L_{moy}} \tag{2.5}$$

where L_{max}, L_{min}, and L_{moy} are respectively the maximum, the minimum, and the mean luminance values in an area. The visibility threshold C_T is the contrast value corresponds to the limit of visibility. Comes, Bruydonckx, and Macq [32] assumed a logarithmic relationship between the visibility threshold C_T and the contrast value of the background C_M for a given perceptual channel, as shown in Figure 2.2 where C_{T0} is the visibility threshold without masking. The shaded area in the figure is below the visibility threshold and represents the invisible error. When $C_M = 0$ (i.e there is no background) in the channel, the visibility is determined by the band-pass filtering effect of the eye. As the background contrast C_M increases, the detection threshold C_T increases following a slope ϵ.

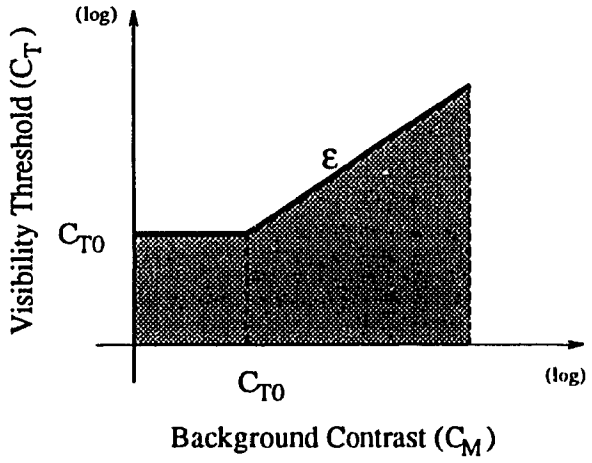

Figure 2.2: Masking Model: logarithmic relation between the visibility threshold C_T and the background contrast C_M

Comes, Bruydonckx, and Macq [32] evaluated the parameters of the masking model assuming that the slope ϵ is equal for all perceptual channels and the detection threshold without masking C_{T0} only depends on the spatial frequency.

2.4.1 Image Quality Criterion

In order to evaluate the quality of a noisy image a knowledge of the noise level is necessary. From the previous subsection, only part of that noise is visible thus

affecting the visual quality of the image. This criterion evaluates image quality after the cancellation of the masked noise defined as *invisible noise*. A *perceptual component* is defined as each pixel in the image. The masked noise is a set of noise perceptual components whom contrast belongs to the shaded area of Figure 2.2.

The noise and the original image are split up into several perceptual channels by means of multi-resolution filters bank performing a polar decomposition with perfect reconstruction. In each perceptual channel, each noise perceptual component is compared to both the contrast of the corresponding perceptual component in the original image and the visibility threshold without masking. The visibility threshold without masking is considered as a constant in a given perceptual channel. The noise perceptual component for a given channel is removed if its contrast belongs to the shaded area of Figure 2.2. Then the unmasked noise is reconstructed with the remaining perceptual channels. The mean square error P_B of the remaining noise is given by [32]:

$$P_B = \frac{1}{MN} \sum_{m=1}^{M} \sum_{n=1}^{N} B^2(m,n) \tag{2.6}$$

where $B(m,n)$ represents the value of the unmasked noise at the location (m,n) of the M×N image.

Two approaches have to be followed to estimate the image quality using P_B:

- *First:* measuring the *PSNR* considering P_B as the power of the noise. The *Masked-PSNR (MPSNR)* is defined as [32]:

$$MPSNR = \frac{(255)^2}{P_B} \tag{2.7}$$

- *Second:* The *quality factor* Q is a measure on the five-grade quality scale recommended by the CCIR 500 [26] and shown in Table 2.1. Q is given by [32]:

$$Q = \frac{5}{1 + KP_B} \tag{2.8}$$

where K is a normalization factor to have Q between 1 and 5.

This method is adequate only when used to compare two noisy versions of an image but not as an absolute criterion. A drawback for this criterion is that the determination of ϵ is experimental and difficult. Another drawback is that this method is not capable of determining the nature of errors.

2.5 Picture Quality Scale Method

Arguing that subjective quality evaluations are based on a number of impairments that can be observed in a degraded image, several years ago Miyahara [45] drew an outline for an objective quality measure called *Picture Quality Scale* (PQS). Later on Algazi, Kato, Miyahara, and Kotani [15, 33] developed the Picture Quality Scale. PQS is an objective approximation of the MOS. It consists of a linear combination of measurable distortion factors F_i, i=1,...,5 that are objectively quantified. These distortion factors which are perceptually weighted measures of image impairments, are function of e(m,n), where e(m,n) is the coding error or the difference between an original and a degraded images.

To provide a more uniform perceptual scale for e(m,n), an original image $P(m,n)$ is transformed by a logarithmic transformation so that [33]

$$x(m,n) = k \log \frac{P(m,n)}{k_o} \tag{2.9}$$

where k and k_o are constants, and [33]

$$e(m,n) = x(m,n) - \hat{x}(m,n) \tag{2.10}$$

where $\hat{x}$(m,n) is a degraded version of x(m,n). A spatial frequency response is modeled approximately by [15]:

$$R(u,v) = S(f)O(\theta,f) \tag{2.11}$$

where S(f) is the spatial frequency response and O(θ,f) accounts for the anisotropy

of vision [15, 46]. S(f) is approximated by [15]:

$$S(f) = 1.5 \exp \frac{(-\sigma 2w^2)}{2} - \exp(-2\sigma^2 w^2) \tag{2.12}$$

$$\sigma = 2, \quad w = \frac{2\pi f}{60}, \quad f = (u^2 + v^2)^{1/2} \tag{2.13}$$

where $u = f\cos\theta, v = f\sin\theta$ are horizontal and vertical spatial frequency respectively and σ^2 is the variance of the Gaussian function.

The distortion factors F_i are defined as numerical functions of e_w(m,n), where e_w(m,n) is the frequency weighted error. e_w(m,n) is obtained by transforming e(m,n) to the spatial frequency domain using the Fast Fourier Transform, then weighting the output of the transform by visual spatial frequency characteristics, at last, the weighted output is transformed to the spatial domain using the inverse Fourier Transform [46]. e_w(m,n) is given by [45]:

$$e_w(m,n) = F^{-1}[F\{e(m,n)\}R(u,v)] \tag{2.14}$$

where F and F^{-1} are the Fourier Transform and its inverse respectively. The frequency weighted error e_w(m,n) is evaluated at each pixel using equation 2.14. Miyahara, Kotani, and Algazi [33] defined five factors as follow:

- F_1 is the weighted mean square error. It represents the random error and is given by:

$$F_1 = \frac{\sum_m \sum_n [e_v(m,n)]^2}{\sum_m \sum_n [P(m,n)]^2} \tag{2.15}$$

  where $e_v(m,n)$ is weighted by the common television noise weighting [15].

- F_2 is a modified version of F_1. It takes into account the threshold of perception of disturbances and is given by:

$$F_2 = \frac{\sum_m \sum_n [e_w(m,n)]^2 T}{\sum_m \sum_n [P(m,n)]^2} \tag{2.16}$$

  where T is a zero-one indicator function for a perceptual threshold of visibility.

- F_3 represents the end of block disturbances which appear in block coders such as transform coder and vector quantization coder. These disturbances are a function of the error discontinuities.

$$F_3 = \{E[\Delta e_w(n, N)] + E[\Delta e_w(M, n)]\}^{1/2} \tag{2.17}$$

with

$$\Delta e_w(n, N) \triangleq [\Delta e_w(m, N) - \Delta e_w(m, N + 1)]^2 \tag{2.18}$$

$$\Delta e_w(M, n) \triangleq [\Delta e_w(M, n) - \Delta e_w(M + 1, n)]^2 \tag{2.19}$$

where M and N are the height and the width of the block respectively and $E[]$ is the expectation operator.

- F_4 represents the general correlation errors. It is given by:

$$F_4 = (R_x^2 + R_y^2)^{1/2} \tag{2.20}$$

where R_x and R_y measure the correlation of errors horizontally and vertically. F_4 is zero if errors are uncorrelated.

- F_5 represents the random error in the vicinity of high contrast image distortions. This factor takes into account the masking effect and is given by:

$$F_5 \triangleq (e_x^2 + e_y^2)^{1/2} \tag{2.21}$$

with

$$e_x = \sum_{p}^{P} \sum_{q}^{Q} \sum_{j=1}^{l} |e_w(p, q - j) M_x(p, q - j)| \tag{2.22}$$

and

$$e_y = \sum_{p}^{P} \sum_{q}^{Q} \sum_{j=1}^{l} |e_w(p, q - j) M_y(p, q - j)| \tag{2.23}$$

where M_x(r,s) and M_y(r,s) are the horizontal and vertical masking functions, taken to be exponential functions of the first differences of the pixels values, that are a measure of image activity. The summation is carried out locally over $2\ l$ pixels and that depends on the viewing distance.

Then Miyahara, Kotani, and Algazi [33] carried out a principal component analysis [45] to quantify the correlation between $F_1, \ldots, F_5$. The largest three eigenvalues of the resulting covariance matrix, which account for 98% of the total error energy, provide a first transformation of the F_i into an effective principal component representative(Z_1,Z_2,Z_3).

Finally, The Picture Quality Scale is a linear combination of the principal components $\{Z_i\}$ so that [33]

$$PQS = b_o + \sum_{j=1}^{3} b_j Z_j \tag{2.24}$$

where b_i are the partial regression coefficients that should be obtained by multiple regression analysis between Equation(2.24) and the MOS.

In a recent paper [34], Algazi, Ohira, Kotani, and Miyahara found that for a high quality image with MOS ≥ 4, only F_4 and F_5 distortion factors are contributing significantly to PQS. So, F_1, F_2, and F_3 can be neglected and PQS can be computed as follow [34]:

$$PQS = 5.435 - 0.654F_4 - 0.0985F_5 \tag{2.25}$$

where the equation can not hold as the error and distortion factors reach zero. However, they found that the regression formula may be usable up to PQS = 4.5, level at which distortions are no longer perceptible.

A drawback to PQS is that the evaluation of the frequency weighted error which is a very basic function in this method, is a very complex process. The main complexity comes from the evaluation of the anisotropy of vision $O(\theta, f)$ where it is not trivial.

2.6 Impairment Quality Rating

The Impairment Quality Rating (IQR) predicts the subjective quality ratings for pairs of degraded versus original real-video sequences. This method produces a

rating on the CCIR-500 [26] five-grade impairment scale shown in Table 2.1. A feature is defined as a quantity of information associated with a specified image. IQR is a linear combination of three features. The first feature measures the spatial distortion while the other two features measure the temporal distortion. Only the first feature and its enhancement are discussed in this section since the subject of this thesis is limited to still images. The output of IQR is a single number that simulates the MOS of subjective tests.

In early work done by Wolf, Pison, Jones, and Webster [36] and work done by Webster, Jones, Pison, Voran, Wolf [35], Sobel filters [5] are used to generate Spatial Features (SF). The sobel filter is a common edge detection FIR filter. It has two 3×3 operators $S_h(x,y)$ and $S_v(x,y)$ shown in Table 2.2. The output of the horizontal filter for a pixel $P(x,y)$, denoted by $S_h(x,y)$, is obtained by centering the 3×3 horizontal filter over the pixel $P(x,y)$, multiplying the filter coefficients by the neighboring pixel values, and adding the nine values together. This is expressed mathematically as

$$\begin{aligned} S_h(x,y) &= P(x-1,y+1) - P(x-1,y-1) + 2 * P(x,y+1) - 2 * P(x,y-1) + \\ &\quad P(x+1,y+1) - P(x+1,y-1) \end{aligned}$$

Similarly the output of the vertical filter for a pixel $P(x,y)$, denoted by $S_v(x,y)$, is calculated as

$$\begin{aligned} S_v(x,y) &= P(x+1,y-1) - P(x-1,y-1) + 2 * P(x+1,y) - 2 * P(x-1,y) + \\ &\quad P(x+1,y+1) - P(x-1,y+1) \end{aligned}$$

The magnitude of the sobel filter for pixel $P(x,y)$, denoted by $S_m(x,y)$, is defined as the square root of the sum of the squares of the horizontal and vertical sobel filter operators outputs for that pixel, i.e.

$$S_m(x,y) = \sqrt{[S_h(x,y)]^2 + [S_v(x,y)]^2} \tag{2.26}$$

-1	-2	-1
0	0	0
1	2	1

-1	0	1
-2	0	2
-1	0	1

Table 2.2: Sobel Operators $S_h(x,y)$ and $S_v(x,y)$

If Y_o and Y_d are the luminance of the original and the degraded images respectively. SF is given by [35]:

$$SF_o = STD_{space}\{S_m[Y_o]\} \tag{2.27}$$

and

$$SF_d = STD_{space}\{S_m[Y_d]\} \tag{2.28}$$

where SF_o and SF_d are the Spatial Features of the original and degraded image respectively, STD_{space} is the standard deviation operator over the horizontal and vertical spatial dimensions of an image.

A parameter is defined as the result of comparison between two features. SF is used to calculate a single parameter P_7 that measures both blurring and blocking artifacts [35]. This parameter is defined as [35]:

$$P_7 = \frac{SF_o - SF_d}{SF_o} \tag{2.29}$$

If P_7 is positive, there is less spatial information in the degraded than the original image. This condition results from impairments such as blurring. While if P_7 is negative, there is more spatial information in the degraded than the original image. This condition results from impairments such as blocking.

In IQR [36], P_7 is used as a measure of the spatial distortion where it is combined with another two temporal impairment features TF_1 and TF_2. The equation

of IQR is of the form [35]:

$$IQR \approx c_o - c_1 \times [RMS_{time}(5.81\,|P_7|)] - c_2 \times TF_1 - c_3 \times TF_2 \tag{2.30}$$

where RMS_{time} denotes the root mean square time-collapsing function, and c_i are weighting coefficients that should be determined to give the best fit to subjective test results using a least squares error criterion. A drawback to the spatial feature of IQR is that it can not determine the nature of error if both blocking and blurring artifacts are present in a degraded image.

The Melcher and Wolf's Method [37] specifically detects the "blocking" artifact produced by digital coding systems. It is an extension to the spatial feature of IQR to overcome the weakness of inability to distinguish between blocking and blurring artifacts when both are present in a degraded image. Melcher and Wolf used features based on the sobel filtered image for measuring spatial distortions. If f is an image, SI_h and SI_v are the outputs of the horizontal and the vertical sobel filter respectively. For a function f located at (h,v), the sobel filtering is done by finding the gradient vector:

$$\vec{\nabla} f = \begin{bmatrix} SI_h \\ SI_v \end{bmatrix} = \begin{bmatrix} \partial f/\partial h \\ \partial f/\partial v \end{bmatrix} \tag{2.31}$$

Where h and v are the horizontal and vertical directions, respectively. An approximation of the magnitude of the gradient vector is used to characterize the edge content of an image:

$$\nabla \approx |SI_h| + |SI_v| \tag{2.32}$$

The direction of the gradient vector is also an important quantity. The direction of the gradient vector f at (h,v) is given by:

$$\theta(h,v) = \arctan\left(\frac{SI_v}{SI_h}\right) \tag{2.33}$$

A feature that takes advantage of the angle information that is present in the gradient image is used in order to detect blocking artifact.

2.6.1 Gradient Magnitude and Angle Histogram

A 2-dimensional histogram can be accumulated while computing the gradient image. A bin is defined as a histogram pixel. Each bin in the histogram is identified by an h and v coordinate. For a pixel $P(h, v)$ in an image, the two components (SI_h,SI_v) of the gradient are computed. Then SI_h and SI_v are used as coordinates to identify a bin in the histogram. The bin at (SI_h,SI_v) is incremented. This process is repeated for all the pixels of an image. The histogram can be displayed as a normal X-Y plot. By assigning a different level of intensity for each range of bin values in the histograms, Figures 2.3, 2.4 show an example image and its gradient magnitude and angle histogram respectively. Lighter pixels in the histograms show bins with higher values.

Melcher and Wolf [37] defined a function SIH(r,θ) as the number of pixels in the gradient image whose gradient radius and angle are r and θ respectively, where in all equations, θ is assumed to be between 0 and 2π. Features that detect the presence of the blocking and blurring artifacts are extracted from SIH(r,θ) as will be illustrated in section 2.6.2.

2.6.2 Features Extracted from SIH(r,θ)

Blocking distortion tends to increase the value of SIH(r,θ) when θ lies along one of the principal axes (e.g. where $\theta = k\pi/2, k = 0, 1, 2, 3$). Melcher and Wolf [37] found that blocking produces a "plus-like" shape in the computed histogram, which shows that more points are gathered at the principal axes. An example is shown by introducing the blocking artifact to the image of Figure 2.3 as shown in Figure 2.5, then plotting their gradient magnitude and angle histograms as shown in Figures 2.4 and 2.6. This observation is very important for the development of the features below.

A feature whose value increases as the sharpness of horizontal and vertical

Figure 2.3: Original 512 × 512 Pepper

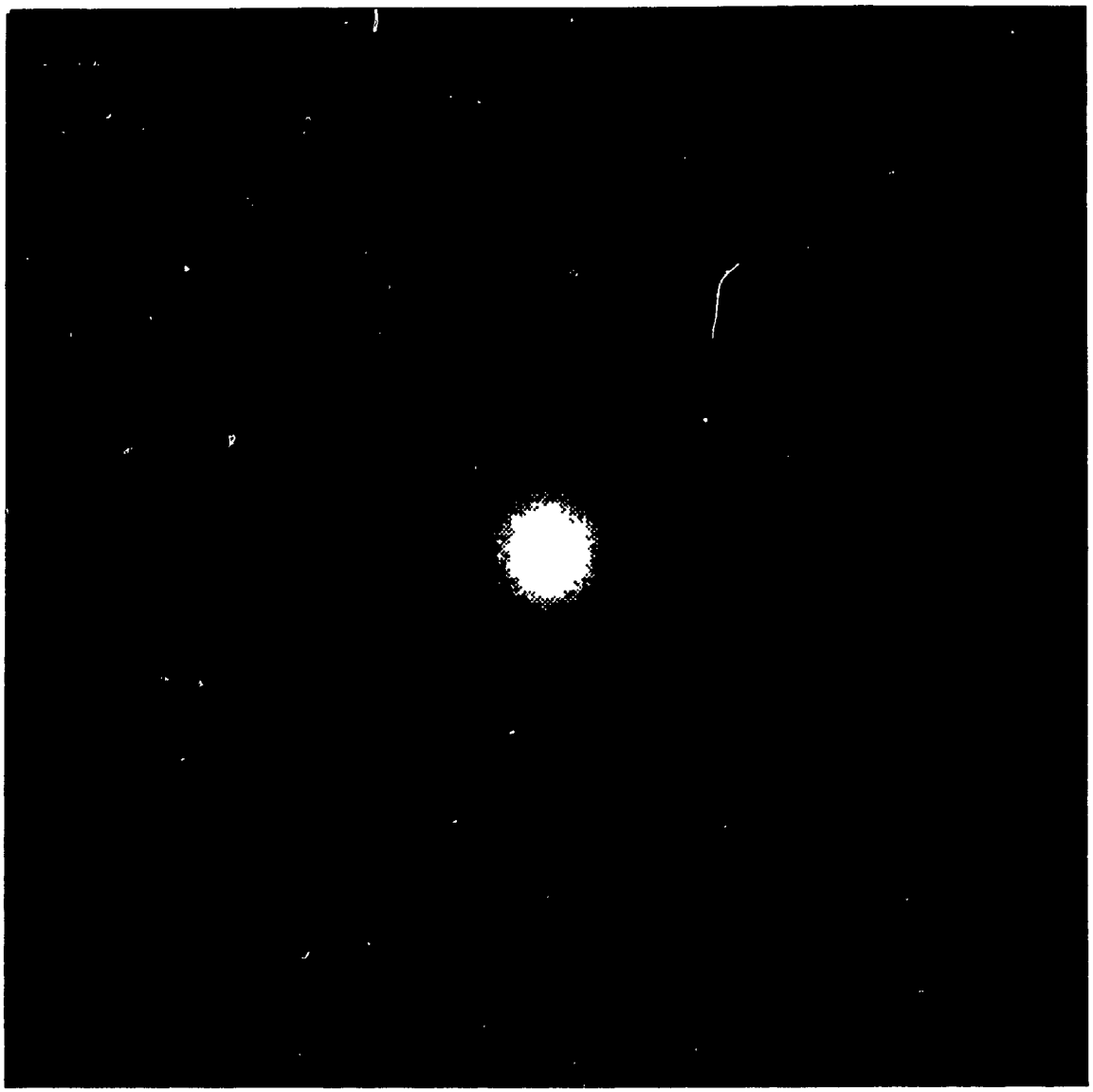

Figure 2.4: SIH(r,θ) of Original Pepper

Figure 2.5: Image Compressed Using PVRG JPEG CODEC at q = 100 compression ratio of 53:1

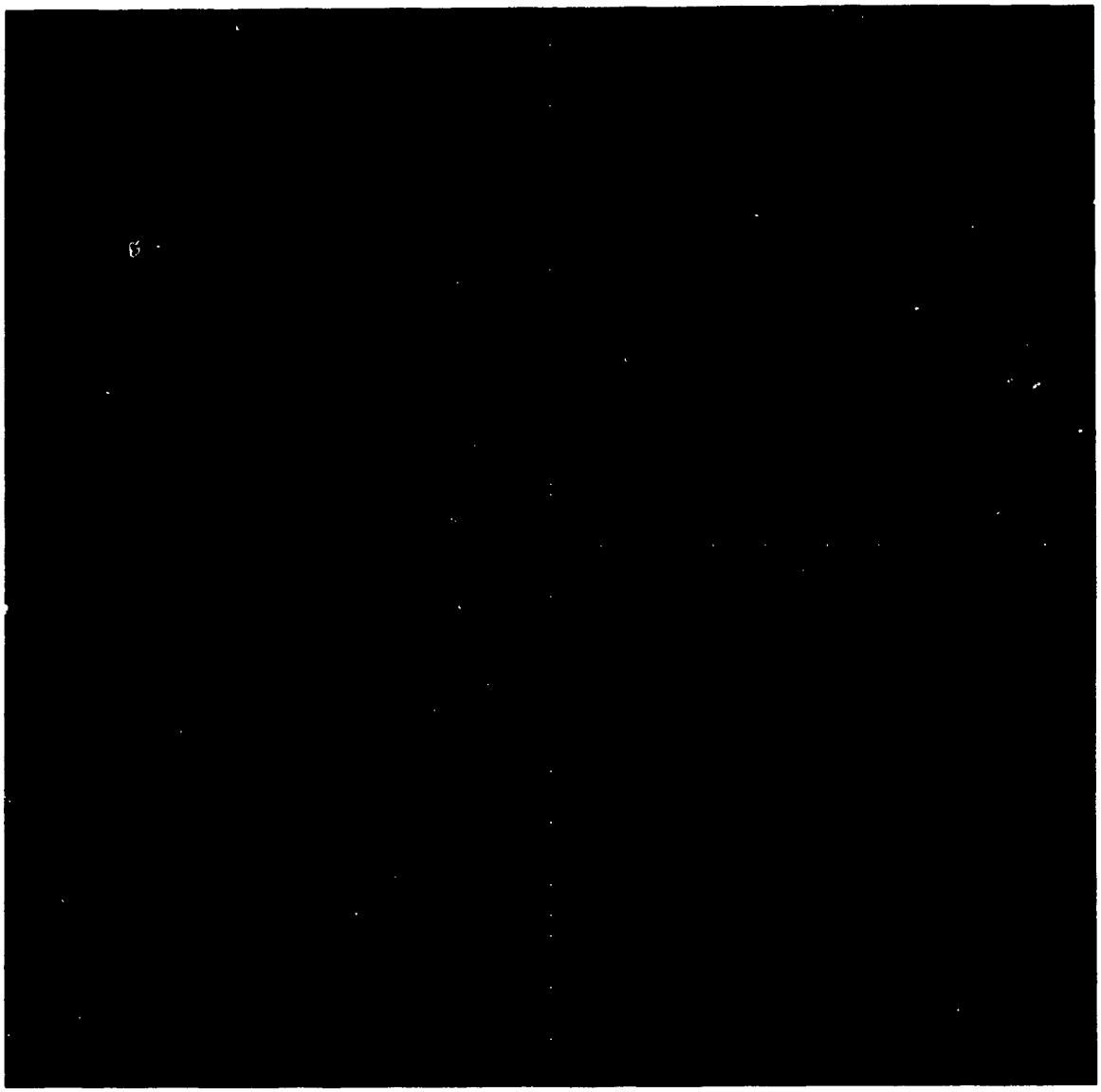

Figure 2.6: SIH(r,θ) of the Degraded Pepper

edges increase is given as [37]:

$$g_{hv} = \frac{1}{p} \cdot \sum_{r} \sum_{\theta} SIH(r, \theta) \cdot r \tag{2.34}$$

$$0 < c_a \leq r \leq c_b \quad \theta = \frac{k\pi}{2} (k = 0, 1, 2, 3)$$

where r and θ are as defined previously, c_a and c_b are clipping limits, and p is the number of pixels in the image. This feature is a weighted sum of the bins that accumulate horizontal and vertical edges in the gradient image.The lower clipping limit is used to restrict the computation to an area where the approximations of angle are more accurate. The higher clipping limit is used to include only the edges of a desired intensity to the measurement.

Melcher and Wolf [37] mentioned that practically, it is useful to include a small wedge of a few degrees around the SIH(r,θ) horizontal and vertical axes. This will be discussed later on in Chapter 3.

The g_{hv} feature characterizes all of the horizontal and vertical edges in an image, natural as well as those produced by blocking artifact. This feature is affected by blurring and blocking, its value decreases when the image get blurred and increases when the image suffers from blocking.

Another feature $g_{hv'}$ is given as [37]:

$$g_{hv'} = \frac{1}{p} \cdot \sum_{r} \sum_{\theta} SIH(r, \theta) \cdot r \tag{2.35}$$

$$0 < c_a \leq r \leq c_b \quad \theta \neq \frac{k\pi}{2} (k = 0, 1, 2, 3)$$

where r, θ, c_a, c_b, and p are as defined previously. $g_{hv'}$ characterizes all edges except the horizontal and vertical ones. This gives it the ability to separate blurring from blocking. In the next section, the extracted features are combined into parameters that measure the amount of distortion.

2.6.3 Combining the Features into Parameters

Two basic features have been described that can be used to characterize the horizontal and vertical edge content of an image (g_{hv}) and the non-horizontal and vertical edge content ($g_{hv'}$). Melcher and Wolf [37] claimed that these features alone can not be used to measure the amount of blocking in an image. The features must be computed for an original and its degraded images then compared in order to detect the presence of blocking in the degraded image.

In order to compare the original and the degraded images, the features are combined into a parameter using the form:

$$P = \frac{d - o}{o} \tag{2.36}$$

Where o denotes the feature computed from the original image, and d is the feature computed from the degraded image. The resulting value is called a parameter. In this case the parameter measures the fractional difference between the original and the degraded features.

Two parameters are used for detecting blocking and blurring artifacts. These parameters can be computed from the above defined features [37]:

$$P_{hv2} = \frac{g_{hvd} - g_{hvo}}{g_{hvo}} \qquad P_{hv2'} = \frac{g_{hv'd} - g_{hv'o}}{g_{hv'o}} \tag{2.37}$$

These two parameters separately measure the fractional change in horizontal and vertical edges and non-horizontal and vertical edges, respectively. If an image is blurred and no extra edges are added to it, the values of these parameters will decrease by roughly the same fraction, showing a global reduction in the edge contents of the degraded image. However, if an image is blurred and has extra horizontal and vertical edges added in the form of blocking, $P_{hv2'}$ will not be affected by the added horizontal and vertical edges and will remain the same as in the first case, while P_{hv2} will increase by some amount that is proportional to the amount of the edge energy added by the blocking artifact.

Another parameter P_{hv4} can be calculated, which represent the difference between P_{hv2} and $P_{hv2'}$ parameters [37]:

$$P_{hv4} = P_{hv2} - P_{hv2'} \tag{2.38}$$

This parameter detects the relative change in horizontal and vertical edges *vs.* non-horizontal and vertical edges. The idea is that if some global degradation has affected the image, P_{hv2} and $P_{hv2'}$ parameters will track and will change by the same fraction resulting in P_{hv4} taking on a value close to zero.

However, if the non-horizontal and vertical edge parameter ($P_{hv2'}$) stays constant, and the horizontal and vertical edge parameter (P_{hv2}) increases due to the addition of some extra horizontal and vertical edges to the degraded image in a form of blocking. Hence, P_{hv4} tends to increase as the amount of blocking increases in the degraded image. A drawback to the added extension of IQR is that it does not locate the errors in degraded images. Another drawback is that while the spatial edge noise contributes to both g_{hv} and g_{nhv}, IQR analyzes the spatial edge noise contributions as a part of the blocking and blurring artifact measurements.

2.7 Conclusions

In this chapter, some image quality measurement techniques are presented. First, the subjective measurement techniques are presented. These techniques are done by humans. Although they are the most reliable quality measures, they are costly, time consuming, and depend on the test conditions. Second, some of the promising objective measures are presented; graphical measures, and numerical measures. Graphical measures presents their outputs in graphical formats such as maps, histograms, plots, or charts. On the other hand, most of the time numerical measures presents their outputs as a single number. The numerical measures that are presented in this chapter are: Measurement based on a multiple channel HVS model, Picture Quality Scale, and Impairment Quality Rating. These numerical measures compute different

distortion factors, but similarly all of them utilize these factors in equations that simulates the MOS of subjective tests. Tables 2.3 and 2.4 summarizes the performance of all the image quality measures introduced in this chapter.

Impairment Quality Rating represents the base of our newly developed Impairments Detection Method which will be illustrated in Chapter 3.

Quality Measures	*Capability of Determining Degradations*		
	Type	*Area*	*Amount*
Subjective	All	Yes	Yes
VDP	All	Yes	Yes
Error Histograms	No	No	Yes
Hosaka Plots	Blocking	Yes	Yes
Eskicioglu Charts	Blocking	Yes	Yes
IQ Criterion	No	No	Yes
PQS	• Blocking • Blurring	No	Yes
IQR	• Blocking • Blurring	No	Yes

Table 2.3: Summary of the Capabilities of the Introduced Image Quality Measures

Quality Measures	*Output Format*	*Measurement Type*
Subjective	Numerical	• Absolute • Relative
VDP	Graphical	Relative
Error Histograms	Graphical	Relative
Hosaka Plots	Graphical	Relative
Eskicioglu Charts	Graphical	Relative
IQ Criterion	Numerical	Relative
PQS	Numerical	Relative
IQR	Numerical	Relative

Table 2.4: Summary of the Output Format and the Measurement Type of the Introduced Image Quality Measures

Chapter 3

Impairments Detection Method

3.1 Introduction

This thesis is dealing with digital images. As discussed in Chapter 1, image compression techniques are used to minimize the cost of storage and transmission of digital images. Unfortunately, such techniques result in impaired reconstructed images. The determination of a good objective quality scale that measures the perceptual impairments in reconstructed images is a difficult problem. In Chapter 2, some promising objective quality measurement methods described in the literature are presented. All of those methods were based on properties of the HVS. In this chapter, the Impairments Detection Method (IDM) is introduced. It is a new objective image quality measure that detects, locates, and measures three common perceptual impairments in reconstructed images based on properties of the HVS.

The HVS is more sensitive to low spatial frequencies [46]. Human observers tend to notice degradation in flat areas (low frequency areas) more than degradation in detailed areas (high frequency areas). In addition, each type of impairment occurs in an a priori known location in a reconstructed image. For example, blocking artifact occurs near block boundaries and ringing artifact occurs near sharp edges. To take advantage of the sensitivity of the HVS to low frequencies and the a priori

known locations of impairments, it is felt that an image should be classified into different regions; flat region, texture region, and sharp edge region. These classification regions are chosen based on the location of occurrence of each type of impairment and based on the location where an impairment is most perceivable by the human observers. For example, the blocking artifact is most perceivable by the human eye in flat regions where there is no activities in the background, and can be hidden in texture region because of the background activities. Another example is the ringing artifact where it can be seen near sharp edges with flat background and it is hidden in texture regions, while the blurring artifact can be seen in sharp edges and texture regions and only for the severe case it can be seen in flat region.

From previous chapter, Melcher and Wolf [37] proposed a new technique for detecting the blocking artifact. In their technique, every pixel in the image is analyzed for measuring blocking and blurring artifacts.

The IDM introduced here is a relative objective measure where original and degraded images are required. It is a modified and extended version of Melcher and Wolf's blocking artifact detection technique [37]. While Melcher and Wolf's technique addresses the problem of detecting blocking artifact, IDM addresses the problem of detecting and measuring three types of impairments that are associated with block transform coding techniques; **Blocking, Blurring,** and **Spatial Edge Noise (Ringing)**. Figure 3.1 shows a block diagram of IDM. The concept behind IDM is centered around the idea of classifying the image into different areas: **Flat Region, Texture Region,** and **Sharp Edge Region.**

- *First:* Since this thesis is dealing with block transform coding techniques where an image is divided into 8×8 blocks, an original image is divided by IDM into 8×8 blocks. Then these blocks are classified into three categories:

  1. Flat Blocks, where Blocking artifact and severe Blurring are more visible.
  2. Sharp Edge Blocks, where Blurring, and Spatial Edge Noise artifacts can

be detected.

3. Texture Blocks, where Blurring artifact can be detected.

where the locations of the blocks of each category are used to categorize the blocks of a degraded image. In section 3.2, the five steps involved in the 8×8 block classification process are illustrated; edge block detector, edge connectivity test, edge contour measurement, edge continuity test, and edge extraction. Edge extraction facilitates the detection of ringing artifact by classifying the sharp edge blocks pixels into background pixels and sharp edge pixels.

- *Second:* Due to the fact that the blocking artifact occurs only at block boundaries, each block is divided into:

  1. Block Frame, where blocking artifact can be detected.
  2. Block Interior, where blurring, and spatial edge noise artifacts can be detected.

In section 3.3, the amount of horizontal and vertical edges (g_{hv}) and the amount of non-horizontal and vertical edges (g_{nhv}) of each category are computed using histograms of the magnitude and angle of image gradient. The construction of these histograms are illustrated in the same section.

g_{hv} and g_{nhv} of each class are used in parameters that detect and measure the presence of artifacts of interest. Section 3.4 illustrates how each type of impairment utilizes certain class parameters for its measurement.

Finally, Lena and PVRG-JPEG CODEC [25] are used in the simulation of IDM. The simulation results are shown and discussed in Section 3.5 and conclusions are presented in Section 3.6.

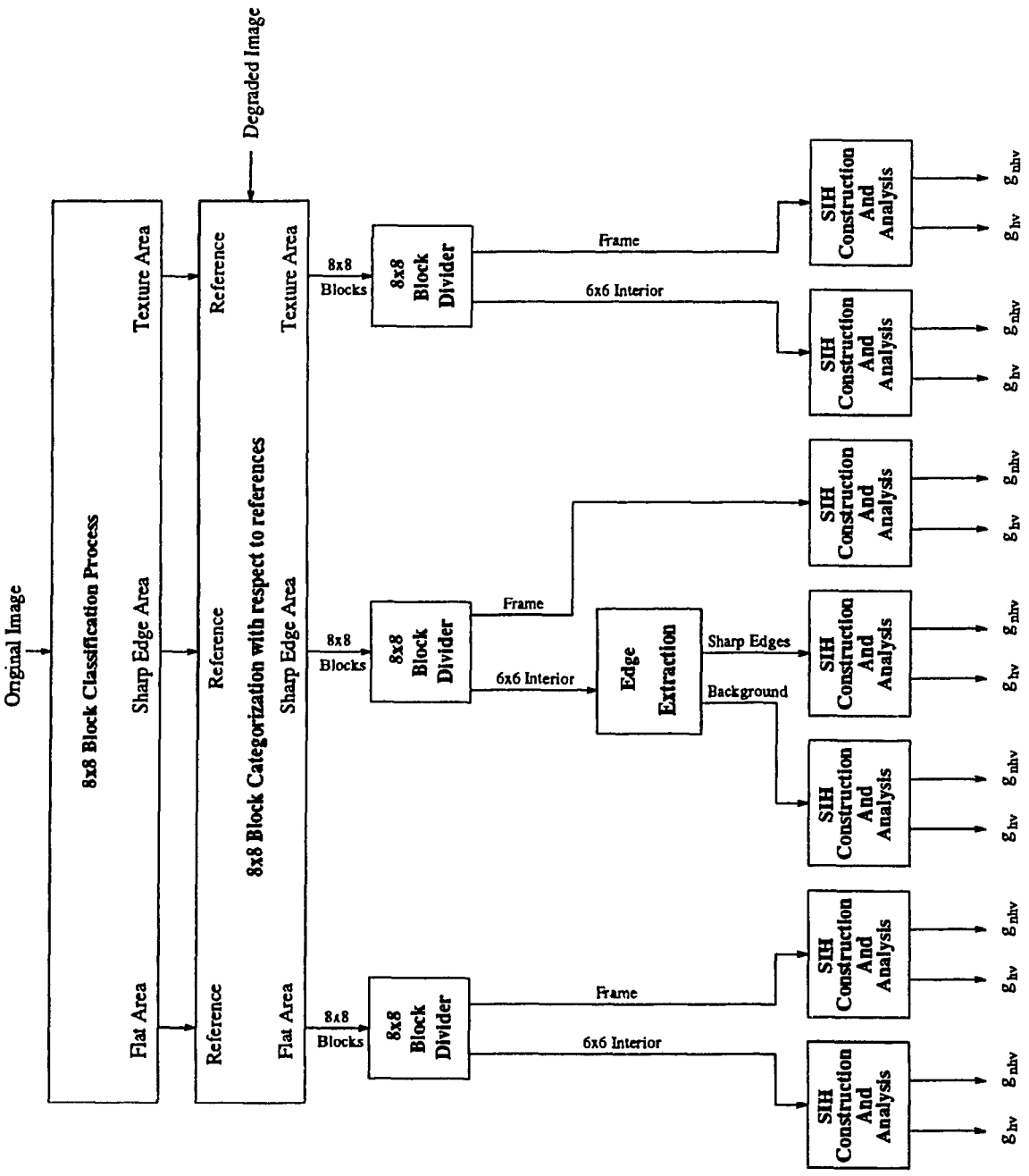

Figure 3.1: IDM Block Diagram

3.2 Block Classification

According to psychophysics of vision [46], an impairment is weighted distinctly by human observers depending on its place of occurrence within the same image. An example is shown in Figure 3.2 where the original Lena of Figure 1.3 is compressed using PVRG-JPEG CODEC [25] with -q = 100 (compression ratio of 18:1), where -q is defined previously in section 1.2. Although the whole image suffers from blocking artifact, it can be seen only across the low frequency area of the image. Figure 3.3 shows another example where the original Lena of Figure 1.3 is passed through 3×3 *neighborhood averaging* low pass filter [5] shown in table 3.1. In Figure 3.3, blurring can be noticed by looking at the high frequency area (i.e sharp edges and texture). Therefore, an image should be pre-classified into different regions before any analysis is done.

In the block classification process, the 8×8 blocks of an image are classified into three main categories: Flat Blocks, Texture Blocks, and Sharp Edge Blocks based on the gradient image.

The gradient image is constructed by computing $S_h(x,y)$ and $S_v(x,y)$ which are defined in Section 2.6, for each pixel $P(x,y)$ of an original image using the two Sobel filter operators shown in Table 2.2. Figure 3.4 shows the magnitude of the sobel filtered Lena of Figure 1.3.

$$\frac{1}{9} \times \begin{array}{|c|c|c|} \hline 1 & 1 & 1 \\ \hline 1 & 1 & 1 \\ \hline 1 & 1 & 1 \\ \hline \end{array}$$

Table 3.1: 3×3 Neighborhood Averaging Low Pass Filter

Figure 3.2: Compressed Lena using PVRG-JPEG CODEC at q=100 compression ratio of 18:1

Figure 3.3. Blurred Lena

Figure 3.4: The Magnitude of the Sobel Filtered Lena

By taking a certain luminance threshold T_l over the sobel filtered image ($T_l = 80$ in this case), the 8×8 blocks of an image can be classified into two categories:

- *First:* Flat Blocks (low frequency blocks).
- *Second:* High Frequency Blocks.

Figures 3.5 and 3.6 show the result of the first stage of classification.

Using the Edge Block Detection Technique of Section 3.2.1, High Frequency Blocks are reclassified into two categories:

1. Sharp Edge Blocks.
2. Texture Blocks.

3.2.1 Edge Block Detector

Lynch's method [47] is used with some modifications. In an image, the edge block detector separates the low variation region from the high variation one (i.e. smooth regions from sharp edges). $S_h(x, y)$ and $S_v(x, y)$ are calculated for each pixel $P(x, y)$ in the high frequency blocks of an original image. Then each pixel is labeled as an edge or a non-edge according to the following equation:

$$\sqrt{[S_h(x, y)]^2 + [S_v(x, y)]^2} \geq T_s \tag{3.1}$$

where T_s is a sharp edge threshold. If a pixel does not satisfy equation 3.1, it is labeled as a non-edge pixel. Figure 3.7 illustrates the mapping of the two sobel operators to the Sharp Edge Region. Shaded region describes the two dimensional Sobel mask of non-edge pixels, while unshaded region describes the two dimensional Sobel mask of edge pixels. In this case, the sharp edge threshold T_s is chosen to be equal to 200 (i.e. $T_s = 200$) while in Lynch's method [47], T_s is a variable and its value depends on the eight surrounding blocks with minimum value of 200. In

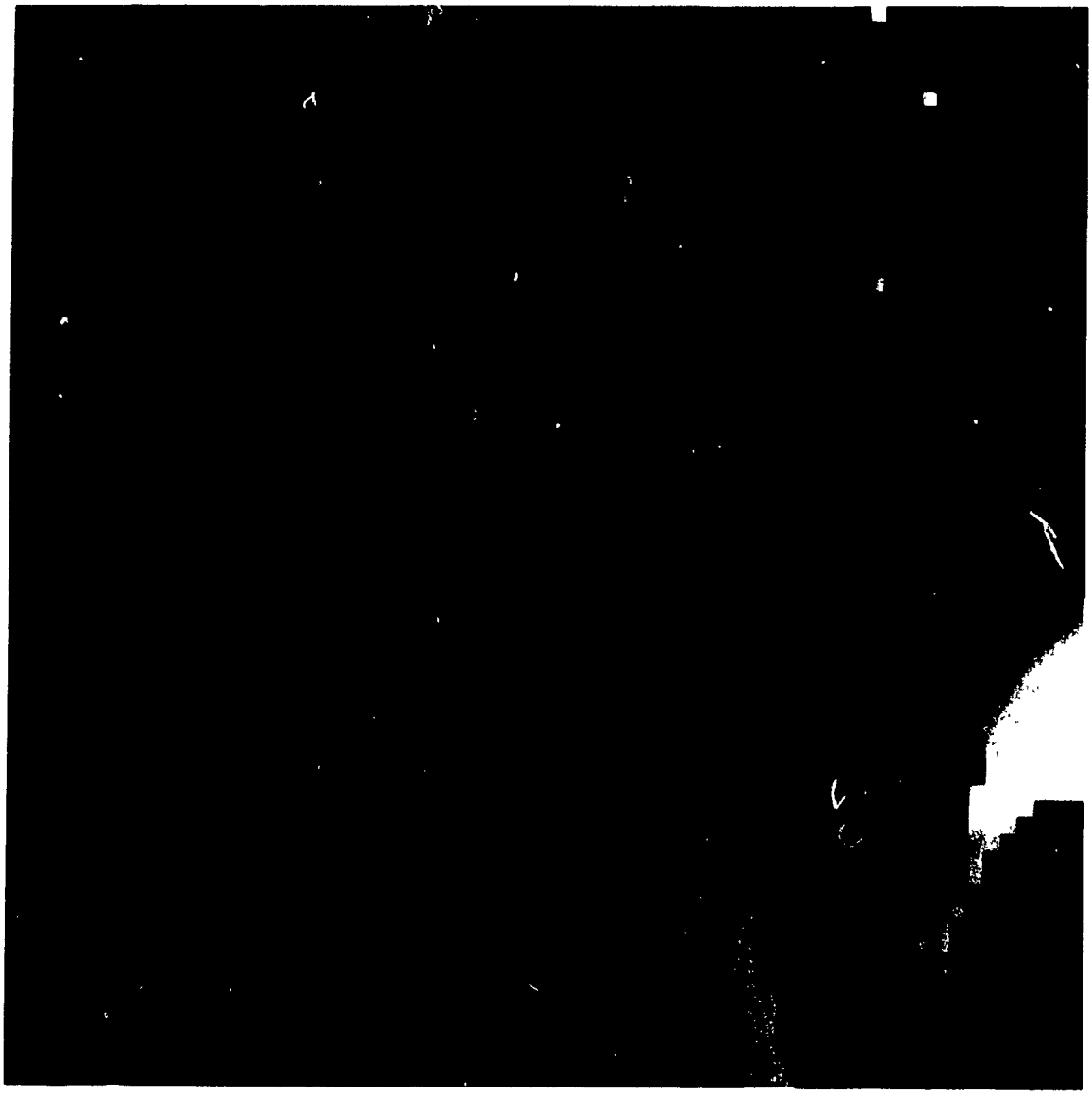

Figure 3.5: Low Frequency Blocks of Original Lena

Figure 3.6: High Frequency Blocks of Original Lena

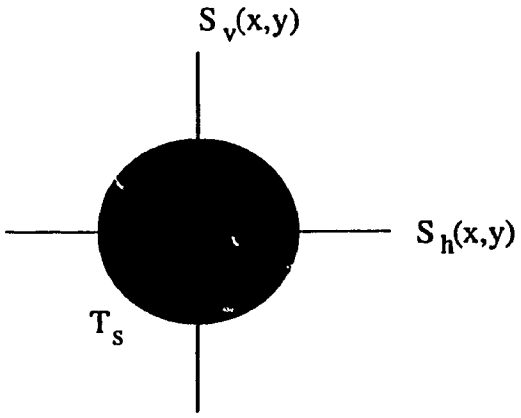

Figure 3.7: Mapping of Two Sobel Operators to the Sharp Edge Region

addition Lynch uses a square mapping of the two sobel operators to the Sharp Edge Region.

After categorizing each pixel in the sobel filtered high frequency blocks of an original image as an edge or a non-edge pixel, each 8×8 block is examined to determine how many connected regions are inside it. There are two acceptable situations to classify a block as a sharp edge block:

1. If a block has one edge area and two non-edge areas

2. If a block has one edge area and one non-edge area

Figure 3.8 illustrates these situations, where the shaded area represents sharp edge pixels. If any of these conditions is not met then the block is classified as a texture block. To decrease the classification error, any edge area of a size less than two pixels is considered as a non-edge area. This consideration is not allowed in Lynch's method [47]. Figure 3.9 and Figure 3.10 show the output of the edge block detector when original Lena of Figure 1.3 is used as an input.

Errors still can happen, for example: some texture blocks may fall within one of the two acceptable situations of sharp edge blocks and are classified as sharp edge blocks as in Figure 3.9, Or some sharp edge blocks may not fall within any of the two acceptable situations such as if a block has two edge area and three non-edge area

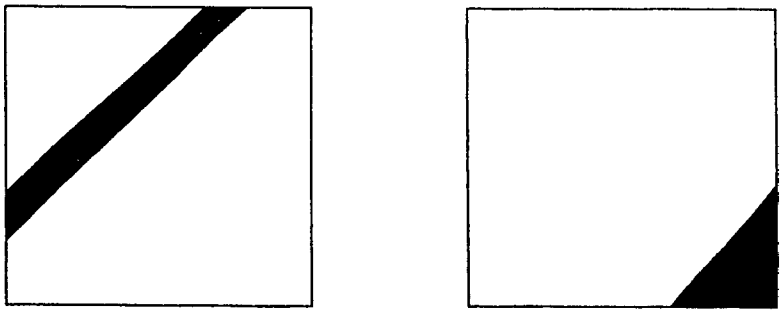

Figure 3.8: Sharp Edge Block Acceptable Situations

as in the case of a Y shape edge or if the block has one edge area and one non-edge area where the size of the edge area is one pixel, these blocks are classified as a part of the texture blocks as shown in Figure 3.10.

In order to minimize such errors, and to put back the wrongly classified blocks into their proper categories, the connectivity and the length of the sharp edges should be checked. This will be discussed in the next section.

3.2.2 Edge Connectivity

There are some problems that are associated with the Edge Block Detection technique, one of them is that some texture blocks may fall within any of the acceptable situations of the sharp edge blocs and will be wrongly classified as sharp edge blocks. With a view of eliminating the block of short edges (which belong to texture blocks) from sharp edge blocks, edges connectivity within sharp edge blocks are checked, followed by edge contours construction. Finally, an edge length threshold is used to reclassify the edges.

For a pixel $P(x, y)$, the 8-neighbors which are defined in Figure 3.11, have the following coordinates

$$(x-1, y), (x-1, y-1), (x-1, y+1), (x, y+1),$$
$$(x+1, y), (x+1, y+1), (x+1, y-1), (x, y-1)$$

To distinguish between the edges in the sharp edge blocks, each sharp edge (defined

Figure 3.9: Output of the Edge Block Detector (Sharp Edge Blocks)

Figure 3.10: Output of the Edge Block Detector (Texture Blocks)

in section 3.2.1) is labeled by a unique edge identification number. Then, the connectivity between each pixel $P(x, y)$ and its 8-neighbors is checked in a pixel by pixel bases for all pixels of the sharp edge blocks. If any two edge pixels are connected, they are labeled by the same edge identification number.

Two pixels are said to be connected [5] if they are:

1. Adjacent (say, if they are 8-neighbors).
2. Sharp edge pixels.

To measure the length of each sharp edge in the sharp edge blocks, a contour is constructed for each sharp edge as will be illustrated in the next section.

3.2.3 Edge Contour

A contour is defined as the boundary between a sharp edge and its background. For a sharp edge pixel, if any of its 4-neighboring pixels which are defined in Figure 3.11, is a background pixel, it is considered as a contour pixel. This check is done for all pixels of the sharp edge blocks on a pixel by pixel bases. The 4-neighbors are the horizontal and vertical neighbors [5] which are defined in Figure 3.11 and whose coordinates are given by:

$$(x+1, y), (x-1, y), (x, y+1), (x, y-1)$$

The length of an edge can be determined by:

Figure 3.11: 8-Neighbors and 4-Neighbors of the Center Pixel

- *First:* Constructing a contour around that edge.
- *Second:* Measuring the length of the constructed contour.

Figure 3.12 shows an example of two edge regions with their edge identification numbers and their constructed contours.

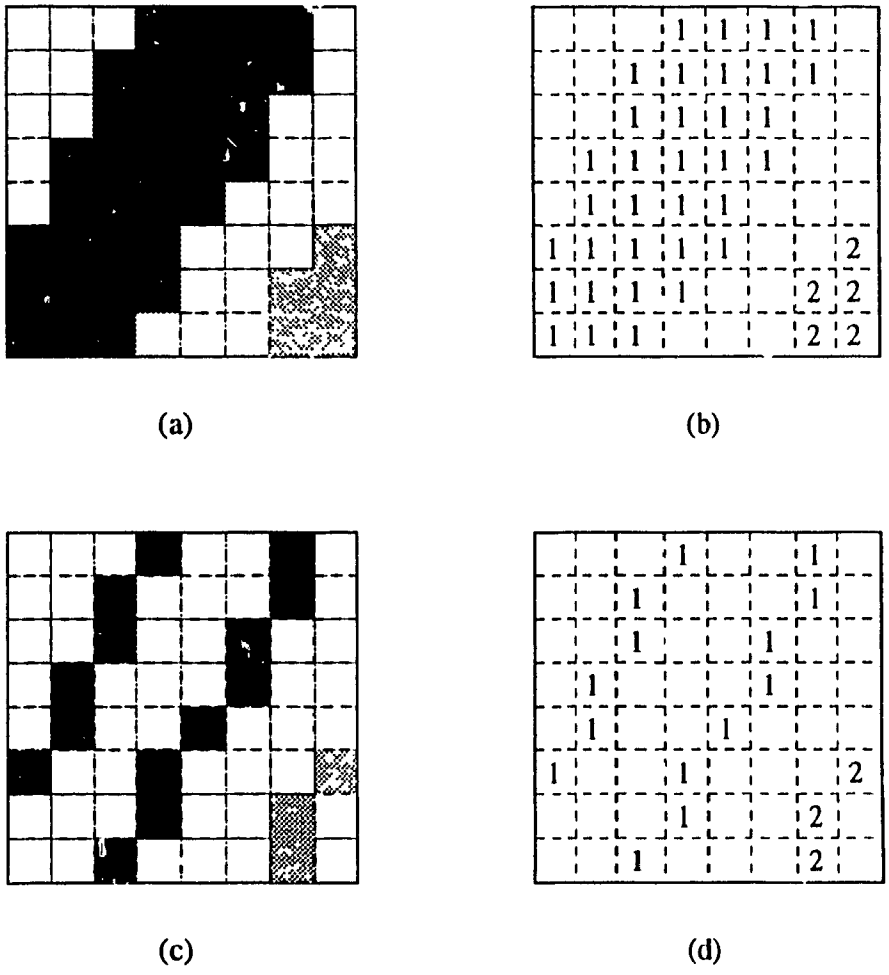

Figure 3.12: (a) Two Edge Regions (b) Their Edge Identification Numbers (c) Their Edge Contours (d) The Edge Identification Numbers of The Contours

Using a contour length threshold T_c, short edges which are found in the output image of the edge connectivity test (which are normally texture), can be separated from long sharp edges. If any only block has short edges inside it, the block is

recategorized as a texture block. (in this case $T_c = 30$). Figure 3.13 shows the sobel filtered sharp edge blocks after having the edge length measurement done.

3.2.4 Edge Continuity

Despite the presence of sharp edge pixels inside some blocks, if these blocks do not fall within one of the two sharp edge block's acceptable situations, these blocks will not be classified as sharp edge blocks. For example: if all the pixels inside a block are sharp edge pixels, or as in most of the cases, if a block has a combination of sharp edge pixels and texture pixels, these blocks will be classified as texture blocks by the Edge Block Detector. Such blocks are needed to be recategorized and put back to their right category. To do so, the continuity of any edge inside a sharp edge block is checked with its 8-neighboring texture blocks. This check is done in a block by block bases. If a sharp edge block share a continuous edge with a texture block, then the texture block is recategorized as a sharp edge block.

First, each 8×8 block in the sharp edge blocks and texture blocks is divided into a block frame and a 6×6 "block interior" as shown in Figure 3.14. Then, an edge is said to be continuous between two neighboring sharp edge blocks if any of its pixels that are in the block frame area has at least one edge neighboring pixel in the block frame area of the other block.

All sharp edge blocks should be checked for edge continuity. Figure 3.15 and Figure 3.16 show the sobel masked images of the sharp edge blocks and the texture blocks respectively after having the edge continuity test done.

3.2.5 Edge Extraction

Further categorization is done in the sharp edge blocks. Specifically, sharp edges are extracted from the background of the blocks. This is useful for measuring the ringing artifact.

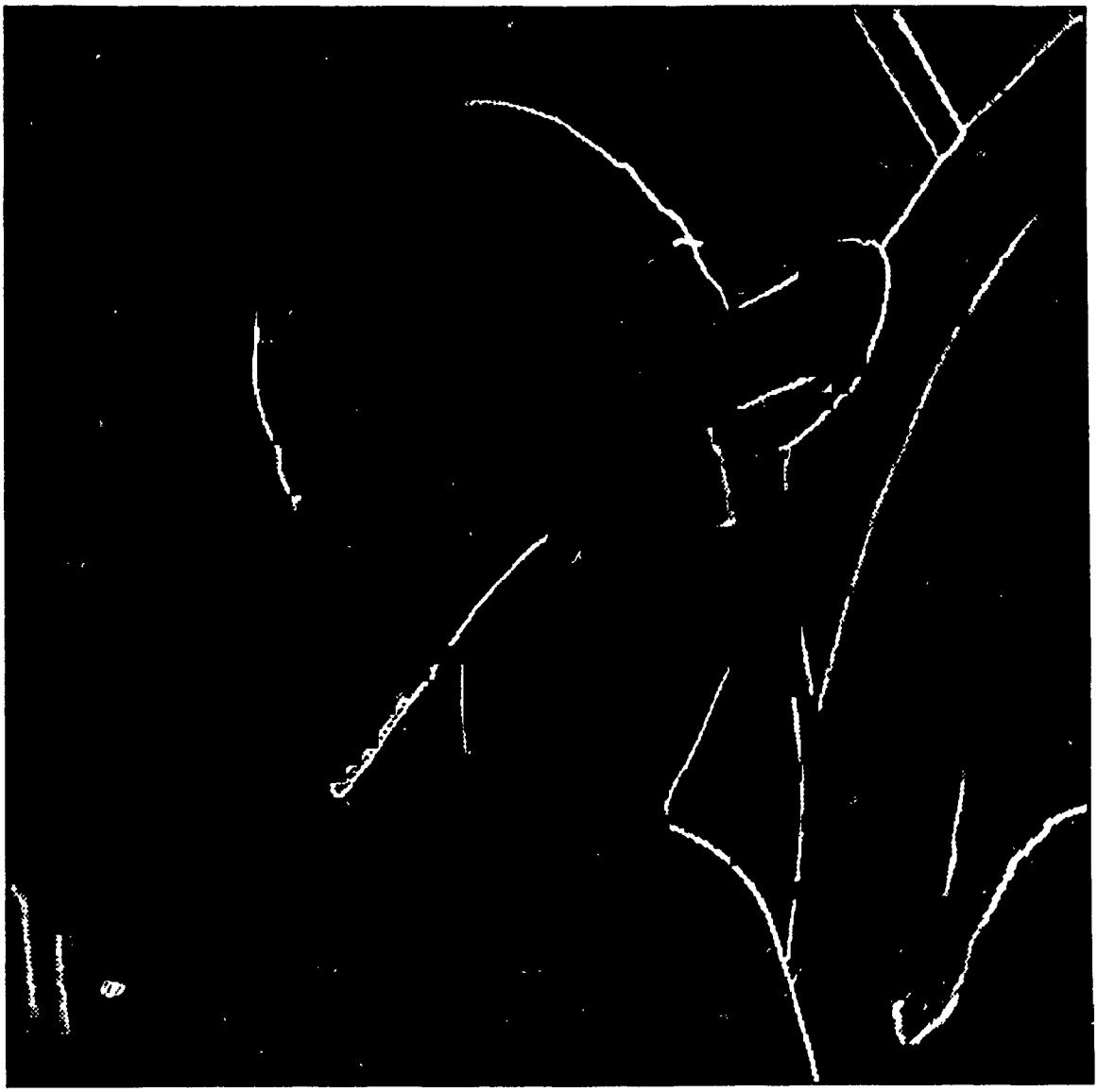

Figure 3.13: The Sharp Edge Region after the Edge Length Test

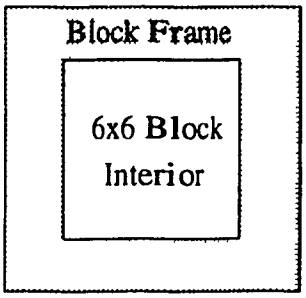

Figure 3.14: 8×8 Block Division into Frame and Interior

Using the same sharp edge threshold T_s that is used in Edge Block Detector (*i.e.* $T_s = 200$), pixels of values greater than or equal to the threshold are labeled as *Sharp Edge Pixels* while the rest of the pixels are labeled as *Background Pixels.* Figure 3.17 shows the sharp edge pixels of the sharp edge blocks of Figure 3.15.

The block categorization process categorizes an image blocks into three classes: *(Flat Blocks, Sharp Edge Blocks, and Texture Blocks).* Table 3.2 shows these classes and summaries their categorization conditions.

Block Class	*Conditions of Acceptance*
Flat Blocks	• The sobel magnitude of each pixel in a block is $\leq T_l$
Sharp Edge Blocks	• *a*) A block fall within one of the two acceptable situations: 1) It has one edge area and two non-edge areas 2) It has one edge area and one non-edge area and *b*) The sharp edge inside the block has a contour length $\geq T_c$ or • The edge inside a block is a continuity to an edge inside a neighboring sharp edge block
Texture Area	• All the blocks that do not belong to the Flat Blocks or the Sharp Edge Blocks or • Sharp Edge Block with a sharp edge of contour length $< T_c$

Table 3.2: Blocks Classes and Their Classification Conditions

Figure 3.15: Sobel Masked Image of the Sharp Edge Blocks after the Continuity Test

Figure 3.16: Sobel Masked Image of the Texture Blocks after the Continuity Test

Figure 3.17: Sharp Edge Pixels

3.3 Image Analysis

The blocking artifact is one of the common types of artifacts that block transform coding produce. It only affects the pixels that lie at the frame of a block which is defined in Figure 3.14, so it is found reasonable to analyze only the block frame pixels in order to detect and measure the blocking artifact.

Spatial Information Histograms are plotted for the block frame and the block interior of each block category of an image as will be illustrated in section 3.3.1. Then the computation of the amount of horizontal and vertical edges and non-horizontal and vertical edges will be discussed in section 3.3.2.

3.3.1 Spatial Information Histogram

A 2-dimensional Spatial Information Histogram shows the distributions of intensity and direction of the edges in an image[37]. SIHs are discussed previously in section 2.6.1.

For each block category of an image, two Spatial Information Histograms SIH(r,θ) are plotted. Here r and θ are the magnitude and the angle of the gradient respectively. One of the SIH(r,θ) is plotted for the block frame pixels, while the other one is for the block interior pixels.

Figure 3.18 shows an example of the construction of a SIH(r,θ), where the horizontal and vertical sobel operators (S_h) and (S_v) which are discussed in section 2.6, are computed for an image pixel $P(x,y)$ (say the results were $S_h = +m$ and $S_v = -n$). Then the bin of the SIH(r,θ) which is located at (S_h, S_v) (in this case the bin at (+m,-n)) is incremented. In constructing each SIH(r,θ), this process is repeated for all the pixels of the block frame or the block interior that belong to the block category under analysis.

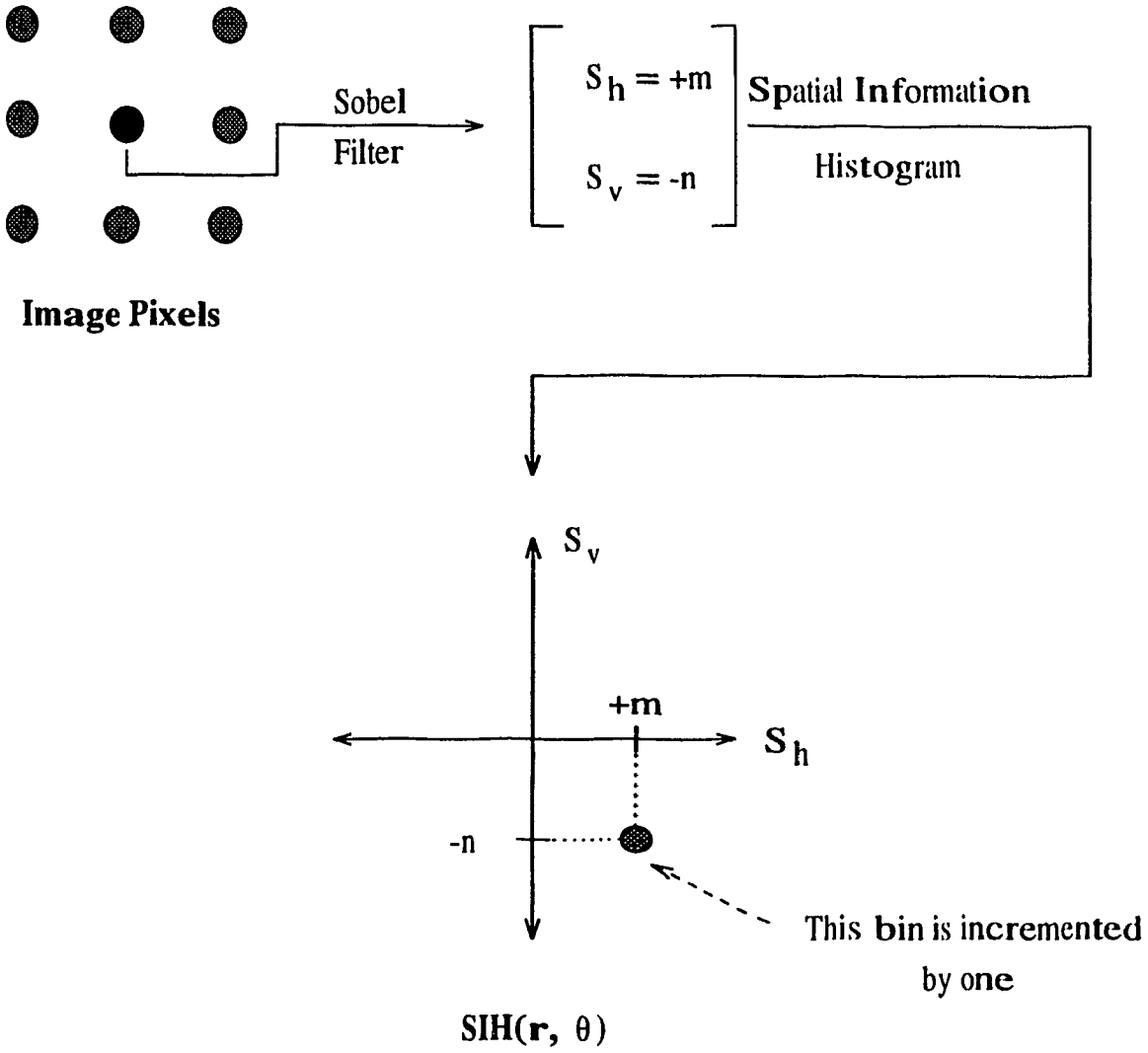

Figure 3.18: An Example of a SIH(r,θ) Construction

3.3.2 Edge Measurements

The blocking artifact affects the amount of horizontal and vertical edges of an image while blurring and ringing artifacts affect the amounts of horizontal and vertical edges as well as non-horizontal and vertical edges of an image. So, the amounts of horizontal and vertical edges and non-horizontal and vertical edges are very important.

As previously defined in section 2.6 a feature is a quantity of information associated with a specified image. The amount of horizontal and vertical edges are computed using the following feature:

$$g_{hv} = \frac{1}{p} \cdot \sum_{r} \sum_{\theta} SIH(r,\theta) \cdot r \tag{3.2}$$

$$0 < c_a \leq r \leq c_b \quad \theta = \tfrac{k\pi}{2} (k = 0, 1, 2, 3)$$

where c_a and c_b are clipping limits, and p is the number of pixels of the area under analysis. Some times the light presence of the blocking artifact in moderately compressed images is affected by a non-purely horizontal and vertical edges, where one of the two sobel operator outputs $S_h(x,y)$ or $S_v(x,y)$ of a pixel $P(x,y)$ is dominating the other (i.e. one has a value away higher than the other). It is thought to be useful to include an area of a small angle α around the horizontal and vertical axes of SIH(r,θ), so that such pixels which contribute to the blocking artifact will be considered as a horizontal and vertical edge and will completely isolate the non-horizontal and vertical edge measurements from being affected by the blocking artifact. Figure 3.19 shows a graphical representation of the location of the horizontal and vertical feature (*shaded area*) in a spatial information histogram.

The amount of non-horizontal and vertical edges are computed using the following feature:

$$g_{nhv} = \frac{1}{p} \cdot \sum_{r} \sum_{\theta} SIH(r,\theta) \cdot r \tag{3.3}$$

$$0 < c_a \leq r \leq c_b \quad \theta \neq \tfrac{k\pi}{2} (k = 0,1,2,3)$$

where c_a, c_b, and p have the same definition as for equation 3.2.

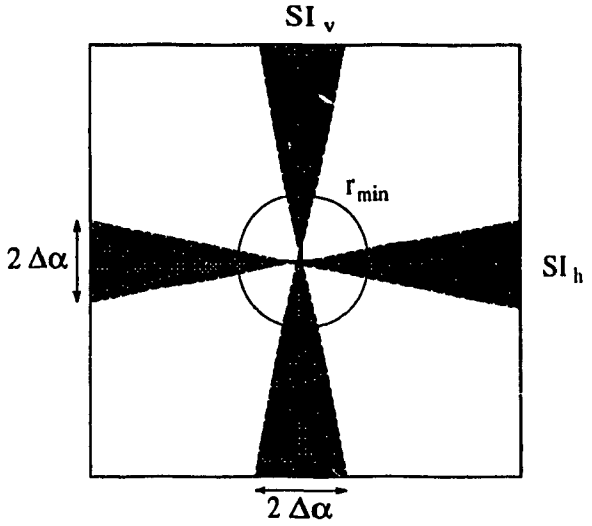

Figure 3.19: Graphical Representation of the Area of the Horizontal and Vertical Feature (*shaded area*)

3.4 Impairments Measurements

The Impairment Detection Method requires both original and degraded images for detecting and measuring impairments. As previously defined in section 2.6, a parameter is defined as the result of comparison between two features. Two parameters are used for detecting blocking, blurring, and spatial edge noise artifacts. These parameters can be computed by computing the difference between the horizontal and vertical edges of an original and a degraded images or between the non-horizontal and vertical edges of an original and a degraded images.

$$P_{hv} = \frac{g_{hvd} - g_{hvo}}{g_{hvo}} \qquad P_{nhv} = \frac{g_{nhvd} - g_{nhvo}}{g_{nhvo}}$$

where o and d are for original and degraded images respectively.

After categorizing the blocks of the image into three categories as described previously, each category is analyzed for certain type of artifacts. It is expected that IDM will provide:

- A parameter that will increase in value as the appearance of the blocking artifact increases in a degraded image,
- A parameter that will increase in value as the appearance of the spatial edge noise artifact increases in a degraded image, and
- A parameter that will decrease in value as the appearance of the blurring artifact increases in a degraded image.

3.4.1 Blurring Artifact

This type of impairment can be perceptually noticed in the sharp edge blocks and the texture blocks of an image as a loss in edge sharpness if an image is moderately or highly compressed or in the flat blocks when spatial details are lost if an image is highly compressed. Blurring artifact is measured by checking:

1. P_{nhv} of block interior of texture blocks.
2. P_{nhv} of sharp edges in block interior of sharp Edge blocks.
3. P_{nhv} of block interior and block frame of flat blocks (in the case of severe blurring).

Note that in all of the above chosen locations of measurement only the blurring artifact contributes to the amount of non-horizontal and vertical edges measured by P_{nhv}. As the blurriness increases in an image more non-horizontal and vertical edge information are lost from a degraded image yielding an increase in the negativeness of P_{nhv}.

3.4.2 Blocking Artifact

The blocking artifact is affecting only the block frame areas where it is represented by purely horizontal and vertical edges. To detect and measure the blocking artifact, all block frame areas of the three block categories of an image are checked. P_{hv} of the block frame area determines the amount of blocking that has affected the degraded image. Since the human visual system is more sensitive to low frequencies [46], a higher weight can be given to P_{hv} of flat blocks when all of these parameters are put together in an equation that simulates the MOS of the subjective tests. Note that blocking increases the amount of horizontal and vertical edges in the block frame area of an image yielding an increase in the positiveness of P_{hv}.

3.4.3 Spatial Edge Noise Artifact *(Ringing)*

Ringing artifact affect the area close to any sharp edge where it contributes to both horizontal and vertical edges and non-horizontal and vertical edges. For detecting and measuring the ringing artifact, the background pixels of the sharp edge blocks are checked. P_{hv} of the background pixels of the block interior area determines the amount of noise that has affected the background of the sharp edge blocks in a degraded image. When the effect of ringing artifact increases in a degraded image, more pixels contribute to the horizontal and vertical edges which increases the positiveness of P_{hv}. Note that P_{nhv} can not detect the presence of the ringing artifact when an image suffers from severe blurring where in that case the spatial information loss in the non-horizontal and vertical edges of a degraded image is much higher than the non-horizontal and vertical edges gain caused by the ringing artifact.

A summary of the required parameters for detecting and measuring blocking, blurring, and spatial edge noise artifacts as well as the measurement locations for each type of artifact are shows in Table 3.3 where $\Uparrow$ and $\Downarrow$ represent an increase and a decrease in the amount of a parameter respectively.

			Blurring	Blocking	Ringing
Flat Blocks	Block Frame	P_{hv}		$\Uparrow$	
		P_{nhv}			
	Block Interior	P_{hv}			
		P_{nhv}	$\Downarrow$		
Sharp Edge Blocks	Block Frame	P_{hv}		$\Uparrow$	
		P_{nhv}			
	Sharp Edges	P_{hv}			
		P_{nhv}	$\Downarrow$		
	Background	P_{hv}			$\Uparrow$
		P_{nhv}			
Texture Blocks	Block Frame	P_{hv}		$\Uparrow$	
		P_{nhv}			
	Block Interior	P_{hv}			
		P_{nhv}	$\Downarrow$		

Table 3.3: Summary of the IDM's Measurement Locations for Each Type of Artifact

3.5 Simulation Results

Original Lena of Figure 1.3 is used as a source image. PVRG-JPEG CODEC v1.1 [25] is used to generate the degraded images by adjusting the Q-Factor option. The Q-Factor and its corresponding compression ratios are defined in Appendix A. For each image, three type of artifacts are isolated namely: blocking, blurring, and spatial edge noise (ringing). Also the context of each type of artifact is separated from each other. Then primitives are computed for each type of artifact in each artifact's context and location. Two simulations are done, one for a wedge angle of $\alpha = 5°$ and the other one when there is no wedge angle i.e. when $\alpha = 0°$. A comparison between the two simulation results will present the benefits of inclusion

of a such small wedge angle around the SIH two principle axes. For both simulations, P_{hv} and P_{nhv} are computed using g_{hv} and g_{nhv} of equations 3.2 and 3.3 respectively, where the clipping limits of $c_a = 0$ and $c_b = 1$ are used. Through this section, all of the simulation results are plotted in line graphs while the result tables are presented in Appendix A.

In Section 3.5.1, a discussion on how to evaluate IDM's results, will be presented. While Sections 3.5.2, 3.5.3, and 3.5.4 will explain the simulation results of low frequency blocks, texture blocks, and sharp edge blocks respectively. In each section, a discussion of the behavior of its curves, and a comparison between the results of the two simulations are presented. Figure 3.20 will be used in all of these sections to illustrate some examples where the areas of interest are magnified and presented in Figures 3.2', 3.22, and 3.23. Finally, in Section 3.5.5 a comparison between the IDM and the IQR will be presented.

3.5.1 Discussion

As the compression ratio is increased for an image, the presence of artifacts in the reconstructed image will increase. So IDM's results can be evaluated by:

- looking at the reconstructed images and reading the artifacts primitives values. If the perceptual presence of an artifact increases in a reconstructed image as the compression ratio increases, then all of its primitives should be monotonic and should have one to one relation with the perceptual presence of its artifact (i.e. the primitive value should reflect any increase or decrease in the perceptual presence of the artifact that is associated with it).

- having an indication that each type of artifact is isolated from the rest of artifacts. Where the presence or the disappearance of a single artifact should not affect any primitive except its own.

- being able to measure the primitives of each type of artifacts in different contexts.

The context of artifact is a very important image quality factor. It is going to be used in the second problem solving step discussed in section 1.3.1. As shown in Table 3.3, IDM separates different types of artifacts into different contexts where primitives for each type of artifact are measured. Not necessarily all of these primitives should be used in the second problem solving step. Only the those who isolate the artifacts and contribute to the amount of perceptual distortion in the context where such distortion is most disturbing to the human observers are going to be used.

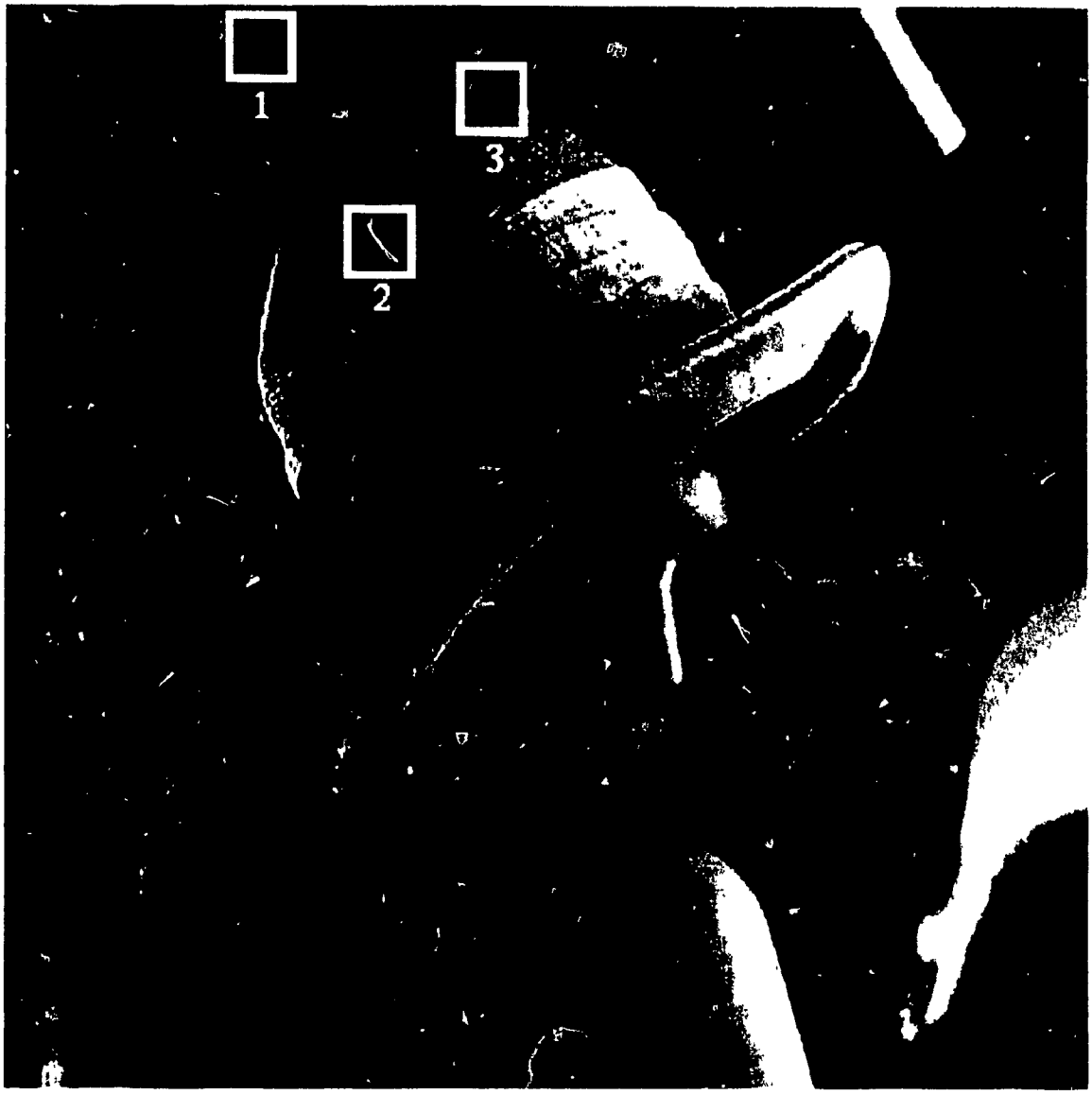

Figure 3.20: Degraded Lena at $q = 100$ Showing the Blocks of Interest

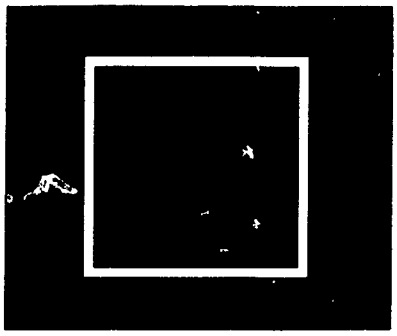

Figure 3.21 Block (8,112) of Degraded Lena at [illegible]

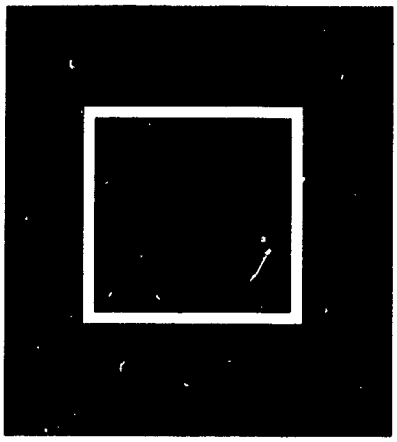

Figure 3.22 Block (112,168) of Degraded Lena at [illegible]

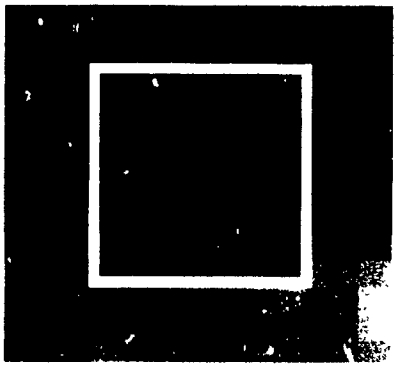

Figure 3.23 Block (40,224) of Degraded Lena at [illegible]

3.5.2 Low Frequency Blocks Results

Since there are no activity in the blocks of this category, any type of distortion will be easily perceived by the human eye. As mentioned earlier, Blocking and severe blurring artifact are expected to be detected and measured in this category. Figure 3.24 shows line graph of the percentage change of the horizontal and vertical edges and the non-horizontal and vertical edges between the original lena and its degraded images as the q factor has changed.

As expected, due to the increase of the q factor, there was an increase in the negativeness of P_{nhv} of the block frame and the block interior. As the q factor was increasing, the degree of blurriness that affected the image was increasing too. As a result, more non-horizontal and vertical edges were lost in the degraded image due to blurriness. g_{nhv} measured the amount of non-horizontal and vertical edges in both the original and the degraded images, while P_{nhv} detected the loss of the spatial information. An example is given by looking at the flat blocks of Figure 1.3 and 3.25. As it is shown, the spatial details were lost in the flat blocks of Figure 3.25. As shown by the simulation results of Table A.3, the original Lena has a non-horizontal and vertical edge value of g_{nhv}=15.96 while after compressing the image with a compression ratio of 65:1 as in the case of Figure 3.25, the non-horizontal and vertical edge value has dropped to g_{nhv}=0.00. As shown by this example and from Table A.3, when the image blurriness increased, the amount of non-horizontal and vertical edges decreased monotonically showing that there were less details in the flat blocks of the degraded image than of the original image.

Blocking artifact produces pure horizontal and vertical edges, as the blockiness increases in an image the strength of the pure horizontal and vertical edges increases. In the simulation, the degree of blockiness increased as the q factor was increasing. The amount of horizontal and vertical edges are measured by g_{hv}. P_{hv} detects the degree of blockiness that affect the image by measuring the percentage change of g_{hv} between the original and degraded Lena. An example is given by looking at the

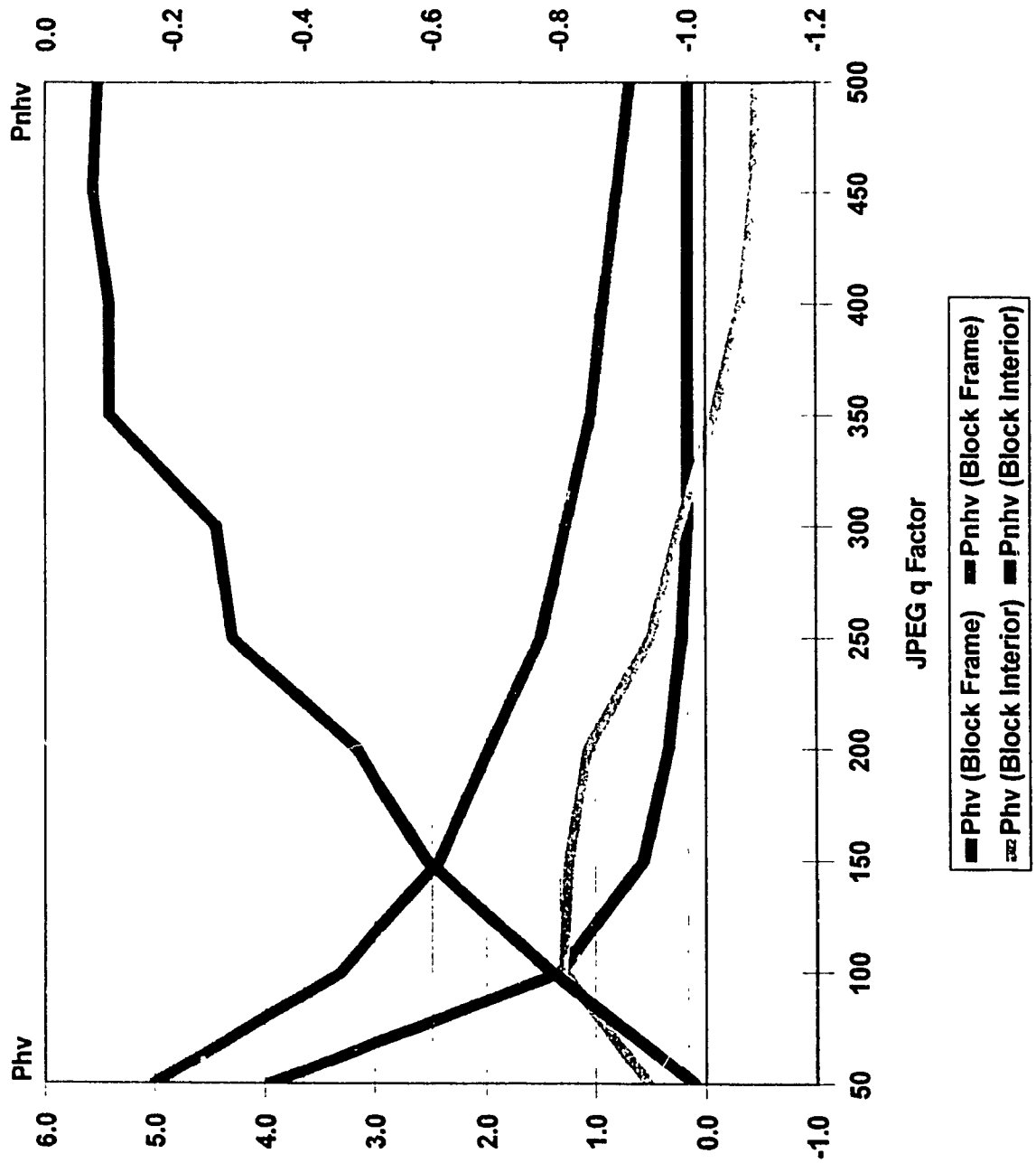

Figure 3.24: Simulation Results of Low Frequency Block, $\alpha = 5°$

Figure 3.25: Compressed Lena Using PVRG JPEG CODEC at $q = 500$ compression ratio of 65:1

flat blocks of Figure 3.2 and 3.25. It is shown that the blockiness in Figure 3.25 is more noticeable due to a higher strength of horizontal and vertical edges. From the simulation results of Table A.2 it shown that the amount of horizontal and vertical edges in the block frame of flat blocks of Figure 3.2 was g_{hv}=5.92 while for Figure 3.25 g_{hv}=15.40 which indicates that the strength of the horizontal and vertical edges has increased showing that the blocking artifact was more noticeable. As shown by this example and from Table A.2, when the blocking artifact increased in an image the amount of the horizontal and vertical edges has increased monotonically showing that the blocking artifact was more noticeable in the flat blocks of the degraded image.

Discussion

From Figure 3.24, the horizontal and vertical edges of the block interior gained some value until $q = 150$. This is due to the presence of horizontal or vertical stripes in the horizontal or vertical sobel filtered block respectively, which can be explained by looking at the block in the frequency domain where the presence of coefficients only at the first column or first row of the DCT block explain the presence of these stripes. As shown, the amount of horizontal and vertical edges started to decrease for $q < 150$. That is because of the horizontal and vertical stripes started to get blurred and started to loose their edge contents that they have already generated.

An illustrative example is shown in Figure 3.28 where it shows the horizontal and vertical sobel filter output of a flat area block located at (8,112) of the original Lena and the degraded Lena of $q = 100$. The formation of vertical stripes can be seen in the vertical sobel filter output of the degraded images block at the same location. This Block is located inside Box 1 of Figure 3.20, where Figure 3.21 shows the blocks of Box 1. As shown in Figure 3.27, the frequency analysis emphasize the presence of these vertical stripes, since there is only AC coefficients at the first row of the DCT block of the degraded image. The DCT coefficients of the original block

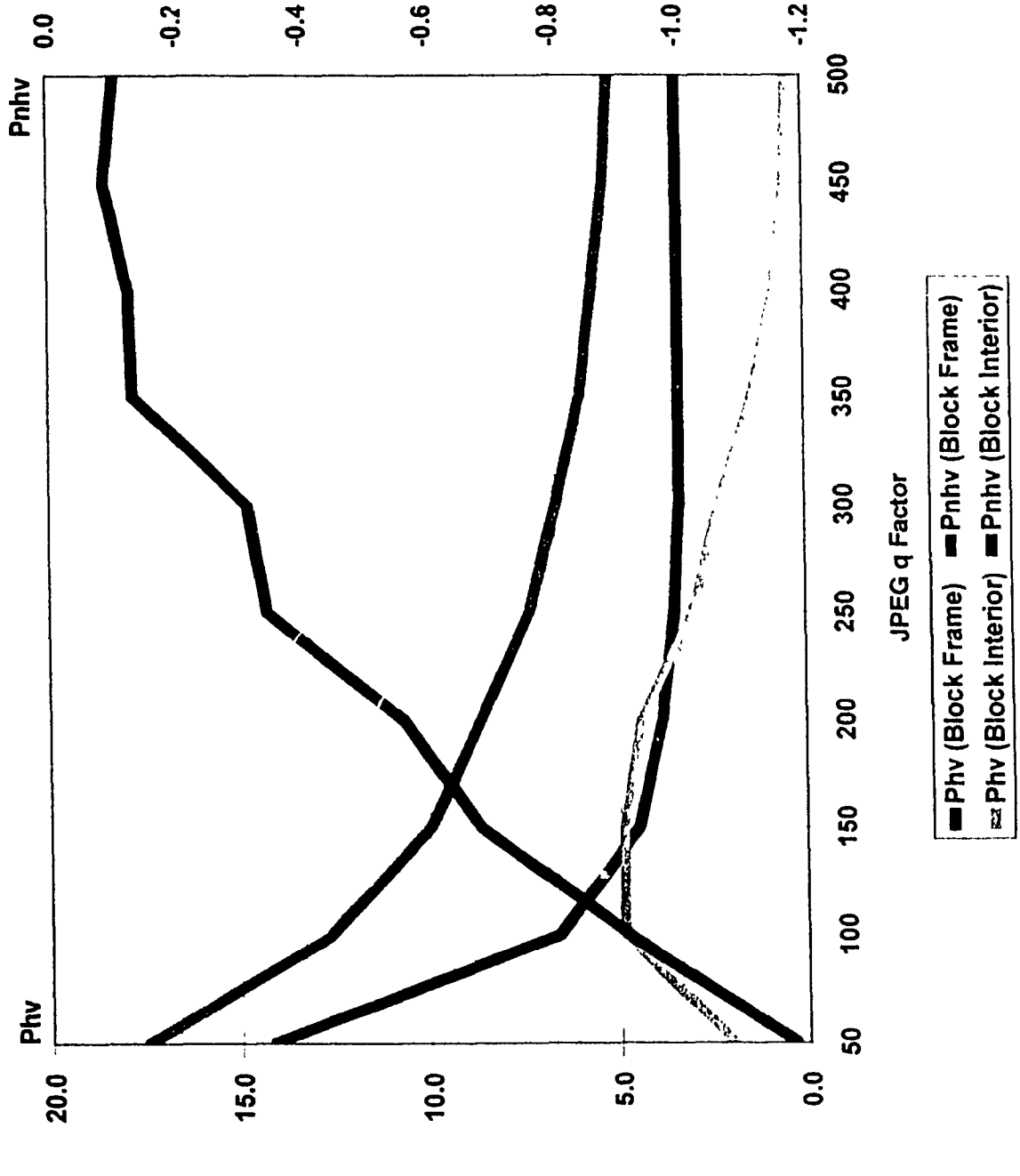

Figure 3.26: Simulation Results of Low Frequency Block, $\alpha = 0°$

also are shown in Figure 3.27.

By comparing the results when $\alpha = 5°$ and the results when $\alpha = 0°$ and by comparing Figure 3.24 and Figure 3.26, it can be seen that an angle of 5 degrees around the two principal axes of $SIH(r, \theta)$ did not have any effect on the characteristics of the curves. All the above discussion is still applied to the simulation results of $\alpha = 0°$.

−312.12	−19.56	−2.86	1.41	−2.13	2.41	−0.03	−1.56
5.17	3.43	−2.16	−2.33	−6.48	7.70	−1.23	−0.06
−1.24	−4.29	3.21	−3.75	−4.06	2.70	1.04	−0.01
−7.47	4.91	0.92	4.41	3.33	2.42	−3.08	0.37
2.12	−3.45	0.94	−2.25	−0.88	−0.82	−4.58	0.26
3.67	0.43	−0.04	−0.05	3.88	−3.23	−1.49	−2.20
−0.70	7.55	−1.21	−0.44	4.25	−1.03	−1.21	−1.16
2.61	3.47	0.74	−2.08	0.11	−0.13	−1.26	−2.61

−320.00	−21.85	0.00	−0.63	0.00	−1.42	0.00	0.58
0.00	0.00	0.00	0.00	0.00	0.00	0.00	0.00
0.00	0.00	0.00	0.00	0.00	0.00	0.00	0.00
0.00	0.00	0.00	0.00	0.00	0.00	0.00	0.00
0.00	0.00	0.00	0.00	0.00	0.00	0.00	0.00
0.00	0.00	0.00	0.00	0.00	0.00	0.00	0.00
0.00	0.00	0.00	0.00	0.00	0.00	0.00	0.00
0.00	0.00	0.00	0.00	0.00	0.00	0.00	0.00

Figure 3.27: DCT Coefficients of the Block Located at (8,112) of the Original Lena (Left) and the Degraded Lena at -q = *100* (Right)

(a)

−24	−25	−19	−23	−28	−14	−1	−4
4	10	12	12	14	6	−6	−2
11	6	−2	10	20	3	−4	0
−2	−15	−22	−17	−8	−4	−1	−3
12	−8	−17	−14	−15	−24	−32	−26
−3	−6	−6	−5	1	4	5	13
−28	1	11	1	−1	14	31	36
−14	9	19	10	−2	3	5	−10

(b)

10	19	15	−11	8	34	−13	−8
10	24	18	−18	12	36	−14	−6
15	20	16	−4	10	13	−10	−2
8	9	12	17	8	2	−3	−7
−10	−6	11	26	7	−2	−4	−2
−23	−16	12	29	9	−10	−3	11
−10	−3	9	23	19	−2	7	14
20	19	7	6	22	15	9	2

(c)

−8	−10	−19	−26	−26	−20	−11	−6
0	0	0	0	0	0	0	0
0	0	0	0	0	0	0	0
0	0	0	0	0	0	0	0
0	0	0	0	0	0	0	0
0	0	0	0	0	0	0	0
0	0	0	0	0	0	0	0
0	0	0	0	0	0	0	0

(d)

2	12	13	14	10	4	3	4
4	8	8	12	12	8	8	4
4	8	8	12	12	8	8	4
4	8	8	12	12	8	8	4
4	8	8	12	12	8	8	4
4	8	8	12	12	8	8	4
4	8	8	12	12	8	8	4
4	8	8	12	12	8	8	4

Figure 3.28: For the Block located at (8,112): (a),(c) Horizontal Sobel Filter of the Original and the Degraded Lena at -q = *100* respectively (b),(d) Vertical Sobel Filter of the Original and the Degraded Lena at -q = *100* Respectively

3.5.3 Texture Blocks Results

In this category, blurring artifact is expected to be detected and measured, where blocking and ringing artifact can be easily hidden in this block category for slightly and moderately compressed images due to the activities of the pixels. From Figure 3.29, it is shown that as the q factor was increasing, the blurriness of the texture blocks of the image were increasing too, so the non-horizontal and vertical edges of the block interior were loosing their edge contents resulting in an increase in the negativeness of P_{nhv} of the block interior which represent the fractional change of the non-horizontal and vertical edges between the original and the degraded images. An example is given by comparing the feather in Figure 1.3 and 3.30. It is shown that the sharpness of the edges of the feather was reduced in Figure 3.30. From the simulation results of Table A.5 it is shown that the original Lena has a non-horizontal and vertical edge value of g_{nhv}=61.90 while after compressing the image with a compression ratio of 25:1 as in the case of Figure 3.30, the non-horizontal and vertical edge value has dropped to g_{nhv}=51.21 (i.e. the degraded image lost %17 of its original value). As shown by this example and from Table A.5, when the image blurriness increased the amount of non-horizontal and vertical edges decreased monotonically showing that there were less details in the texture blocks of the degraded image than of the original image.

Discussion

Although blocking artifact can be hidden in this category for slightly and moderately compressed images, blocking artifact can still be detected and measured in this category. This doesn't mean the contribution of blocking artifact primitive of this category should be taken into consideration. As the q factor increases, stronger horizontal and vertical edges appear at the block frame of the blocks resulting in an increase in the degree of blockiness that is affecting the texture blocks. This was detected by the continuous increase of the positiveness of P_{hv} of the block frame.

The amount of horizontal and vertical edges of the block interior in this case was increasing as the q factor was increasing. This is due to the presence of horizontal or vertical stripes in the horizontal or vertical sobel filtered block respectively, which can be explained by looking at the blocks in the frequency domain where the presence of coefficients only at the first column or first row of the DCT blocks explain the presence of these stripes. These stripes are purely horizontal or vertical edges and it contribute directly to g_{hv}. An example that explains what is going on is given by looking at the texture block located at (112,168). Box 2 in Figure 3.20 shows the area of the block of interest, where Figure 3.22 shows the blocks of Box 2. By looking at the sobel filter output of this block as shown in Figure 3.32, the formation of vertical stripes can be seen.

As shown in Figure 3.33, the Frequency analysis emphasize the presence of these vertical stripes, since there is only AC coefficients at the first row of the DCT block. The DCT coefficients of the original block also is shown in Figure 3.33.

By comparing the results when $\alpha = 5°$ and the results when $\alpha = 0°$ and by comparing Figure 3.29 and Figure 3.31, it can be seen that an angle of 5 degrees around the two principal axes of $SIH(r, \theta)$ did not have any effect on the characteristics of the curves. All the above discussion is still applied to the simulation results of $\alpha = 0°$.

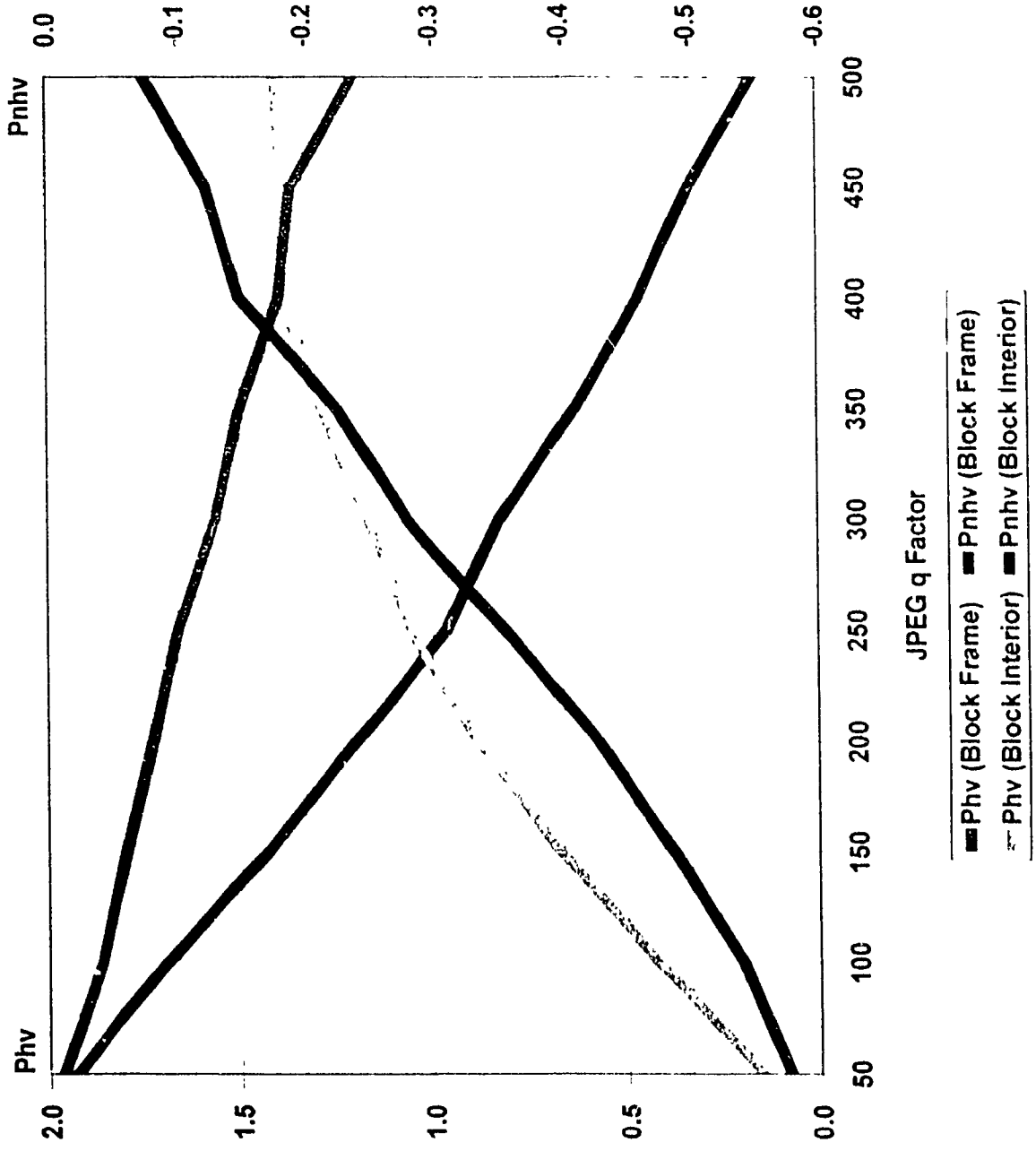

Figure 3.29: Simulation Results of Texture Blocks, $\alpha = 5°$

Figure 3.30 Compressed Lena Using PVRG JPEG CODEC at q = 150 compression ratio of 25:1

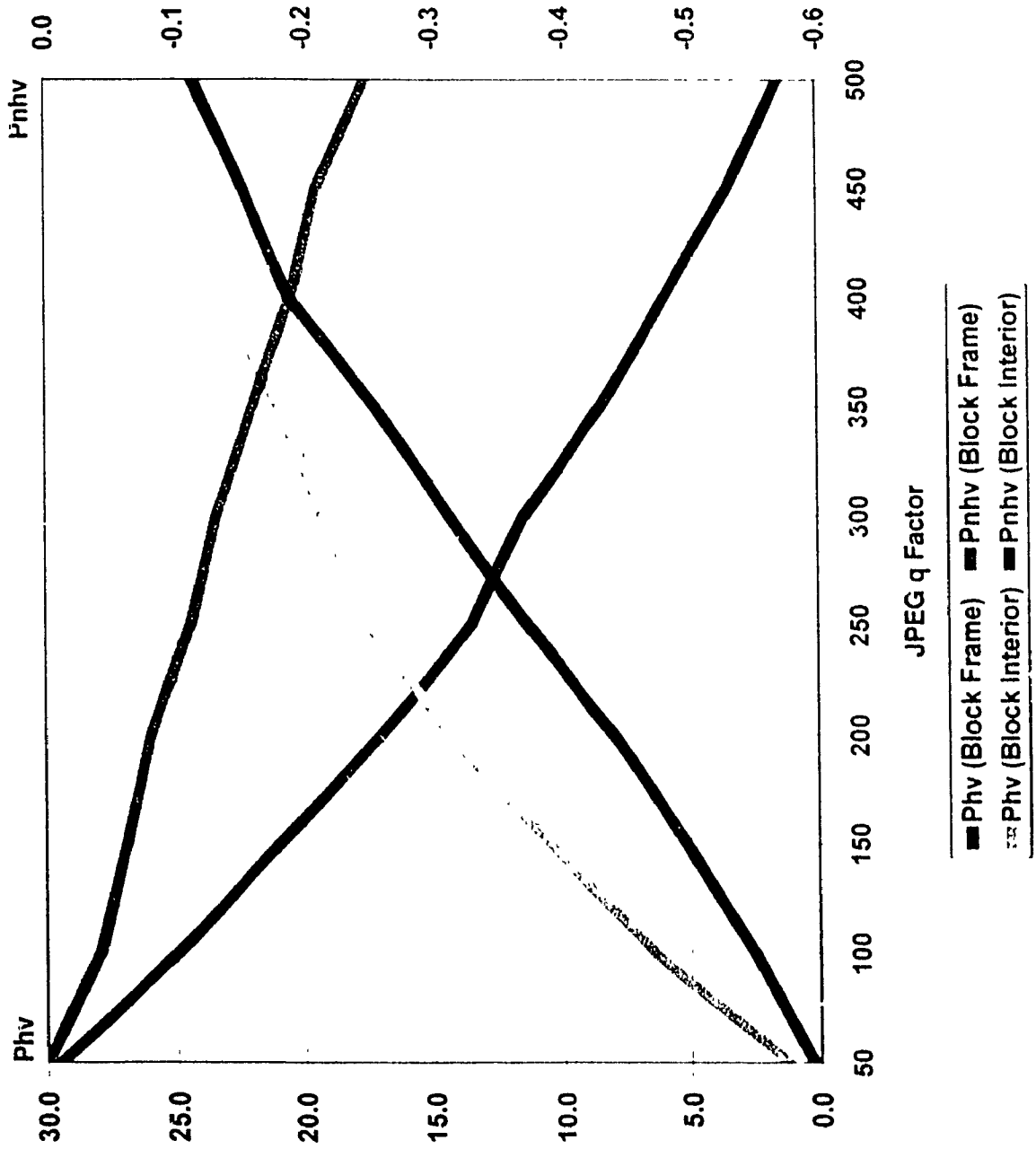

Figure 3.31: Simulation Results of Texture Blocks, $\alpha = 0°$

	14	29	12	−4	−5	18	51	59
	52	0	−45	−26	26	27	1	−10
	−20	−6	26	47	32	1	−6	0
(a)	−10	35	46	20	−14	5	49	50
	26	5	−15	−35	- 21	14	6	−15
	7	−29	−13	20	32	6	−36	−39
	−8	−5	6	16	2	−29	−25	−4
	28	3	−25	−34	−17	5	23	17

	30	37	24	−12	−5	−10	5	57
	32	−2	1	14	20	−11	13	46
	10	−18	4	51	20	−41	10	44
(b)	40	11	18	32	−10	−23	29	32
	62	13	7	−3	5	16	26	15
	19	−1	17	0	28	2	−10	27
	−16	1	42	18	8	−35	−11	46
	−28	−9	35	26	3	−39	15	35

	0	12	22	28	28	20	10	5
	0	0	0	0	0	0	0	3
	0	0	0	0	0	0	0	4
(c)	0	0	0	0	0	0	0	4
	0	0	0	0	0	0	0	4
	0	0	0	0	0	0	0	4
	0	0	0	0	0	0	0	3
	−9	−18	−12	−4	4	12	18	−12

	30	2	4	10	14	14	12	−1
	36	8	8	12	12	8	8	1
	36	8	8	12	12	8	8	8
(d)	36	8	8	12	12	8	8	16
	36	8	8	12	12	8	8	24
	36	8	8	12	12	8	8	32
	36	8	8	12	12	8	8	39
	25	10	12	16	16	12	10	10

Figure 3.32: For the Block located at (112,168): (a),(c) Horizontal Sobel Filter of the Original and the Degraded Lena at *-q = 100* respectively (b),(d) Vertical Sobel Filter of the Original and the Degraded Lena at *-q = 100* respectively

−247.63	−17.09	−5.20	−1.85	9.87	−6.97	9.33	5.84
−8.97	−2.03	1.91	−4.59	−5.11	−3.08	−1.85	1.21
−11.28	5.07	−5.69	−3.79	1.17	2.92	5.96	1.96
3.34	−0.01	1.45	−5.82	−12.59	8.92	2.37	0.72
2.37	−0.64	−3.25	−19.85	−1.63	2.98	−5.55	1.39
−4.09	0.80	−19.61	−3.17	3.41	−0.25	−1.75	1.41
−9.26	3.15	−1.54	4.31	−1.43	−1.49	5.44	3.13
−1.01	1.70	−0.78	−0.05	−2.89	−4.16	−3.12	1.61

−256.00	−21.85	0.00	−0.63	0.00	−1.42	0.00	0.58
0.00	0.00	0.00	0.00	0.00	0.00	0.00	0.00
0.00	0.00	0.00	0.00	0.00	0.00	0.00	0.00
0.00	0.00	0.00	0.00	0.00	0.00	0.00	0.00
0.00	0.00	0.00	0.00	0.00	0.00	0.00	0.00
0.00	0.00	0.00	0.00	0.00	0.00	0.00	0.00
0.00	0.00	0.00	0.00	0.00	0.00	0.00	0.00
0.00	0.00	0.00	0.00	0.00	0.00	0.00	0.00

Figure 3.33: DCT Coefficients of the Block Located at (112,168) of the Original Lena (Left) and the Degraded Lena at *-q = 100* (Right)

3.5.4 Sharp Edge Blocks Results

In this category blurring is expected to be seen at the sharp edges while ringing is expected to be seen at the background pixels. As expected, when the q factor increased, the strength of the non-horizontal and vertical edges of the sharp edges was affected by the blurriness and decreased in value. Figure 3.34 shows that the negativeness of P_{nhv} of the sharp edges was increasing for the same reason. An example is given by looking at the sharp edge blocks of Figure 1.3 and 1.5. As it is shown in Figure 1.5, the sharpness of the edges of Lena was reduced (e.g. the edge of Lena's right shoulder). From the simulation results of Table A.7 it is shown that the original Lena has a non-horizontal and vertical edge value of g_{nhv}=124.99 while after compressing the image with a compression ratio of 42:1 as in the case of Figure 1.5, the non-horizontal and vertical edge value has dropped to g_{nhv}=111.30 (i.e. the

degraded image lost %11 of its original value). As shown by this example and from Table A.7, when the image blurriness increased the amount of non-horizontal and vertical edges decreased monotonically showing less sharpness and less strength for the sharp edges of the sharp edge blocks in the degraded image than in the original image.

Ringing artifact can be checked by comparing the background pixels of the original blocks to the background pixels of the degraded blocks, as shown in Figure 3.34 the horizontal and vertical edges g_{hv} and the non-horizontal and vertical edges g_{nhv} have gained some value until a certain q factor level (in this case $q = 150$). This shows that the spatial edge noise was affecting the background. When the q factor increased, g_{hv} was increasing too, resulting in an increase in the positiveness of P_{hv} of the background, and showing an increase in the degree of the spatial edge noise. At the same time, g_{nhv} was affected by the blurriness and kept loosing its edge contents, resulting in a decrease of P_{nhv} of the background. An example is given by looking at the sharp edge blocks of Figure 1.3 and 1.5. The ringing artifact can be noticed near the edge of Lena's right shoulder in Figure 1.5. From the simulation results of Table A.8 it is shown that the original Lena has a horizontal and vertical edge value of g_{hv}=4.07 while after compressing the image with a compression ratio of 42:1 as in the case of Figure 1.5, the horizontal and vertical edge value has increased to g_{hv}=10.82 (i.e. the degraded image has gained %166 of its original value showing more activity). As shown by this example and from Table A.8, when the image compression increased the amount of horizontal and vertical edges of the background pixels increased monotonically showing more and stronger horizontal and vertical edges were gained by the background pixels of the sharp edge blocks in the degraded image than in the original image which indicates stronger presence of the ringing artifact.

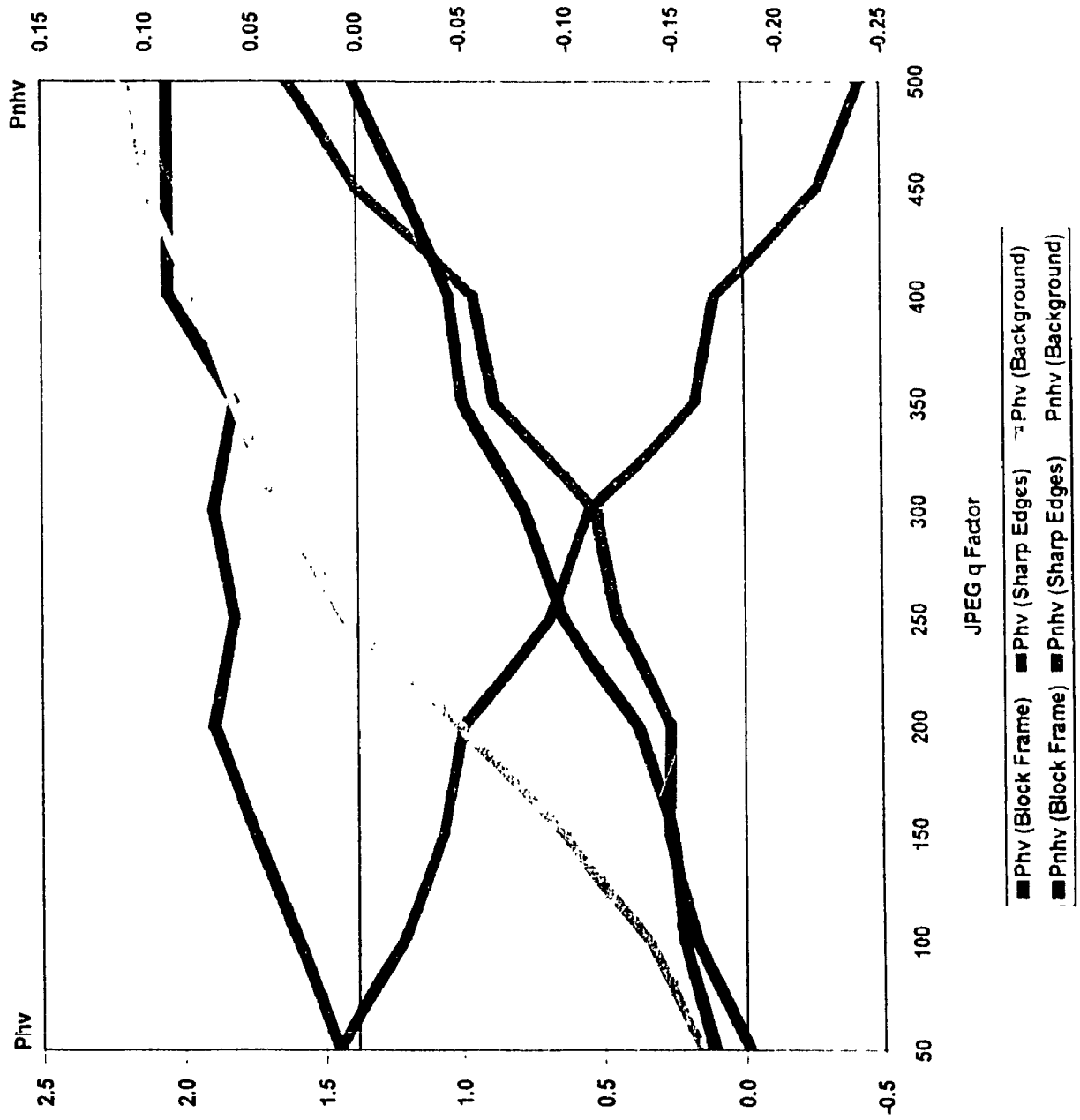

Figure 3.34: Simulation Results of Sharp Edge Blocks, $\alpha = 5°$

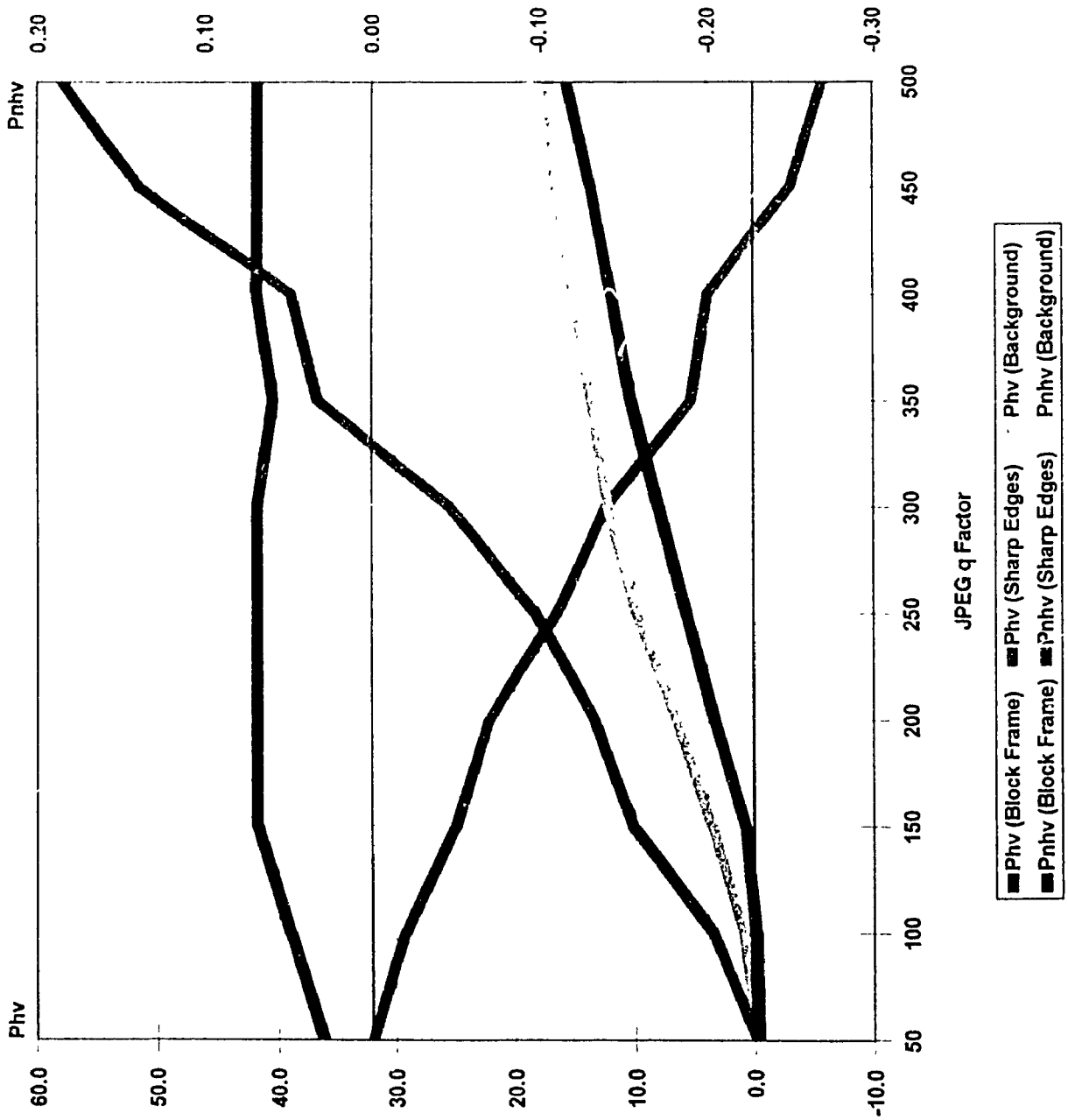

Figure 3.35: Simulation Results of Sharp Edge Blocks, $\alpha = 0°$

Discussion

As the blurriness increases, the horizontal and vertical edge components of the pixels will decrease. Some pixels will loose one of their two edge components before the other one, which will make these pixels contribute to the amount of the horizontal and vertical edges g_{hv} and increase it. This was the case for P_{hv} of the sharp edges in Figure 3.34 where its value increased as the q factor was increasing.

Blocking is less perceivable in this category than in flat blocks category, but it is still can be detected and measure in this category. Again, the degree of blockiness increased as the quantization level of the CODEC was increasing. From the table A.6, the strength of the horizontal and vertical edges of the blocks frame increased showing more blockiness and resulting in an increase in the positiveness of P_{hv} of the block frame. In this case, g_{nhv} of the block frame wasn't affected by the blurriness and had a small increase which made it contribute to the degree of blockiness.

Box 3 of Figure 3.20 shows an example of the sharp edge area blocks. Figure 3.23 shows the block which is located at (40,224), this block will be used as an example to show what is going on in the sharp edge area blocks. By looking at the sobel filter output of the original block shown in Figure 3.36 and of the degrade block at -q = *100* shown in Figure 3.37 (a) and (c), one can see that the non-horizontal and vertical pixels of the block interior formed a horizontal and vertical stripes in the horizontal and vertical sobel operators outputs respectively. The spatial edge noise that can be seen in this block is a result of the existence of these stripes. From Figure 3.37 (b) and (d), the block has lost all of its vertical edge component in the block interior and most of it in the block frame as a result of the increase in the q factor which introduced more blurriness to the image. That caused an increase in g_{hv} and P_{hv} of the block interior and the block frame as can be seen in Figure 3.34. An explanation to what happened is that by looking at Figure 3.38 (c) the coefficients are only at the first column of the DCT block of the degraded image of q = *400*.

By comparing the results when $\alpha = 5°$ and the results when $\alpha = 0°$ and by

	−20	−3	9	11	5	1	9	14
	−13	−10	−3	−2	−6	−3	−11	−20
	13	−8	1	10	−3	−12	−1	−5
(a)	119	75	64	92	90	45	27	43
	199	183	246	291	256	203	198	210
	119	226	257	180	166	245	274	237
	105	125	14	−21	65	105	61	84
	69	−29	−27	31	12	−32	20	100

	8	−5	−9	−5	15	3	1	−2
	17	6	−1	−10	10	7	−3	−2
	−1	6	15	−16	−1	12	−5	−13
(b)	−43	−17	36	0	−32	−11	11	−17
	−101	−19	90	19	−88	−53	30	−8
	−89	60	105	−28	−90	−25	26	−29
	25	73	12	−47	1	3	−17	0
	31	−11	−13	1	20	−20	14	72

Figure 3.36: For the Block Located at (40,224): (a) Horizontal Sobel Filter of the Original Lena (b) Vertical Sobel Filter of the Original Lena

	−40	−27	−13	−1	5	3	3	11
	−11	−4	−4	−4	−4	−4	−4	−11
	−10	−12	−12	−12	−12	−12	−12	13
(a)	113	89	88	88	88	88	89	86
	254	228	228	228	228	228	228	215
	208	215	216	216	216	216	215	221
	38	76	76	76	76	76	76	111
	24	14	−8	−19	−10	18	53	56

	8	13	13	3	−9	−17	−17	23
	21	20	20	8	−8	−20	−20	8
	26	20	20	8	−8	−20	−20	−3
(b)	1	19	20	8	−8	−20	−19	8
	−48	18	20	8	−8	−20	−18	−25
	−68	19	20	8	−8	−20	−19	31
	−24	20	20	8	−8	−20	−20	11
	16	8	10	7	2	−2	−3	32

	−24	−20	−20	−20	−20	−20	−20	29
	−34	−44	−44	−44	−44	−44	−44	−44
	−1	−16	−16	−16	−16	−16	−16	−16
(c)	74	56	56	56	56	56	56	56
	162	144	144	144	144	144	144	144
	207	192	192	192	192	192	192	192
	173	164	164	164	164	164	164	164
	13	48	48	48	48	48	48	48

	20	0	0	0	0	0	0	0
	14	0	0	0	0	0	0	0
	−11	0	0	0	0	0	0	0
(d)	−44	0	0	0	0	0	0	0
	−80	0	0	0	0	0	0	0
	−113	0	0	0	0	0	0	0
	−137	0	0	0	0	0	0	0
	−111	0	0	0	0	0	0	0

Figure 3.37: For the Block Located at (40,224): (a),(c) Horizontal Sobel Filter of the Degraded Lena at *-q = 100 and 400* respectively (b),(d) Vertical Sobel Filter of the the Degraded Lena at *-q = 100 and 400* respectively

	−116.25	3.87	−9.84	−6.03	9.00	3.59	7.59	−0.34
	−227.43	−4.87	7.92	1.24	−1.84	4.36	−3.25	0.86
	83.80	−3.87	8.79	8.37	−14.97	−17.04	2.17	−5.34
(a)	27.96	−3.01	−14.46	−18.02	9.19	12.14	−1.14	3.41
	−33.50	11.27	10.89	19.86	19.25	−9.58	−1.80	1.98
	8.63	−10.22	0.28	−12.95	−26.86	7.27	0.90	4.71
	11.56	−1.54	−7.83	−0.34	24.60	4.45	1.71	0.33
	−0.77	8.27	−3.50	10.42	−11.40	−3.45	−2.62	−5.88

	−128.75	0.00	−21.21	0.00	0.25	0.00	0.40	0.00
	−240.79	0.00	−0.09	0.00	−0.07	0.00	−0.04	0.00
	83.44	0.00	−0.43	0.00	−0.33	0.00	−0.18	0.00
(b)	28.49	0.00	0.26	0.00	0.20	0.00	0.11	0.00
	−36.75	0.00	0.33	0.00	0.25	0.00	0.14	0.00
	0.44	0.00	−0.38	0.00	−0.29	0.00	−0.16	0.00
	0.89	0.00	−0.18	0.00	−0.14	0.00	−0.07	0.00
	0.50	0.00	0.45	0.00	0.35	0.00	0.19	0.00

	−128.00	0.00	0.00	0.00	0.00	0.00	0.00	0.00
	−192.61	0.00	0.00	0.00	0.00	0.00	0.00	0.00
	112.92	0.00	0.00	0.00	0.00	0.00	0.00	0.00
(c)	−1.52	0.00	0.00	0.00	0.00	0.00	0.00	0.00
	0.00	0.00	0.00	0.00	0.00	0.00	0.00	0.00
	0.93	0.00	0.00	0.00	0.00	0.00	0.00	0.00
	0.85	0.00	0.00	0.00	0.00	0.00	0.00	0.00
	0.82	0.00	0.00	0.00	0.00	0.00	0.00	0.00

Figure 3.38: DCT Coefficients of the Block Located at (40,224), (a) the Original Lena, (b) the Degraded Lena at -q = *100*, (c) the Degraded Lena at -q = *400*

comparing Figure 3.34 and Figure 3.35, it can be seen that an angle of 5 degrees around the two principal axes of $SHH(r,\theta)$ did not have any effect on the characteristics of the curves. All the above discussion is still applied to the simulation results of $\alpha = 0°$.

3.5.5 IDM vs. IQR

In the following sections, the compression ratio of each block category is increased, one block category at a time, and the rest of the image blocks are left without compression. Then IDM and IQR simulations are carried out to illustrate the superiority of IDM over IQR. Such type of compression is practically done by the compressor where it compress certain parts of the image more coarsely than the other parts, based on a decision the compressor takes about the importance of each part to the user.

Compressing the Texture Blocks

In original Lena, the feather blocks of Lena's hat were compressed coarsely (Figure 3.39) where blocking artifact is introduced by compressing the feather blocks using PVRG-JPEG CODEC with -q = 200. In this simulation, the amount of compression is increased step by step where for each step the primitives of IDM and the parameters of IQR are computed. From the masking phenomenon of vision, it is known that texture blocks will mask most of the degradation, i.e. the degradation will not be noticeable unless it is severe. But from Figure 3.40, the IQR indicated that the whole image suffers from blocking artifact (which is not true), while from the same figure one can notice that IDM indicated that only the texture blocks of the reconstructed image suffer from blocking artifact. For example, the fractional change of horizontal and vertical edges between the original Lena and the image of Figure 3.39 computed by Melcher and Wolf method is P_{hv}=1.26 indicating global blocking. While the IDM show that the fractional change of horizontal and vertical

edges in the block frame of the texture blocks between original Lena and the image of Figure 3.39 is P_{hv}=1.27 while for flat blocks P_{hv}=0.00 showing that blocking artifact affected only the texture blocks of the degraded image.

Since the flat blocks of the reconstructed image do not indicate that they suffer from blocking artifact as it can be seen from Figure 3.40, so IDM do not indicate that the reconstructed image suffers from blocking. As it can be seen in this case, IQR gave a false detection for blocking artifact and it couldn't determine the context nor the location of error, while IDM determined the context and the location of degradation and gave the user a chance to decide if this type of degradation in that context and location should be taken into account or not.

Compressing the Sharp Edge Blocks

In this example, ringing and blocking artifacts are introduced to the sharp edge blocks of Lena as in Figure 3.41 where the sharp edge blocks are compressed using PVRG-JPEG CODEC with -q = 300. In this simulation, the amount of compression is increased step by step where for each step the primitives of IDM and the parameters of IQR are computed. From Figure 3.42, it can be seen that IQR indicated that the whole image of Figure 3.41 suffers from light blocking artifact, while IDM indicated that only the sharp edge blocks of Figure 3.41 suffer from blocking artifact and ringing artifact which are presented by P_{hv} of the block frame and the background pixels respectively. For Figure 3.41 the fractional change of horizontal and vertical edges between the original Lena and the degraded image computed by Melcher and Wolf method is P_{hv}=0.11 indicating light global blocking. While the IDM show that the fractional change of horizontal and vertical edges in the block frame of the sharp edge blocks between original Lena and the degraded image is P_{hv}=0.36 indicating that blocking artifact is affecting the sharp edge blocks. While the fractional change of horizontal and vertical edges in the background pixels of the sharp edge blocks between original Lena and the degraded image is P_{hv}=1.17 indicating that ringing

Figure 3.39: The Feather Blocks of Lena are Compressed at a Rate 8:1

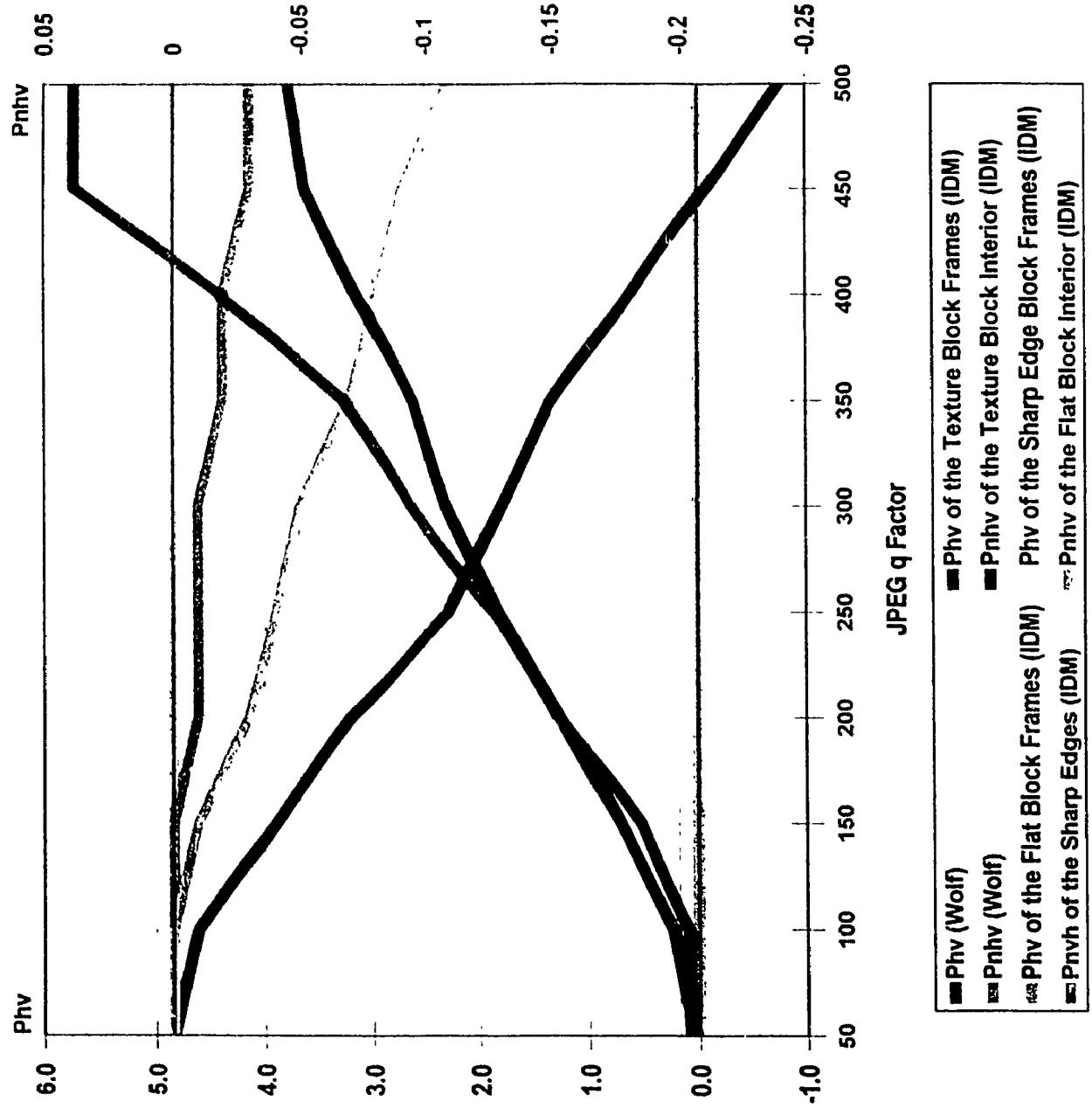

Figure 3.40: Simulation Results of Changing the Compression Ratio for Lena's Feather Blocks

artifact is affecting the sharp edge blocks.

As it can be seen in this case, IQR gave a false detection for blocking artifact and it couldn't determine the context nor the location of error, in addition IQR couldn't detect or measure the ringing artifact. While IDM determined the context and the location of degradation in addition to the type of degradation since it detected blocking and ringing artifact and showed that these artifacts are present in the sharp edge blocks of the reconstructed image.

Compressing the Flat Blocks

In this example, the flat blocks of lena are compressed coarsely. As a result, the flat blocks suffered from blocking and blurring artifacts. Figures 3.43 and 3.44 shows Lena where the flat blocks are compressed using PVRG-JPEG CODEC with -q = 250 and 450 respectively. In this simulation, the amount of compression is increased step by step where for each step the primitives of IDM and the parameter of IQR are computed. From Figure 3.45, it can be seen that IQR indicated that the whole image suffers from blocking and slight blurring. While from the same Figure, IDM indicated that the flat blocks of lena suffer from blocking artifact and from severe blurring artifact where as in the case of Figure 3.44, the whole spatial details of the flat blocks were wiped out. For example, the fractional change of horizontal and vertical edges between the original Lena and the images of Figures 3.43 and 3.44 computed by Melcher and Wolf method are P_{hv}=0.25 for both indicating that there no change in the degree of blockiness (which can be seen that it is not true). Again P_{nhv}=-0.11 for both images indicating hat there no change in the degree of blurriness (also it can be seen that it is not true). While the IDM showed that P_{hv}=3.45 for Figures 3.43 and P_{hv}=4.67 for Figures 3.44 which shows that the degree of blockiness has increased. For blurriness P_{nhv}=-1.00 for both images indicating that all the spatial information in the flat blocks were wiped out. It can be seen that although there were no spatial detail left in the flat blocks, the IQR could not show that, instead it showed a light

Figure 3.11: Sharp Edge Blocks of Lena are Compressed with a Compression Ratio of 12:1

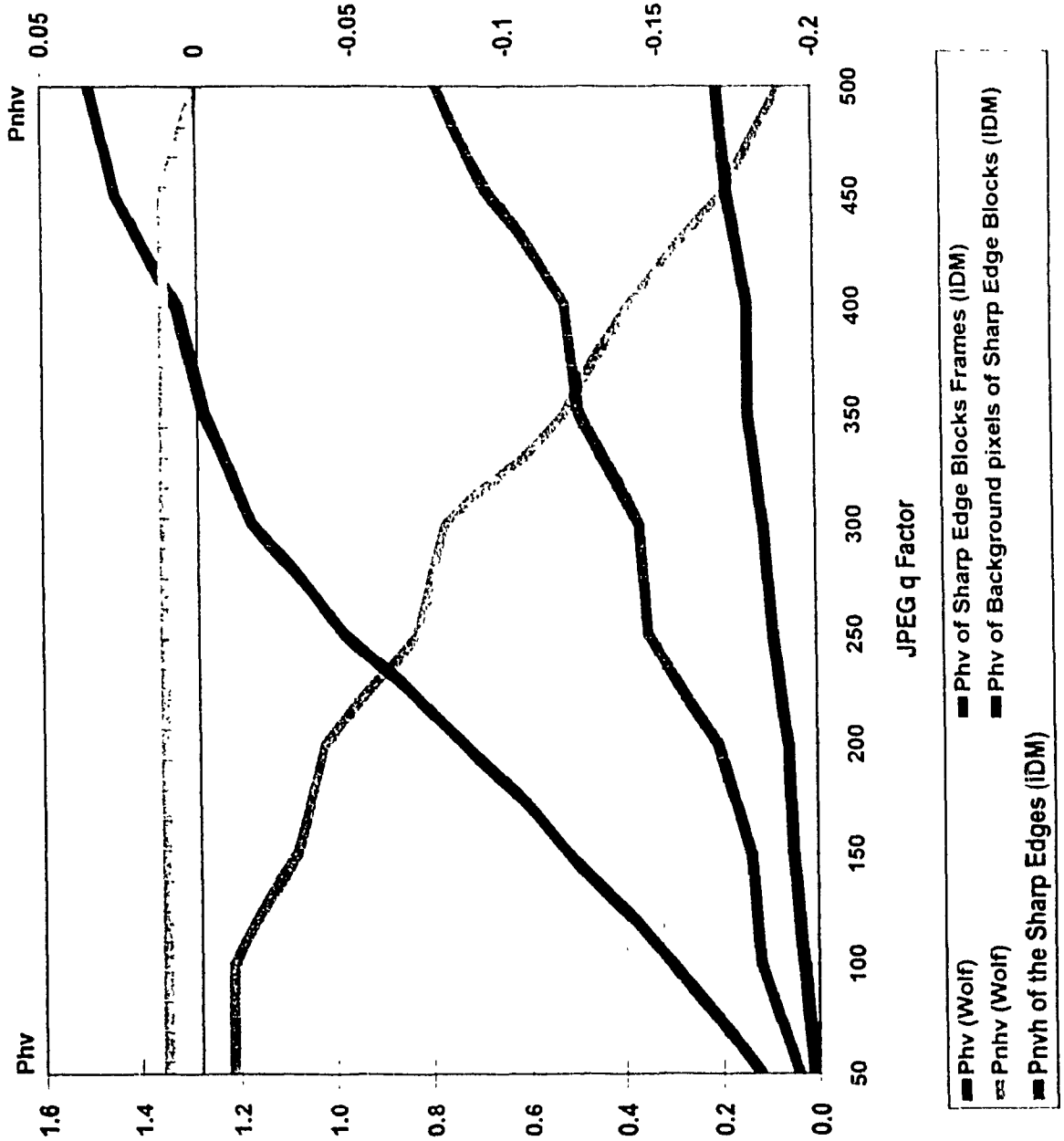

Figure 3.42: Simulation Results of Changing the Compression Ratio for Lena's Sharp Edge Blocks

blurriness affecting the degraded images.

It can be seen that although the blocking and blurring were severe in some of the images, the IQR couldn't present it and couldn't determine the location of degradation. Again in this case, IDM shows superiority over IQR in producing monotonic primitives that measure the amount of the degradation and determine the context and the location of degradation.

3.5.6 Results of Other Images

Different images are used in IDM's simulation namely: Lena, Pepper, Bank, Girl, and House images shown in Figures 1.3, 2.3, 3.46, 3.47, and 3.48 respectively. All of input images produced similar successful output results. Note that the simulation results for different type of images are shown in Appendix A.

Figure 3.13: Flat Blocks of Lena are Compressed with a Compression Ratio of 30:1

Figure 3.11: Flat Blocks of Lena are Compressed with a Compression Ratio of 9:1

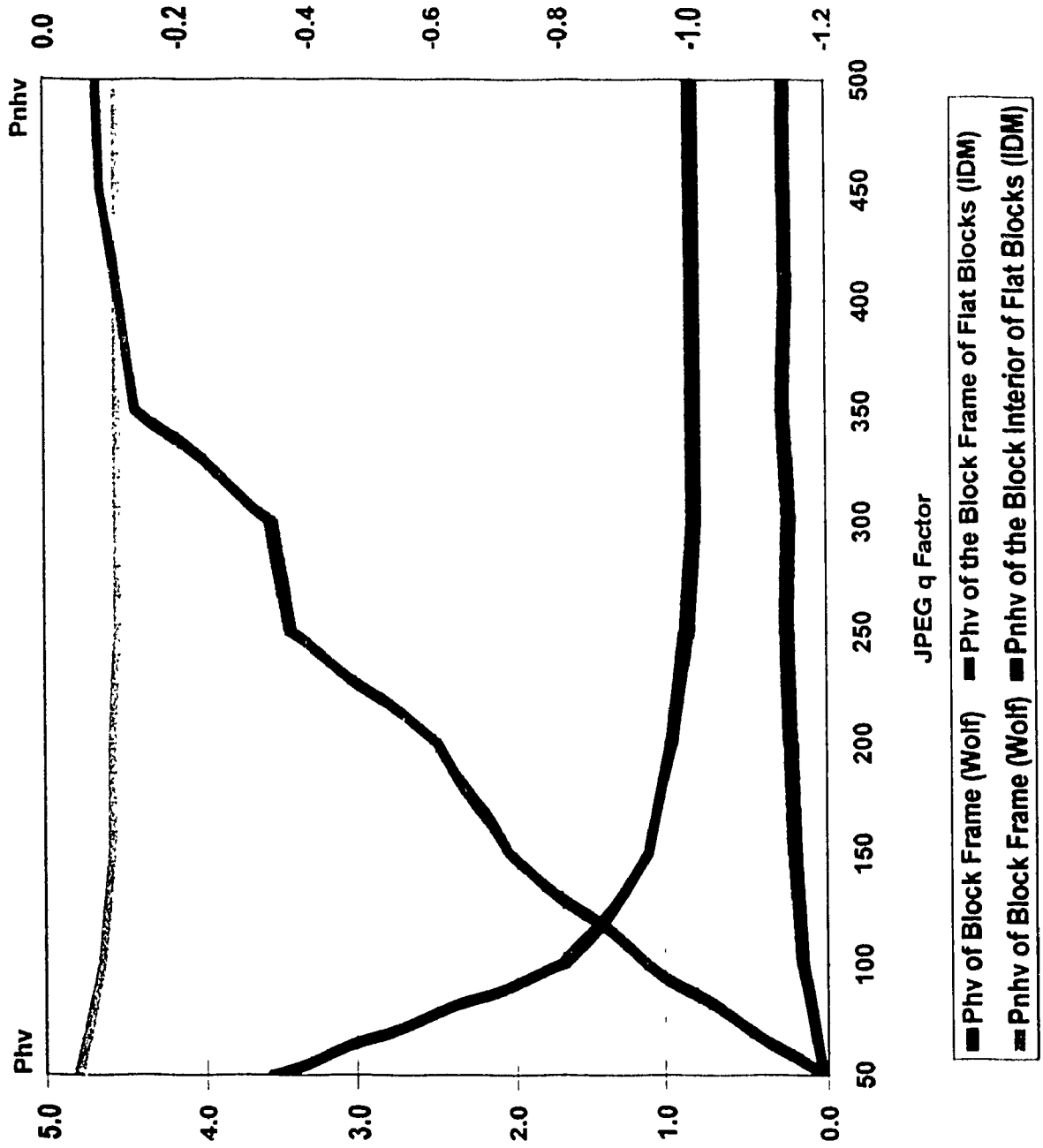

Figure 3.45: Simulation Results of Changing the Compression Ratio for Lena's Flat Blocks

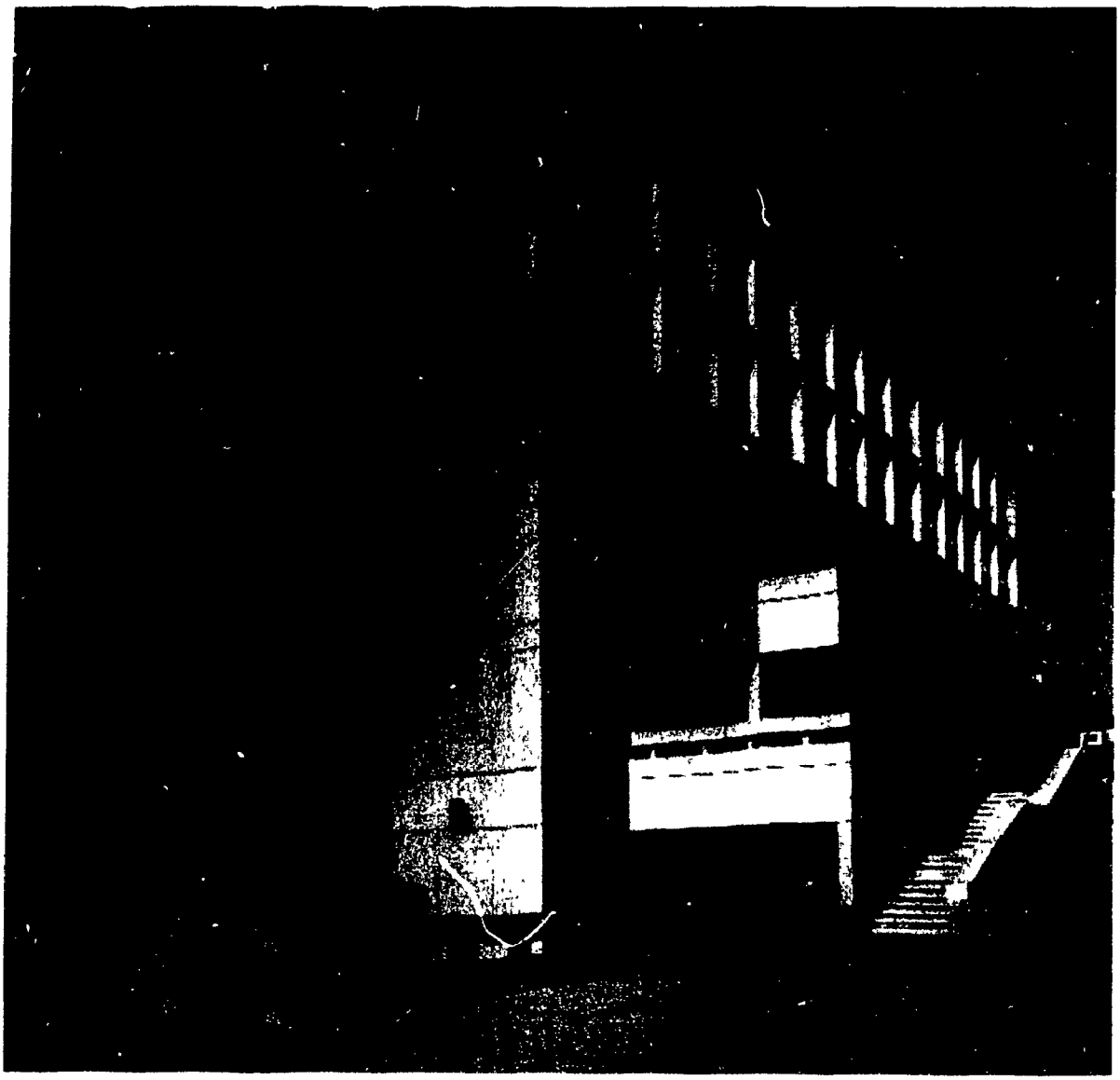

Figure 3.10: Original 512 × 512 Bank

Figure 3.17: Original 256 × 256 Girl

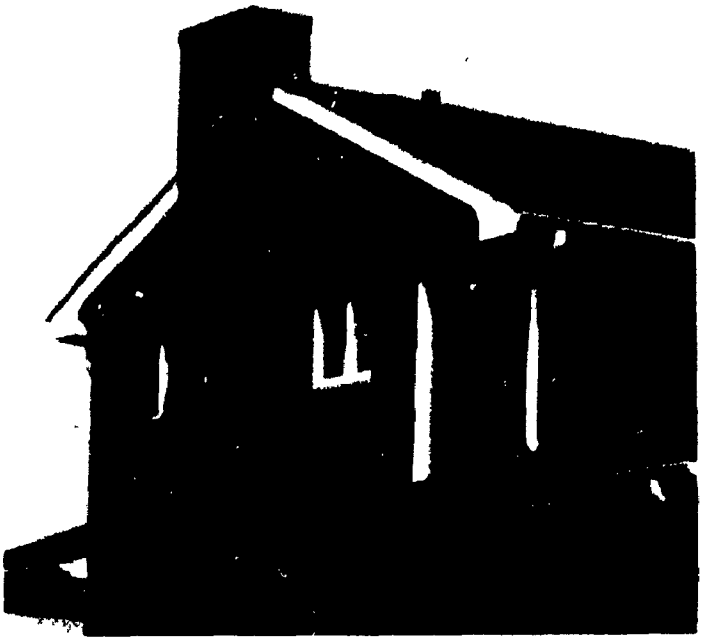

Figure 3.18: Original 256 × 256 House

3.6 Conclusions

From the simulation results, it can be concluded that the Impairment Detection Method succeeded in isolating three types of impairments, namely: *Blocking, Blurring,* and *Spatial edge noise (Ringing).* Also, it succeeded in isolating the context and the locations of the artifacts. In addition, the IDM primitives are good measures since they showed that they are monotonic and have one to one relation with the perceived distortions.

The goals set in the problem solving mechanism were achieved. From all the above, the Impairment Detection Method showed superiority over its original method (the Impairment Quality Rating). When only a certain part of an image is compressed, IQR appeared to be mainly dealing with the artifacts or the texture blocks of that image.

Finally, the extension of the horizontal and vertical edges measurement region in the spatial information histogram $SIH(r, \theta)$ by a wedge angle α around the two principal axes does not provide any help.

Chapter 4

Conclusions and Further Research

4.1 Conclusions

The main work in this thesis is a first step toward solving the problem of objectively evaluating the subjective goodness of transform coding compressed images. From experimental results presented earlier and in Appendix A, the first problem tackling step mentioned in section 1.3.1 was successfully addressed by the IDM.

The measurement of three types of artifacts that are common with transform coding techniques were successfully isolated from each other:

1. Blocking Distortion.
2. Blurring.
3. Spatial Edge Noise (*ringing*).

and the masking phenomenon of vision was taken into consideration by successfully determining and isolating the context of artifacts. Also from the simulation results, the measured primitives for each type of artifact of different images were monotonic and had one to one relation with the perceived distortions. So it can be concluded that the goals set in the problem tackling mechanism of section 1.3.1 were achieved.

When only certain part of an image was compressed, the Impairment Quality Rating appeared to be mainly dealing with the artifacts that were affecting the texture area of that image and it didn't give a correct detection and measurement of these artifacts. In addition, IQR was not able to detect the spatial edge noise artifact.

Using the evaluation criterion set earlier in section 1.3.2, it can be shown that the primitives produced by the IDM are good measures. And from all the above, the IDM showed superiority over its original method (the Impairment Quality Rating).

The IDM is similar to the objective measures that are introduced earlier in Chapter 2 by the means of utilizing the properties of the Human Visual System. Although, the IDM is similar to the PQS, Hosaka plots, and Eskicioglu charts in computing different error factors, it does not combine these factors in an equation that simulates the Mean Opinion Score of subjective evaluations yet as in the case of the PQS, and it is different than Hosaka plots, and Eskicioglu charts by producing numerical primitives output that will be combined in the future in an equation that simulates the MOS, where each primitive can be given different weighting depending on how each type of artifact is weighted by the HVS.

4.2 Further Research

In order to achieve better impairments detection and measurement, and to reach an image quality rating that produces a single number that is highly correlate with subjective measurements results, the following tasks are recommended in the future:

MOS Emulation

All the developed artifacts primitives should be integrated into an equation that correlates well with subjective results and should emulates the Mean Opinion Score (MOS) of the subjective evaluations. This can be achieved through the utilization of joint statistical analysis (regression analysis) of the subjective and objective data sets. This step identifies a subset of the candidate objective measurements that provide useful image quality information. Then the best measurement will be selected by exhaustive search.

Subjective evaluation results are needed in order to be able to use statistical analysis to put the developed artifacts primitives together in a single equation that reflects the MOS. Such results are not commonly available, so subjective evaluation tests need to be carried out properly despite the fact that such tests are expensive and time consuming. These test can be conducted by setting certain test conditions such as the test room size, the size of the display, the viewing distance, the viewing angle, number of assessors, and the testing images.

The human eye weights image impairments in a non linear and a complex way based on their type and their location in an image. For example, subjective studies showed that blocking distortion is ten times more objectionable than equal energy white noise [18] and blocking artifact is more noticeable and objectionable in flat areas than in detailed areas. Such non linearity can be tackled by non-linear regression analysis where different weights are assigned to the primitives of an artifact based on the artifact context and location, and by assigning different

weights for different primitives that are associated with different types of artifacts. Investigation on weighting the developed artifacts primitives should be done.

Inclusion of More Types of Artifacts

Sensitivity to other types of artifacts such as edge discontinuity and color errors should be studied. Adding more primitives to the IDM to cover more types of impairments would make the IDM produce more precise output that is in higher correlation with subjective evaluation results. Edge discontinuity should be checked at the block frame of two adjacent blocks where if an edge is continuous through certain pixels at the block frame of two adjacent blocks in an original image they should remain continuous through the same pixels location at the block frame of the corresponding two adjacent blocks of a reconstructed image.

There are certain types of color artifacts that are associated with transform coding techniques such as color bleeding which occurs near at sharp edges and color fading which is a global error that covers the whole image. Color bleeding artifact can be checked my measuring the the gain in the chrominance energy at the corresponding location of sharp edges in the chrominance part of a reconstructed image. While color fading artifact can be measured by computing the amount of loss in the chrominance energy of the whole reconstructed image.

In order to extend the use of IDM to moving pictures, temporal artifacts such as mosquito noise [11] and jerkiness [11] should be studied. The presence of ringing artifact in some consecutive frames of a sequence of images, would develop the mosquito noise artifact, so by measuring the change in ringing artifacts in each frame, the mosquito noise artifact can be measured. Jerkiness artifact are perceived by an observer when a an originally smooth and continuous motion is perceived as a series of distinct snapshots. Such artifact can be measured by checking the frame repetition.

Practical Problems and Refining

Some CODECs result in a spatially shifted reconstructed images. So the addition of a technique that check and correct the spatial coordination of reconstructed images with respect to original images prior to categorization of image blocks should be investigated. A spatial coordination correction can be achieved by choosing a block of certain size in an original image, then trying to find the its corresponding matching block in the reconstructed image. By checking the coordination of the block in the original image and the constructed image, the amount of horizontal and vertical shifts can be determined.

The use of adaptive techniques to determine the required IDM threshold values such as: sharp edge threshold (T_s) and contour length threshold (T_c) should be investigated. Adaptive techniques that adjust threshold values lead to a better and more precise results. For the sharp edge threshold it can be determined in a block by block basis by checking the maximum and the minimum gray level of the eight surrounding blocks of the sobel image. Contour length threshold can be determined by checking the width and the length of the image, the maximum, and the minimum lengths of the contours of the sharp edges in sharp edge blocks output of the edge block detector.

Bibliography

[1] N. S. Jayant and Peter Noll, *Digital Coding of Waveforms: Principles and Applications to Speech and Video*, Prentice Hall, 1984.

[2] William B. Pennebaker and Joan L. Mitchell, *JPEG Still Image Compression Standard*, Van Nostrand Reinhold, 1993.

[3] Anil K. Jain, *Fundumentals of Digital Image Processing*, Prentice Hall, 1989.

[4] Arun N. Netravali, *Digital Pictures: Representation, Compression, and Standards*, Plenum Press, 1995.

[5] R. C. Gonzalez and R. E. Woods, *Digital Image Processing*, Addison-Wesley, 1992.

[6] Andrew B. Watson, *Digital Images and Human Vision*, MIT Press, 1993.

[7] A. M. Eskicioglu and Paul S. Fisher, "A Survey of Quality Measures for Gray Scale Image Compression", *in Proceeding of 1993 Space and Earth Science Data Compression Workshop, NASA Conference Publication 3191*, pp. 49–61, Snowbird, Utah, April 1993.

[8] Gregory K. Wallace, "The JPEG Picture Compression Standard", *IEEE Trans. Consumer Electronics*, vol. 38, pp. 18–34, February 1992.

[9] Simulation Model Editorial Group, *MPEG Video Simulation Model Three (SM3)*, International Organisation for Standardisation, ISO-IEC JTC1/SC2/WG8, 1990.

[10] International Telegraph and Telephone Consultative Committee, *Video Codec for Audiovisual Services at p x 64 kbit/s. Recommendation H.261*, CCITT, August 1990.

[11] "American National Standard for Telecommunications, Digital Transport of Video Teleconferencing/ Video Telephony Signals Performance Terms, Definitions, and Examples", ANSI T1.801.02-1995, American National Standards Institute, New York, 1995.

[12] K. Taylor, C. Carey-Smith, and I. Goodwin, "Objective Assessment of Video Coding Techniques", *in Proceedings of ITU/BR Workshop on Enhanced Television*, Auckland, New Zealand, October 1993.

[13] C. F. Hall, "Subjective Evaluation of a Perceptual Quality Metric", *in Proceedings of SPIE*, vol. 310, pp. 200–204, 1981.

[14] J. A. Saghri, P. S. Cheatham, and A. Habibi, "Image Quality Measure Based on a Human Visual System Model", *Journal of Optical Engineering*, vol. 28, pp. 813–818, July 1989.

[15] V. R. Algazi, Y. Kato, M. Miyahara, and K. Kotani, "Comparison of Image Coding Techniques with a Picture Quality Scale", *in Proceedings of the SPIE Technical Program on Photonics Instrumentation Conference*, vol. 1771, pp. 396–405, San Diego, CA, July 1992.

[16] J. Vaisey and A. Gersho, "Image Compression with Variable Block Size Segmentation", *IEEE Trans. Signal Processing*, vol. 40, pp. 2040–2060, August 1992.

[17] F. X. J. Lukas and Z. L. Budrikis, "Picture Quality Prediction Based on a Visual Model", *IEEE Transactions on Communications*, vol. COM-30, pp. 1679–1692, July 1982.

[18] Paul M. Farrelle, *Recursive Block Coding for Image Data Compression*, Springer-Verlag, 1990.

[19] A. Puri and R. Aravind, "Motion-Compensated Video Coding with Adaptive Perceptual Quantization", *IEEE Transactions on Circuit and Systems for Video Technology*, vol. 1, pp. 351–361, December 1991.

[20] Hans Marmolin, "Subjective MSE Measures", *IEEE Transactions on Systems, Man, and Cybernetics*, vol. SMC-16, pp. 486–489, May/June 1986.

[21] Ahmet M. Eskicioglu, Paul S. Fisher, and Siyuan Chen, "Image Quality Measures and Their Performance", *in Proceeding of 1994 Space and Earth Science Data Compression Workshop, NASA Conference Publication 3255*, pp. 55–67, Salt Lake City, Utah, April 1994.

[22] Bernd Girod, "What's Wrong with Mean-Squared Error?", in Andrew B. Watson, editor, *Digital Images and Human Vision*, chapter 3, pp. 207–220. MIT Press, Cambridge, MA, USA, 1993.

[23] A. M. Eskicioglu, "An Improved Graphical Quality Measure for Monochrome Compressed Images", *in Proceeding of Optical Engineering Midwest '95, SPIE*, Chicago, IL, May 1995.

[24] Ahmet M. Eskicioglu and Paul S. Fisher, "The Variance of the Difference Image: an Alternative Quality Measure", *in Proceeding of Picture Coding Symposium 1994, CIPIC*, pp. 88–91, Sacramento, California, September 1994.

[25] Portable Video Research Group, Ftp address [36.2.0.35], *PVRG-JPEG CODEC 1.2*, June 1993.

[26] CCIR Recommendation 500-3, "Methods for the Subjective Assessment of the Quality of the Television Pictures", vol. XI, Part 1. XVIth Plenary Assembly, Recommendations and Reports of the CCIR, 1986.

[27] Patrick C. Teo and David J. Heeger, "Perceptual Image Distortion", *in Proceedings of 1st IEEE International Conference on Image Processing*, vol. 1, pp. 982–986, Austin, Texas, 1994.

[28] S. A. Karunasekera and N. G. Kingsbury, "A Distortion Measure for Blocking Artifacts in Images Based on Human Visual Sensitivity", *IEEE Transactions on Image Processing*, vol. 4, pp. 713–724, June 1995.

[29] Albert J. Ahumada, Jr., and Cynthia H. Null, "Image Quality: A Multidimensional Problem", in Andrew B. Watson, editor, *Digital Images and Human Vision*, chapter 3, pp. 141–148. MIT Press, Cambridge, MA, USA, 1993.

[30] Paul J. Hearty, "Achieving and Confirming Optimum Image Quality", in Andrew B. Watson, editor, *Digital Images and Human Vision*, chapter 3, pp. 149–162. MIT Press, Cambridge, MA, USA, 1993.

[31] S. Comes and B. Macq, "Human Visual Quality Criterion", *in Visual communications and Image Processing, SPIE*, vol. 1360, pp. 2–13, Lausanne, October 1990.

[32] S. Comes, O. Bruyndonckx, and B. Macq, "Image Quality Criterion Based on the Cancelation of the Masked Noise", *in Proceedings of ICASSP '95*, vol. 4, pp. 2635–2638, Detroit, Michigan, May 1995.

[33] V. R. Algazi, M. Miyahara, and K. Kotani, "Objective Picture Quality Scale (PQS) for Image Coding", *in SID'92 Digest, Society for Information Display Int'l Symposium*, vol. XXIII, pp. 859–862, Boston, MA, May 1992.

[34] V. R. Algazi, M. Miyahara, K. Kotani, H. Ohiro, and Y. Kato, "Important Distortion Factors in the Encoding of Very High Quality Images", *in Application of Digital Image Processing, SPIE*, vol. XVII, pp. 113–116, San Diego, CA, July 1994.

[35] A. A. Webster, C. T. Jones, M.H. Pinson, S. D. Voran, and S. Wolf, "An Objective Video Quality Assessment System Based on Human Perception", *in Proceedings of SPIE, Human Vision, Visual Processing, and Digital Display IV*, vol. 1913, San Jose, California, February 1993.

[36] S. Wolf, M. Pinson, C. Jones, and A. Webster, "A Summary of Methods of Measurement for Objective Video Quality Parameters Based on the Sobel Filtered Image and Motion Difference Image", T1A1.93/-152, NTIA/ITS, November 1993.

[37] Dwight Melcher and Stephen Wolf, "Objective Measures for Detecting Digital Tiling", T1A1.5/95-104, NTIA/ITS, January 1995.

[38] Nagato Narita, "Subjective Evaluation Method or Quality of Coded Images", *IEEE Transactions on Broadcasting*, vol. 40, pp. 7–13, March 1994.

[39] A. M. Eskicioglu, "A Multi-Dimensional Measure for Image Quality", *in Proceeding of 1995 Space and Earth Science Data Compression Workshop, NASA Conference Publication*, pp. 83–92, Salt Lake City, Utah, March 1995.

[40] Scott Daly, "The Visible Differences Predictor: An Algorithm for the Assessment of Image Fidelity", in Andrew B. Watson, editor, *Digital Images and Human Vision*, chapter 3, pp. 179–206. MIT Press, Cambridge, MA, USA, 1993.

[41] William K. Pratt, *Digital Image Processing*, Wiley-Interscience Publication, 1991.

[42] A. M. Eskicioglu, "Application of Multi-Dimensional Quality Measures to Reconstructed Medical Images", *in Proceeding of CBMS'95, The 8th IEEE Symposium on Computer-Based Medical Systems*, pp. 6-15, Lubbock, Texas, July 1995.

[43] C. Zetzsche and G. Hauske, "Multiple channel model for the prediction of subjective image quality", *in Human Vision, Visual Processing, and Digital Display, SPIE*, vol. 1077, pp. 209–216, Los Angeles, California, January 1989.

[44] S. J. P. Westen, R. L. Lagendijk, and J. Biemond, "Perceptual Image Quality Based on a Multible Channel HVS Model", *in Proceedings of ICASSP '95*, vol. 4, pp. 2351–2354, Detroit, Michigan, May 1995.

[45] Makoto Miyahara, "Quality Assessments for Visual Service", *IEEE Communication Magazine*, vol. 26, pp. 51–60, October 1988.

[46] Tom N. Sweetcorn, *Visual Perception*, NY: Academic Press, 1970.

[47] W.E. Lynch, Amy R. Reibman, and Bede Liu, "Edge Compensated Transform Coding", *in Proceedings of ICIP*, pp. 105-109, 1994.

Appendix A

IDM and IQR Simulation Results

This appendix contains the simulation results of the IDM and of Melcher and Wolf's Method. Two sets of tables are presented, one for the simulation results when $\alpha = 5°$ and the other for the simulation results when $\alpha = 0°$. In addition, the simulation results of IDM when Bank, Girl, House, and Pepper are used as input images and when $\alpha = 0°$ are presented. PVRG-JPEG CODEC v1.1 is used to generate the degraded images required for the simulation, where the output compression ratio is adjusted by adjusting the (-q) option. The Q-Factor option (-q) specifies a multiplicative factor for the quantization: each quantization coefficient of the default quantization matrix is scaled by (-q/50). Table A.1 shows the compression ratios achieved for different -q factors.

Degradation	*Compression Ratio*
PVRG-JPEG -q 50	11:1
PVRG-JPEG -q 100	18:1
PVRG-JPEG -q 150	25:1
PVRG-JPEG -q 200	31:1
PVRG-JPEG -q 250	36:1
PVRG-JPEG -q 300	42:1
PVRG-JPEG -q 350	49:1
PVRG-JPEG -q 400	53:1
PVRG-JPEG -q 450	59:1
PVRG-JPEG -q 500	65:1

Table A.1: Image Compression Ratios of the Used Q-Factor ($-q$)

Degradation	Block Frame			
	g_{hv}	g_{nhv}	P_{hv}	P_{nhv}
NULL	2.36	15.93	N/A	N/A
PVRG-JPEG -q 50	2.63	13.13	0.11	-0.17
PVRG-JPEG -q 100	5.92	8.56	1.42	-0.46
PVRG-JPEG -q 150	8.37	6.13	2.55	-0.61
PVRG-JPEG -q 200	9.83	4.82	3.17	-0.69
PVRG-JPEG -q 250	12.51	3.63	4.30	-0.77
PVRG-JPEG -q 300	12.87	2.96	4.45	-0.81
PVRG-JPEG -q 350	15.14	2.34	5.42	-0.85
PVRG-JPEG -q 400	15.14	2.05	5.42	-0.87
PVRG-JPEG -q 450	15.54	1.72	5.58	-0.89
PVRG-JPEG -q 500	15.40	1.40	5.53	-0.91

Table A.2: Lena, Low Frequency Blocks (Block Frame), $\alpha = 5°$

Degradation	Block Interior			
	g_{hv}	g_{nhv}	P_{hv}	P_{nhv}
NULL	2.37	15.96	N/A	N/A
PVRG-JPEG -q 50	3.63	10.27	0.53	-0.35
PVRG-JPEG -q 100	5.46	3.22	1.30	-0.80
PVRG-JPEG -q 150	5.33	1.15	1.25	-0.93
PVRG-JPEG -q 200	4.91	0.49	1.07	-0.97
PVRG-JPEG -q 250	3.59	0.13	0.51	-0.99
PVRG-JPEG -q 300	2.95	0.05	0.24	-1.00
PVRG-JPEG -q 350	2.20	0.03	-0.07	-1.00
PVRG-JPEG -q 400	1.62	0.04	-0.32	-1.00
PVRG-JPEG -q 450	1.36	0.00	-0.43	-1.00
PVRG-JPEG -q 500	1.29	0.00	-0.46	-1.00

Table A.3: Lena, Low Frequency Blocks (Block Interior), $\alpha = 5°$

Degradation	Block Frame			
	g_{hv}	g_{nhv}	P_{hv}	P_{nhv}
NULL	9.26	60.69	N/A	N/A
PVRG-JPEG -q 50	10.03	59.98	0.08	-0.01
PVRG-JPEG -q 100	11.13	58.23	0.20	-0.04
PVRG-JPEG -q 150	12.75	57.06	0.38	-0.06
PVRG-JPEG -q 200	14.66	56.04	0.58	-0.08
PVRG-JPEG -q 250	16.86	54.34	0.82	-0.10
PVRG-JPEG -q 300	19.21	52.82	1.07	-0.13
PVRG-JPEG -q 350	20.81	51.37	1.25	-0.15
PVRG-JPEG -q 400	23.19	49.90	1.50	-0.18
PVRG-JPEG -q 450	24.02	48.90	1.59	-0.19
PVRG-JPEG -q 500	25.49	46.29	1.75	-0.24

Table A.4: Lena, Texture Blocks (Block Frame), $\alpha = 5°$

Degradation	Block Interior			
	g_{hv}	g_{nhv}	P_{hv}	P_{nhv}
NULL	9.30	61.90	N/A	N/A
PVRG-JPEG -q 50	10.73	60.93	0.15	-0.02
PVRG-JPEG -q 100	13.20	56.25	0.42	-0.09
PVRG-JPEG -q 150	15.59	51.21	0.68	-0.17
PVRG-JPEG -q 200	17.62	47.02	0.89	-0.24
PVRG-JPEG -q 250	19.20	42.74	1.06	-0.31
PVRG-JPEG -q 300	20.15	40.21	1.17	-0.35
PVRG-JPEG -q 350	21.28	36.74	1.29	-0.41
PVRG-JPEG -q 400	22.24	33.72	1.39	-0.46
PVRG-JPEG -q 450	22.22	30.80	1.39	-0.50
PVRG-JPEG -q 500	22.38	27.98	1.41	-0.55

Table A.5: Lena, Texture Blocks (Block Interior), $\alpha = 5°$

Degradation	Block Frame			
	g_{hv}	g_{nhv}	P_{hv}	P_{nhv}
NULL	10.18	83.55	N/A	N/A
PVRG-JPEG -q 50	11.34	84.55	0.11	0.01
PVRG-JPEG -q 100	12.44	86.05	0.22	0.03
PVRG-JPEG -q 150	12.86	87.92	0.26	0.05
PVRG-JPEG -q 200	14.15	89.10	0.39	0.07
PVRG-JPEG -q 250	16.82	88.59	0.65	0.06
PVRG-JPEG -q 300	18.27	89.41	0.79	0.07
PVRG-JPEG -q 350	20.32	88.90	1.00	0.06
PVRG-JPEG -q 400	20.89	90.74	1.05	0.09
PVRG-JPEG -q 450	22.60	90.81	1.22	0.09
PVRG-JPEG -q 500	24.31	90.97	1.39	0.09

Table A.6: Lena, Sharp Edge Blocks (Block Frame), $\alpha = 5°$

Degradation	Block Interior (Sharp Edge Pixels)			
	g_{hv}	g_{nhv}	P_{hv}	P_{nhv}
NULL	9.54	124.99	N/A	N/A
PVRG-JPEG -q 50	9.46	125.61	-0.01	0.01
PVRG-JPEG -q 100	11.19	122.63	0.17	-0.02
PVRG-JPEG -q 150	12.18	119.55	0.28	-0.04
PVRG-JPEG -q 200	12.11	118.20	0.27	-0.05
PVRG-JPEG -q 250	13.89	113.12	0.46	-0.09
PVRG-JPEG -q 300	14.64	111.30	0.53	-0.11
PVRG-JPEG -q 350	18.06	105.12	0.89	-0.16
PVRG-JPEG -q 400	18.74	103.44	0.96	-0.17
PVRG-JPEG -q 450	22.69	97.69	1.38	-0.22
PVRG-JPEG -q 500	25.13	94.59	1.63	-0.24

Table A.7: Lena, Sharp Edge Blocks (Sharp Edge pixels), $\alpha = 5°$

Degradation	Block Interior (Background Pixels)			
	g_{hv}	g_{nhv}	P_{hv}	P_{nhv}
NULL	4.07	24.90	N/A	N/A
PVRG-JPEG -q 50	4.70	27.04	0.15	0.09
PVRG-JPEG -q 100	5.49	27.65	0.35	0.11
PVRG-JPEG -q 150	6.73	27.71	0.65	0.11
PVRG-JPEG -q 200	8.20	26.83	1.01	0.08
PVRG-JPEG -q 250	9.90	25.46	1.43	0.02
PVRG-JPEG -q 300	10.82	24.87	1.66	0.00
PVRG-JPEG -q 350	11.50	24.06	1.83	-0.03
PVRG-JPEG -q 400	12.03	23.71	1.96	-0.05
PVRG-JPEG -q 450	12.72	23.12	2.13	-0.07
PVRG-JPEG -q 500	12.96	22.08	2.18	-0.11

Table A.8: Lena, Sharp Edge Blocks (Background pixels), $\alpha = 5°$

Degradation	g_{hv}	g_{nhv}	P_{hv}	P_{nhv}
NULL	6.66	46.13	N/A	N/A
PVRG-JPEG -q 50	7.61	44.38	0.14	-0.04
PVRG-JPEG -q 100	9.54	40.66	0.43	-0.12
PVRG-JPEG -q 150	11.05	38.37	0.66	-0.17
PVRG-JPEG -q 200	12.27	36.77	0.84	-0.20
PVRG-JPEG -q 250	13.63	34.83	1.05	-0.25
PVRG-JPEG -q 300	14.43	33.76	1.17	-0.27
PVRG-JPEG -q 350	15.50	32.29	1.33	-0.30
PVRG-JPEG -q 400	16.27	31.17	1.44	-0.32
PVRG-JPEG -q 450	16.68	30.01	1.51	-0.35
PVRG-JPEG -q 500	17.13	28.53	1.57	-0.38

Table A.9: Lena, Simulation Results of IQR, $\alpha = 5°$

Degradation	Block Frame			
	g_{hv}	g_{nhv}	P_{hv}	P_{nhv}
NULL	0.78	17.31	N/A	N/A
PVRG-JPEG -q 50	1.08	14.68	0.38	-0.15
PVRG-JPEG -q 100	4.52	9.77	4.80	-0.44
PVRG-JPEG -q 150	7.54	6.96	8.67	-0.60
PVRG-JPEG -q 200	9.09	5.55	10.70	-0.68
PVRG-JPEG -q 250	11.91	4.23	14.30	-0.76
PVRG-JPEG -q 300	12.33	3.50	14.80	-0.80
PVRG-JPEG -q 350	14.68	2.81	17.80	-0.84
PVRG-JPEG -q 400	14.74	2.44	17.90	-0.86
PVRG-JPEG -q 450	15.22	2.03	18.50	-0.88
PVRG-JPEG -q 500	14.96	1.83	18.20	-0.89

Table A.10: Lena, Low Frequency Blocks (Block Frame), $\alpha = 0°$

Degradation	Block Interior			
	g_{hv}	g_{nhv}	P_{hv}	P_{nhv}
NULL	0.90	17.24	N/A	N/A
PVRG-JPEG -q 50	2.72	11.18	2.00	-0.35
PVRG-JPEG -q 100	5.31	3.37	4.90	-0.80
PVRG-JPEG -q 150	5.31	1.18	4.90	-0.93
PVRG-JPEG -q 200	4.90	0.50	4.40	-0.97
PVRG-JPEG -q 250	3.59	0.14	3.00	-0.99
PVRG-JPEG -q 300	2.95	0.05	2.30	-1.00
PVRG-JPEG -q 350	2.20	0.03	1.40	-1.00
PVRG-JPEG -q 400	1.62	0.04	0.80	-1.00
PVRG-JPEG -q 450	1.36	0.00	0.50	-1.00
PVRG-JPEG -q 500	1.29	0.00	0.40	-1.00

Table A.11: Lena, Low Frequency Blocks (Block Interior), $\alpha = 0°$

Degradation	Block Frame			
	g_{hv}	g_{nhv}	P_{hv}	P_{nhv}
NULL	0.78	69.18	N/A	N/A
PVRG-JPEG -q 50	1.00	69.01	0.28	0.00
PVRG-JPEG -q 100	2.80	66.56	2.59	-0.04
PVRG-JPEG -q 150	4.83	64.98	5.19	-0.06
PVRG-JPEG -q 200	7.09	63.60	8.10	-0.08
PVRG-JPEG -q 250	9.64	61.56	11.40	-0.11
PVRG-JPEG -q 300	11.99	60.04	14.40	-0.13
PVRG-JPEG -q 350	14.24	57.94	17.26	-0.16
PVRG-JPEG -q 400	16.84	56.25	20.60	-0.19
PVRG-JPEG -q 450	18.27	54.65	22.40	-0.21
PVRG-JPEG -q 500	19.78	52.00	24.36	-0.25

Table A.12: Lena, Texture Blocks (Block Frame), $\alpha = 0°$

Degradation	Block Interior			
	g_{hv}	g_{nhv}	P_{hv}	P_{nhv}
NULL	0.80	70.40	N/A	N/A
PVRG-JPEG -q 50	1.81	69.86	1.26	-0.01
PVRG-JPEG -q 100	6.01	63.44	6.51	-0.10
PVRG-JPEG -q 150	9.27	57.53	10.59	-0.18
PVRG-JPEG -q 200	12.34	52.30	14.40	-0.26
PVRG-JPEG -q 250	14.81	47.12	17.50	-0.33
PVRG-JPEG -q 300	16.27	44.08	19.34	-0.37
PVRG-JPEG -q 350	17.60	40.42	21.00	-0.43
PVRG-JPEG -q 400	19.33	36.63	23.16	-0.48
PVRG-JPEG -q 450	19.64	33.38	23.55	-0.53
PVRG-JPEG -q 500	20.16	30.20	24.20	-0.57

Table A.13: Lena, Texture Blocks (Block Interior), $\alpha = 0°$

Degradation	Block Frame			
	g_{hv}	g_{nhv}	P_{hv}	P_{nhv}
NULL	0.95	92.78	N/A	N/A
PVRG-JPEG -q 50	0.71	95.18	-0.25	0.03
PVRG-JPEG -q 100	0.88	97.61	-0.07	0.05
PVRG-JPEG -q 150	1.70	99.08	0.79	0.07
PVRG-JPEG -q 200	4.25	99.01	3.47	0.07
PVRG-JPEG -q 250	6.48	98.94	5.80	0.07
PVRG-JPEG -q 300	8.69	98.98	8.15	0.07
PVRG-JPEG -q 350	10.79	98.43	10.36	0.06
PVRG-JPEG -q 400	12.34	99.29	12.00	0.07
PVRG-JPEG -q 450	14.04	99.37	13.78	0.07
PVRG-JPEG -q 500	16.02	99.26	15.86	0.07

Table A.14: Lena, Sharp Edge Blocks (Block Frame), $\alpha = 0°$

Degradation	Block Interior (Sharp Edge Pixels)			
	g_{hv}	g_{nhv}	P_{hv}	P_{nhv}
NULL	0.38	134.14	N/A	N/A
PVRG-JPEG -q 50	0.31	134.76	-0.18	0.00
PVRG-JPEG -q 100	1.75	132.07	3.61	-0.02
PVRG-JPEG -q 150	4.25	127.47	10.18	-0.05
PVRG-JPEG -q 200	5.48	124.84	13.42	-0.07
PVRG-JPEG -q 250	7.35	119.66	18.34	-0.11
PVRG-JPEG -q 300	10.06	115.88	25.47	-0.14
PVRG-JPEG -q 350	14.32	108.86	36.68	-0.19
PVRG-JPEG -q 400	15.16	107.01	38.90	-0.20
PVRG-JPEG -q 450	19.98	100.41	51.57	-0.25
PVRG-JPEG -q 500	22.43	97.29	58.03	-0.27

Table A.15: Lena, Sharp Edge Blocks (Sharp Edge pixels), $\alpha = 0°$

Degradation	Block Interior (Background Pixels)			
	g_{hv}	g_{nhv}	P_{hv}	P_{nhv}
NULL	0.60	28.37	N/A	N/A
PVRG-JPEG -q 50	0.48	31.26	-0.20	0.10
PVRG-JPEG -q 100	1.18	31.96	0.97	0.13
PVRG-JPEG -q 150	2.84	31.59	10.18	0.11
PVRG-JPEG -q 200	4.57	30.46	6.62	0.07
PVRG-JPEG -q 250	6.53	28.82	9.88	0.02
PVRG-JPEG -q 300	7.96	27.73	12.27	-0.02
PVRG-JPEG -q 350	8.87	26.69	13.77	-0.06
PVRG-JPEG -q 400	9.75	25.99	15.25	-0.08
PVRG-JPEG -q 450	10.62	25.21	16.70	-0.11
PVRG-JPEG -q 500	10.99	24.05	17.32	-0.15

Table A.16: Lena, Sharp Edge Blocks (Background pixels), $\alpha = 0°$

Degradation	g_{hv}	g_{nhv}	P_{hv}	P_{nhv}
NULL	0.82	51.97	N/A	N/A
PVRG-JPEG -q 50	1.57	50.42	0.91	-0.03
PVRG-JPEG -q 100	4.27	45.93	4.20	-0.12
PVRG-JPEG -q 150	6.29	43.13	6.67	-0.17
PVRG-JPEG -q 200	8.06	40.98	8.83	-0.21
PVRG-JPEG -q 250	9.75	38.71	10.89	-0.26
PVRG-JPEG -q 300	10.83	37.37	12.21	-0.28
PVRG-JPEG -q 350	12.14	35.65	13.80	-0.31
PVRG-JPEG -q 400	13.22	34.22	15.12	-0.34
PVRG-JPEG -q 450	13.90	32.79	15.95	-0.37
PVRG-JPEG -q 500	14.47	31.19	16.65	-0.40

Table A.17: Lena, Simulation Results of IQR, $\alpha = 0°$

Degradation	Block Frame	
	P_{hv}	P_{nhv}
PVRG-JPEG -q 50	1.77	-0.23
PVRG-JPEG -q 100	6.00	-0.48
PVRG-JPEG -q 150	8.27	-0.61
PVRG-JPEG -q 200	10.00	-0.68
PVRG-JPEG -q 250	11.46	-0.74
PVRG-JPEG -q 300	11.87	-0.78
PVRG-JPEG -q 350	12.31	-0.80
PVRG-JPEG -q 400	13.00	-0.81
PVRG-JPEG -q 450	13.06	-0.82
PVRG-JPEG -q 500	13.30	-0.82

Table A.18: Bank, Low Frequency Blocks (Block Frame), $\alpha = 0°$

Degradation	Block Interior	
	P_{hv}	P_{nhv}
PVRG-JPEG -q 50	3.25	-0.52
PVRG-JPEG -q 100	3.75	-0.87
PVRG-JPEG -q 150	2.55	-0.96
PVRG-JPEG -q 200	1.10	-0.99
PVRG-JPEG -q 250	0.27	-1.00
PVRG-JPEG -q 300	-0.31	-1.00
PVRG-JPEG -q 350	-0.55	-1.00
PVRG-JPEG -q 400	-0.73	-1.00
PVRG-JPEG -q 450	-0.82	-1.00
PVRG-JPEG -q 500	-0.96	-1.00

Table A.19: Bank, Low Frequency Blocks (Block Interior), $\alpha = 0°$

Degradation	Block Frame	
	P_{hv}	P_{nhv}
PVRG-JPEG -q 50	0.18	0.05
PVRG-JPEG -q 100	2.11	0.05
PVRG-JPEG -q 150	4.58	0.01
PVRG-JPEG -q 200	6.75	-0.01
PVRG-JPEG -q 250	8.58	-0.04
PVRG-JPEG -q 300	10.15	-0.07
PVRG-JPEG -q 350	11.89	-0.11
PVRG-JPEG -q 400	14.26	-0.13
PVRG-JPEG -q 450	14.75	-0.14
PVRG-JPEG -q 500	16.06	-0.18

Table A.20: Bank, Texture Blocks (Block Frame), $\alpha = 0°$

Degradation	Block Interior	
	P_{hv}	P_{nhv}
PVRG-JPEG -q 50	1.58	0.03
PVRG-JPEG -q 100	7.13	-0.06
PVRG-JPEG -q 150	11.83	-0.16
PVRG-JPEG -q 200	14.24	-0.22
PVRG-JPEG -q 250	15.44	-0.28
PVRG-JPEG -q 300	16.77	-0.33
PVRG-JPEG -q 350	17.22	-0.38
PVRG-JPEG -q 400	17.59	-0.41
PVRG-JPEG -q 450	18.13	-0.44
PVRG-JPEG -q 500	18.63	-0.47

Table A.21: Bank, Texture Blocks (Block Interior), $\alpha = 0°$

Degradation	Block Frame	
	P_{hv}	P_{nhv}
PVRG-JPEG -q 50	0.01	0.06
PVRG-JPEG -q 100	1.58	0.08
PVRG-JPEG -q 150	3.46	0.09
PVRG-JPEG -q 200	4.72	0.11
PVRG-JPEG -q 250	7.20	0.09
PVRG-JPEG -q 300	9.28	0.09
PVRG-JPEG -q 350	11.06	0.08
PVRG-JPEG -q 400	11.91	0.08
PVRG-JPEG -q 450	13.88	0.07
PVRG-JPEG -q 500	15.96	0.05

Table A.22: Bank, Sharp Edge Blocks (Block Frame), $\alpha = 0°$

Degradation	Sharp Edge Pixels	
	P_{hv}	P_{nhv}
PVRG-JPEG -q 50	1.10	-0.01
PVRG-JPEG -q 100	6.34	-0.08
PVRG-JPEG -q 150	10.15	-0.13
PVRG-JPEG -q 200	13.80	-0.18
PVRG-JPEG -q 250	19.27	-0.25
PVRG-JPEG -q 300	22.26	-0.28
PVRG-JPEG -q 350	24.85	-0.33
PVRG-JPEG -q 400	26.01	-0.35
PVRG-JPEG -q 450	27.68	-0.38
PVRG-JPEG -q 500	30.01	-0.41

Table A.23: Bank, Sharp Edge Blocks (Sharp Edge Pixels), $\alpha = 0°$

Degradation	Background pixels	
	P_{hv}	P_{nhv}
PVRG-JPEG -q 50	1.19	0.19
PVRG-JPEG -q 100	5.03	0.22
PVRG-JPEG -q 150	8.30	0.24
PVRG-JPEG -q 200	11.08	0.25
PVRG-JPEG -q 250	14.27	0.21
PVRG-JPEG -q 300	17.16	0.17
PVRG-JPEG -q 350	18.95	0.13
PVRG-JPEG -q 400	20.00	0.12
PVRG-JPEG -q 450	22.00	0.08
PVRG-JPEG -q 500	23.95	0.03

Table A.24: Bank, Sharp Edge Blocks (Background pixels), $\alpha = 0°$

Degradation	Block Frame	
	P_{hv}	P_{nhv}
PVRG-JPEG -q 50	3.38	-0.28
PVRG-JPEG -q 100	6.75	-0.43
PVRG-JPEG -q 150	9.51	-0.55
PVRG-JPEG -q 200	12.31	-0.59
PVRG-JPEG -q 250	13.75	-0.69
PVRG-JPEG -q 300	14.90	-0.70
PVRG-JPEG -q 350	16.69	-0.79
PVRG-JPEG -q 400	18.84	-0.82
PVRG-JPEG -q 450	19.00	-0.86
PVRG-JPEG -q 500	19.36	-0.88

Table A.25: Girl, Low Frequency Blocks (Block Frame), $\alpha = 0°$

Degradation	Block Interior	
	P_{hv}	P_{nhv}
PVRG-JPEG -q 50	4.18	-0.51
PVRG-JPEG -q 100	5.94	-0.80
PVRG-JPEG -q 150	6.44	-0.91
PVRG-JPEG -q 200	4.90	-0.95
PVRG-JPEG -q 250	3.64	-0.99
PVRG-JPEG -q 300	2.65	-1.00
PVRG-JPEG -q 350	0.56	-1.00
PVRG-JPEG -q 400	0.32	-1.00
PVRG-JPEG -q 450	0.21	-1.00
PVRG-JPEG -q 500	0.03	-1.00

Table A.26: Girl, Low Frequency Blocks (Block Interior), $\alpha = 0°$

Degradation	Block Frame	
	P_{hv}	P_{nhv}
PVRG-JPEG -q 50	0.23	0.01
PVRG-JPEG -q 100	0.38	0.01
PVRG-JPEG -q 150	1.37	0.01
PVRG-JPEG -q 200	3.97	-0.02
PVRG-JPEG -q 250	7.00	-0.06
PVRG-JPEG -q 300	8.87	-0.08
PVRG-JPEG -q 350	12.64	-0.09
PVRG-JPEG -q 400	15.62	-0.12
PVRG-JPEG -q 450	18.09	-0.14
PVRG-JPEG -q 500	23.22	-0.20

Table A.27: Girl, Texture Blocks (Block Frame), $\alpha = 0°$

Degradation	Block Interior	
	P_{hv}	P_{nhv}
PVRG-JPEG -q 50	0.67	0.01
PVRG-JPEG -q 100	3.81	-0.05
PVRG-JPEG -q 150	8.08	-0.13
PVRG-JPEG -q 200	14.18	-0.23
PVRG-JPEG -q 250	17.74	-0.31
PVRG-JPEG -q 300	20.78	-0.38
PVRG-JPEG -q 350	21.94	-0.42
PVRG-JPEG -q 400	26.35	-0.49
PVRG-JPEG -q 450	28.85	-0.55
PVRG-JPEG -q 500	30.57	-0.61

Table A.28: Girl, Texture Blocks (Block Interior), $\alpha = 0°$

Degradation	Block Frame	
	P_{hv}	P_{nhv}
PVRG-JPEG -q 50	0.30	0.05
PVRG-JPEG -q 100	0.89	0.06
PVRG-JPEG -q 150	1.06	0.10
PVRG-JPEG -q 200	1.32	0.10
PVRG-JPEG -q 250	1.48	0.11
PVRG-JPEG -q 300	3.22	0.11
PVRG-JPEG -q 350	5.86	0.12
PVRG-JPEG -q 400	7.00	0.12
PVRG-JPEG -q 450	7.90	0.13
PVRG-JPEG -q 500	8.37	0.16

Table A.29: Girl, Sharp Edge Blocks (Block Frame), $\alpha = 0°$

Degradation	Sharp Edge Pixels	
	P_{hv}	P_{nhv}
PVRG-JPEG -q 50	0.09	-0.01
PVRG-JPEG -q 100	0.1	-0.01
PVRG-JPEG -q 150	0.21	-0.04
PVRG-JPEG -q 200	0.32	-0.05
PVRG-JPEG -q 250	0.43	-0.05
PVRG-JPEG -q 300	0.48	-0.05
PVRG-JPEG -q 350	0.57	-0.10
PVRG-JPEG -q 400	2.74	-0.13
PVRG-JPEG -q 450	6.04	-0.18
PVRG-JPEG -q 500	9.30	-0.24

Table A.30: Girl, Sharp Edge Blocks (Sharp Edge Pixels), $\alpha = 0°$

Degradation	Background pixels	
	P_{hv}	P_{nhv}
PVRG-JPEG -q 50	0.01	0.18
PVRG-JPEG -q 100	0.08	0.28
PVRG-JPEG -q 150	0.71	0.33
PVRG-JPEG -q 200	2.33	0.36
PVRG-JPEG -q 250	3.29	0.40
PVRG-JPEG -q 300	4.00	0.41
PVRG-JPEG -q 350	5.82	0.42
PVRG-JPEG -q 400	6.55	0.35
PVRG-JPEG -q 450	8.53	0.37
PVRG-JPEG -q 500	13.63	0.27

Table A.31: Girl, Sharp Edge Blocks (Background pixels), $\alpha = 0°$

Degradation	Block Frame	
	P_{hv}	P_{nhv}
PVRG-JPEG -q 50	1.67	-0.30
PVRG-JPEG -q 100	3.73	-0.50
PVRG-JPEG -q 150	8.39	-0.70
PVRG-JPEG -q 200	8.00	-0.77
PVRG-JPEG -q 250	4.92	-0.79
PVRG-JPEG -q 300	6.17	-0.83
PVRG-JPEG -q 350	10.20	-0.86
PVRG-JPEG -q 400	13.53	-0.86
PVRG-JPEG -q 450	15.48	-0.87
PVRG-JPEG -q 500	19.33	-0.87

Table A.32: House, Low Frequency Blocks (Block Frame), $\alpha = 0°$

Degradation	Block Interior	
	P_{hv}	P_{nhv}
PVRG-JPEG -q 50	1.11	-0.47
PVRG-JPEG -q 100	2.74	-0.85
PVRG-JPEG -q 150	1.48	-0.97
PVRG-JPEG -q 200	0.68	-0.9
PVRG-JPEG -q 250	0.23	-1.00
PVRG-JPEG -q 300	-0.06	-1.00
PVRG-JPEG -q 350	-0.46	-1.00
PVRG-JPEG -q 400	-0.38	-1.00
PVRG-JPEG -q 450	-0.65	-1.00
PVRG-JPEG -q 500	-0.80	-1.00

Table A.33: House, Low Frequency Blocks (Block Interior), $\alpha = 0°$

Degradation	Block Frame	
	P_{hv}	P_{nhv}
PVRG-JPEG -q 50	0.05	0.01
PVRG-JPEG -q 100	0.79	-0.01
PVRG-JPEG -q 150	3.75	-0.06
PVRG-JPEG -q 200	6.67	-0.11
PVRG-JPEG -q 250	8.52	-0.14
PVRG-JPEG -q 300	12.15	-0.18
PVRG-JPEG -q 350	16.43	-0.19
PVRG-JPEG -q 400	17.60	-0.24
PVRG-JPEG -q 450	18.07	-0.28
PVRG-JPEG -q 500	19.99	-0.29

Table A.34: House, Texture Blocks (Block Frame), $\alpha = 0°$

Degradation	Block Interior	
	P_{hv}	P_{nhv}
PVRG-JPEG -q 50	0.42	0.01
PVRG-JPEG -q 100	2.50	-0.08
PVRG-JPEG -q 150	8.90	-0.20
PVRG-JPEG -q 200	11.82	-0.28
PVRG-JPEG -q 250	17.82	-0.37
PVRG-JPEG -q 300	21.32	-0.41
PVRG-JPEG -q 350	25.51	-0.47
PVRG-JPEG -q 400	28.53	-0.52
PVRG-JPEG -q 450	30.57	-0.58
PVRG-JPEG -q 500	31.21	-0.58

Table A.35: House, Texture Blocks (Block Interior), $\alpha = 0°$

Degradation	Block Frame	
	P_{hv}	P_{nhv}
PVRG-JPEG -q 50	2.49	0.01
PVRG-JPEG -q 100	4.84	0.04
PVRG-JPEG -q 150	13.29	-0.02
PVRG-JPEG -q 200	15.25	-0.02
PVRG-JPEG -q 250	16.39	-0.02
PVRG-JPEG -q 300	19.13	-0.03
PVRG-JPEG -q 350	24.31	-0.09
PVRG-JPEG -q 400	27.23	-0.09
PVRG-JPEG -q 450	29.01	-0.10
PVRG-JPEG -q 500	38.14	-0.12

Table A.36: House, Sharp Edge Blocks (Block Frame), $\alpha = 0°$

Degradation	Sharp Edge Pixels	
	P_{hv}	P_{nhv}
PVRG-JPEG -q 50	8.67	-0.12
PVRG-JPEG -q 100	12.97	-0.19
PVRG-JPEG -q 150	15.13	-0.23
PVRG-JPEG -q 200	16.83	-0.27
PVRG-JPEG -q 250	17.87	-0.29
PVRG-JPEG -q 300	18.79	-0.31
PVRG-JPEG -q 350	23.03	-0.39
PVRG-JPEG -q 400	25.32	-0.45
PVRG-JPEG -q 450	28.57	-0.51
PVRG-JPEG -q 500	32.15	-0.56

Table A.37: House, Sharp Edge Blocks (Sharp Edge Pixels), $\alpha = 0°$

Degradation	Background pixels	
	P_{hv}	P_{nhv}
PVRG-JPEG -q 50	2.03	0.07
PVRG-JPEG -q 100	8.86	0.02
PVRG-JPEG -q 150	13.32	0.02
PVRG-JPEG -q 200	19.77	0.01
PVRG-JPEG -q 250	22.57	0.01
PVRG-JPEG -q 300	23.06	0.00
PVRG-JPEG -q 350	27.92	-0.09
PVRG-JPEG -q 400	30.71	-0.18
PVRG-JPEG -q 450	34.11	-0.24
PVRG-JPEG -q 500	40.52	-0.3

Table A.38: House, Sharp Edge Blocks (Background pixels), $\alpha = 0°$

Degradation	Block Frame	
	P_{hv}	P_{nhv}
PVRG-JPEG -q 50	0.45	-0.14
PVRG-JPEG -q 100	4.31	-0.38
PVRG-JPEG -q 150	7.57	-0.55
PVRG-JPEG -q 200	10.37	-0.62
PVRG-JPEG -q 250	14.04	-0.70
PVRG-JPEG -q 300	17.24	-0.75
PVRG-JPEG -q 350	17.28	-0.79
PVRG-JPEG -q 400	17.94	-0.82
PVRG-JPEG -q 450	19.19	-0.83
PVRG-JPEG -q 500	19.20	-0.86

Table A.39: Pepper, Low Frequency Blocks (Block Frame), $\alpha = 0°$

Degradation	Block Interior	
	P_{hv}	P_{nhv}
PVRG-JPEG -q 50	2.17	-0.32
PVRG-JPEG -q 100	5.98	-0.78
PVRG-JPEG -q 150	5.85	-0.92
PVRG-JPEG -q 200	5.33	-0.97
PVRG-JPEG -q 250	3.50	-0.99
PVRG-JPEG -q 300	2.36	-1.00
PVRG-JPEG -q 350	1.27	-1.00
PVRG-JPEG -q 400	0.47	-1.00
PVRG-JPEG -q 450	0.14	-1.00
PVRG-JPEG -q 500	-0.39	-1.00

Table A.40: Pepper, Low Frequency Blocks (Block Interior), $\alpha = 0°$

Degradation	Block Frame	
	P_{hv}	P_{nhv}
PVRG-JPEG -q 50	0.07	0.00
PVRG-JPEG -q 100	0.85	-0.02
PVRG-JPEG -q 150	2.88	-0.04
PVRG-JPEG -q 200	5.95	-0.05
PVRG-JPEG -q 250	10.45	-0.08
PVRG-JPEG -q 300	13.80	-0.10
PVRG-JPEG -q 350	17.75	-0.11
PVRG-JPEG -q 400	22.93	-0.14
PVRG-JPEG -q 450	26.75	-0.16
PVRG-JPEG -q 500	29.23	-0.19

Table A.41: Pepper, Texture Blocks (Block Frame), $\alpha = 0°$

Degradation	Block Interior	
	P_{hv}	P_{nhv}
PVRG-JPEG -q 50	0.24	0.00
PVRG-JPEG -q 100	3.18	-0.08
PVRG-JPEG -q 150	7.43	-0.17
PVRG-JPEG -q 200	11.43	-0.24
PVRG-JPEG -q 250	14.61	-0.31
PVRG-JPEG -q 300	17.35	-0.36
PVRG-JPEG -q 350	19.17	-0.41
PVRG-JPEG -q 400	20.64	-0.46
PVRG-JPEG -q 450	21.93	-0.49
PVRG-JPEG -q 500	22.22	-0.53

Table A.42: Pepper, Texture Blocks (Block Interior), $\alpha = 0°$

Degradation	Block Frame	
	P_{hv}	P_{nhv}
PVRG-JPEG -q 50	0.03	0.03
PVRG-JPEG -q 100	0.26	0.06
PVRG-JPEG -q 150	1.87	0.07
PVRG-JPEG -q 200	3.31	0.09
PVRG-JPEG -q 250	4.66	0.11
PVRG-JPEG -q 300	7.26	0.12
PVRG-JPEG -q 350	8.87	0.13
PVRG-JPEG -q 400	11.61	0.12
PVRG-JPEG -q 450	14.64	0.12
PVRG-JPEG -q 500	19.46	0.10

Table A.43: Pepper, Sharp Edge Blocks (Block Frame), $\alpha = 0°$

Degradation	Sharp Edge Pixels	
	P_{hv}	P_{nhv}
PVRG-JPEG -q 50	4.91	0.00
PVRG-JPEG -q 100	7.91	-0.01
PVRG-JPEG -q 150	30.45	-0.04
PVRG-JPEG -q 200	51.73	-0.06
PVRG-JPEG -q 250	82.09	-0.09
PVRG-JPEG -q 300	112.82	-0.13
PVRG-JPEG -q 350	137.45	-0.16
PVRG-JPEG -q 400	153.55	-0.19
PVRG-JPEG -q 450	195.00	-0.23
PVRG-JPEG -q 500	234.82	-0.28

Table A.44: Pepper, Sharp Edge Blocks (Sharp Edge Pixels), $\alpha = 0°$

Degradation	Background pixels	
	P_{hv}	P_{nhv}
PVRG-JPEG -q 50	0.33	0.09
PVRG-JPEG -q 100	1.91	0.13
PVRG-JPEG -q 150	4.16	0.15
PVRG-JPEG -q 200	6.88	0.18
PVRG-JPEG -q 250	10.40	0.17
PVRG-JPEG -q 300	13.70	0.14
PVRG-JPEG -q 350	15.42	0.14
PVRG-JPEG -q 400	17.81	0.10
PVRG-JPEG -q 450	22.02	0.06
PVRG-JPEG -q 500	24.86	-0.01

Table A.45: Pepper, Sharp Edge Blocks (Background pixels), $\alpha = 0°$